



2004

TESTING AND VALIDATION OF A CORRELATION BASED TRANSITION MODEL USING LOCAL VARIABLES

Srinivas Reddy Likki

University of Kentucky, srinivas@engr.uky.edu

[Right click to open a feedback form in a new tab to let us know how this document benefits you.](#)

Recommended Citation

Likki, Srinivas Reddy, "TESTING AND VALIDATION OF A CORRELATION BASED TRANSITION MODEL USING LOCAL VARIABLES" (2004). *University of Kentucky Master's Theses*. 319.
https://uknowledge.uky.edu/gradschool_theses/319

This Thesis is brought to you for free and open access by the Graduate School at UKnowledge. It has been accepted for inclusion in University of Kentucky Master's Theses by an authorized administrator of UKnowledge. For more information, please contact UKnowledge@lsv.uky.edu.

ABSTRACT OF THESIS

TESTING AND VALIDATION OF A CORRELATION BASED TRANSITION MODEL USING LOCAL VARIABLES

A systematic approach of testing and validating transition models is developed and employed in testing of a recently developed transition model. The testing methodology uses efficient computational tools and a wide range of test cases. The computational tools include a boundary layer code, single zone Navier Stokes solver, and a multi-block Navier Stokes solver which uses MPI and is capable of handling complex geometries and moving grids. Test cases include simple flat plate experiments, cascade experiments, and unsteady wake/blade interaction experiments. The test cases are used to test the predicting capabilities of the transition model under various effects such as free stream turbulence intensity, Reynolds number variations, pressure gradient, flow separation, and unsteady wake/blade interaction. Using the above test cases and computational tools a method is developed to validate transition models. The transition model is first implemented in boundary layer code and tested for simple flat plate cases. Then the transition model is implemented in single zone Navier Stokes solver and tested for hysteresis effects for flat plate cases. Finally the transition model is implemented in multi zone Navier Stokes solver and tested for compressor and turbine cascade cases followed by unsteady wake/blade interaction experiments.

Using the method developed a new correlation based transition model (Menter et al. 2004) which uses local variables is tested and validated. The new model predicted good results for high free stream turbulence and high Reynolds number cases. For low free stream turbulence and low Reynolds number cases, the results were satisfactory.

KEYWORDS: Transition Modeling, Transition Model Validation, Intermittency, Transport Equation, Flow Separation.

Srinivas Reddy Likki

04/19/2004

Copyright © Srinivas Reddy Likki 2004

TESTING AND VALIDATION OF A CORRELATION BASED
TRANSITION MODEL USING LOCAL VARIABLES

By

Srinivas Reddy Likki

Dr. George Huang

Director of Thesis

Dr. George Huang

Director of Graduate Studies

04/19/2004

RULES FOR THE USE OF THESIS

Unpublished thesis submitted for the Master's degree and deposited in the University of Kentucky Library are as a rule open for inspection, but are to be used only with due regard to the rights of the authors. Bibliographical references may be noted, but quotations or summaries of parts may be published only with the permission of the author, and with the usual scholarly acknowledgements.

Extensive copying or publication of the thesis in whole or in part also requires the consent of the Dean of the Graduate School of the University of Kentucky.

THESIS

Srinivas Reddy Likki

The Graduate School
University of Kentucky

2004

TESTING AND VALIDATION OF A CORRELATION BASED
TRANSITION MODEL USING LOCAL VARIABLES

THESIS

A thesis submitted in partial fulfillment of the
requirements for the degree of Master of Science in Mechanical Engineering in the
College of Engineering at the University of Kentucky

By

Srinivas Reddy Likki

Lexington, Kentucky

Director: Dr. George Huang, Professor of Mechanical Engineering

Lexington, Kentucky

2004

Copyright © Srinivas Reddy Likki 2004

Dedication

To my family, specially my father who inspired me to reach greater heights in life and taught me to strive for the best.

ACKNOWLEDGEMENTS

The following thesis is the result of unending guidance and patience shown by Dr.George Huang and Dr.Yildirim Bora Suzen. Although the thesis has one author, it is the result of many people who worked very hard and guided me until the final stages of the project. The thesis looks incomplete until I thank some of the contributors of this thesis. I would like to thank Dr.George Huang for having confidence in me and assigning this project. He has shown complete faith, instilled interest and confidence in me. I would like to thank Dr.Yildirim Bora Suzen, who is my unofficial advisor for his everlasting support, his willingness to share knowledge and for the time he spent for the project including some weekends. I would like to thank Dr. Florian Menter and Dr. Robin Langtry of ANSYS-CFX, Germany for their contribution on the Modeling part. I would like to thank GE Global Research Center for sponsoring this project and my research work. I would like to thank all the members of UKCFD group for their cooperation throughout my graduate study and also providing me with the computer resources. I would also like to thank Dr.Vincent Capece and Dr. Jamey Jacob for being on my thesis committee.

Finally I would like to thank my family for the never ending support they rendered to me throughout my life and particularly during my graduate study at University of Kentucky. I would also like to thank all my friends for their cooperation during my stay here at University of Kentucky.

TABLE OF CONTENTS

Acknowledgements.....	iii
List of Tables.....	vii
List of Figures.....	viii
List of Files.....	xii
Chapter	
1. Introduction.....	1
1.1 Introduction to Transition.....	1
1.2 Motivation.....	2
2. Transition Review.....	5
2.1 Flow Transition.....	5
2.2 Modes of Transition.....	5
2.2.1 Natural Transition.....	5
2.2.2 Bypass Transition.....	6
2.2.3 Separated - Flow Transition.....	6
2.2.4 Periodic - Unsteady Transition.....	6
2.2.5 Reverse Transition or Relaminarization.....	7
2.3 Factors Affecting Flow Transition.....	7
2.3.1 Free Stream Turbulence.....	7
2.3.2 Pressure Gradient.....	7
2.3.3 Surface Roughness.....	8
2.3.4 Curvature.....	8
2.3.5 Compressibility.....	8
2.3.6 Heat Transfer.....	9
2.3.7 Film Cooling.....	9
2.3.8 Acoustic Disturbances.....	9
2.4 Transition – Turbomachinery Applications.....	9
2.4.1 Transition Phenomena in Compressors.....	10
2.4.2 Transition Phenomena in Combustors.....	10
2.4.3 Transition Phenomena in Turbines.....	10
2.5 Transition Prediction Methods.....	11

2.6 Transition Model Validation.....	14
3. Method of Testing and Validation.....	16
3.1 Test Cases.....	16
3.1.1 T3 Flat Plate Experiments of Savill (1993a, 1993b).....	17
3.1.2 Pak-B Low-Pressure Turbine Blade Experiments of Huang et al. (2003)....	17
3.1.3 Highly Loaded Compressor Cascade Experiments of Zierke and Deutsch (1989).....	18
3.1.4 Large Scale Turbine Cascade Experiments of Ubaldi et al. (1996).....	19
3.1.5 Unsteady Wake/blade Interaction Experiments of Stieger et al. (2003).....	19
3.2 Computational Tools.....	20
3.2.1 Boundary Layer Code.....	21
3.2.2 Single Zone Navier Stokes Solver.....	21
3.2.3 Navier Stokes Solver “GHOST”.....	21
3.3 Method of Validation.....	22
4. Results and Discussion.....	31
4.1 T3 Flat Plate Experiments of Savill (1993a, 1993b).....	31
4.1.1 Grid Dependence Study.....	34
4.1.2 Study on Effect of y^+	35
4.2 Pak-B Low-Pressure Turbine Blade Experiments of Huang et al. (2003).....	36
4.2.1 Parametric Study for Low Freestream Turbulence and Low Reynolds Number Case.....	39
4.3 Highly Loaded Compressor Cascade Experiments of Zierke and Deutsch (1989).....	42
4.4 Large Scale Turbine Cascade Experiments of Ubaldi et al. (1996).....	43
4.5 Unsteady Wake/blade Interaction Experiments of Stieger et al. (2003).....	43
5. Conclusions and Future Work.....	87
5.1 Conclusions.....	87
5.2 Future Work.....	89
Appendix.....	90
A1. Nomenclature.....	90

A2. A Correlation Based Transition Model Using Local Variables (Menter et al., 2004).....	92
A3. SST Turbulence Model (Menter, 1994).....	96
References.....	98
Vita.....	102

LIST OF TABLES

Table 3.1 : List of Test Cases.....	24
Table 3.2 : Details of T3 Flat Plate Experiments of Savill (1993a, 1993b).....	24
Table 3.3 : Details of Experiments of Huang et al. (2003).....	25
Table 3.4 : Cascade Geometry for Genoa Cascade Experiments of Ubaldi et al. (1996).....	25
Table 3.5 : Details of T106 Cascade for Experiments of Stieger et al. (2003).....	26
Table 4.1 : Inflow Conditions for T3 Flat Plate Experiments of Savill (1993a, 1993b).....	45
Table 4.2 : Inflow Conditions for Cascade Cases.....	46
Table 4.3 : Modifications for the Parametric Study for Experiments of Huang et al. (2003).....	47

LIST OF FIGURES

Figure 1.1 : Details of Project Collaboration.....	4
Figure 3.1 : Schematic Diagram of Computational Grid for Flat Plate Experiments of Savill (1993a, 1993b).....	26
Figure 3.2 : Pressure Coefficient Profile for Variable Pressure Gradient Flat Plate Experiments of Savill (1993a, 1993b).....	27
Figure 3.3 : Details of P&W PAK-B Blade Cascade (Huang et al., 2003).....	27
Figure 3.4 : Details of Genoa Blade Cascade (Ubaldi et al., 1996).....	28
Figure 3.5 : Bar Passing Cascade With T106 Profile (Stieger et al., 2003).....	29
Figure 3.6 : T106 Cascade Arrangement for Unsteady Transition due to Wake Impingement (Stieger et al., 2003).....	30
Figure 4.1 : Variation of Freestream Turbulence Intensity Along the Flat Plate for T3A Case...	48
Figure 4.2 : Variation of Skin Friction Coefficient Along the Flat Plate for T3A Case.....	49
Figure 4.3 : Variation of Reynolds Number Based on Momentum Thickness Along the Flat Plate for T3A Case.....	49
Figure 4.4 : Variation of Shape Factor Along the Flat Plate for T3A Case.....	50
Figure 4.5 : Variation of Freestream Turbulence Intensity Along the Flat Plate for T3B Case....	50
Figure 4.6 : Variation of Skin Friction Coefficient Along the Flat Plate for T3B Case.....	51
Figure 4.7 : Variation of Reynolds Number Based on Momentum Thickness Along the Flat Plate for T3B Case.....	51
Figure 4.8 : Variation of Shape Factor Along the Flat Plate for T3B Case.....	52
Figure 4.9 : Variation of Freestream Turbulence Intensity Along the Flat Plate for T3A- Case..	52
Figure 4.10 : Variation of Skin Friction Coefficient Along the Flat Plate for T3A- Case.....	53
Figure 4.11 : Variation of Reynolds Number Based on Momentum Thickness Along the Flat Plate for T3A- Case.....	53
Figure 4.12 : Variation of Shape Factor Along the Flat Plate for T3A- Case.....	54
Figure 4.13 : Variation of Freestream Turbulence Intensity Along the Flat Plate for T3C1 Case.....	54
Figure 4.14 : Variation of Skin Friction Coefficient Along the Flat Plate for T3C1 Case.....	55

Figure 4.15 : Variation of Reynolds Number Based on Momentum Thickness Along the Flat Plate for T3C1 Case.....	55
Figure 4.16 : Variation of Shape Factor Along the Flat Plate for T3C1 Case.....	56
Figure 4.17 : Variation of Freestream Turbulence Intensity Along the Flat Plate for T3C2 Case.....	56
Figure 4.18 : Variation of Skin Friction Coefficient Along the Flat Plate for T3C2 Case.....	57
Figure 4.19 : Variation of Reynolds Number Based on Momentum Thickness Along the Flat Plate for T3C2 Case.....	57
Figure 4.20 : Variation of Shape Factor Along the Flat Plate for T3C2 Case.....	58
Figure 4.21 : Effect of Grid Dependence for T3A Case.....	58
Figure 4.22 : Effect of Grid Dependence for T3B Case.....	59
Figure 4.23 : Effect of Grid Dependence for T3A- Case.....	59
Figure 4.24 : Effect of y^+ for T3A Case	60
Figure 4.25 : Computational Grid for FSTI = 0.08% Case of Huang et al. (2003).....	60
Figure 4.26 : Computational Grid for FSTI = 2.35% and FSTI = 6.0% Case of Huang et al. (2003).....	61
Figure 4.27 : Pressure Coefficient Comparison for FSTI=0.08% & Re=100000.....	61
Figure 4.28 : Velocity Profile for FSTI=0.08% & Re=100000.....	62
Figure 4.29 : Pressure Coefficient Comparison for FSTI=0.08% & Re=75000.....	62
Figure 4.30 : Velocity Profile for FSTI=0.08% & Re=75000.....	63
Figure 4.31 : Pressure Coefficient Comparison for FSTI=0.08% & Re=50000.....	63
Figure 4.32 : Velocity Profile for FSTI=0.08% & Re=50000.....	64
Figure 4.33 : Streamlines and Effective Intermittency Contours for PAK B Cascade (FSTI = 0.08% & Re = 50000).....	64
Figure 4.34 : Streamlines and Turbulent Kinetic Energy Contours for PAK B Cascade (FSTI = 0.08% & Re = 50000).....	65
Figure 4.35 : Pressure Coefficient Comparison for FSTI=6.0% & Re=100000.....	65
Figure 4.36 : Velocity Profile for FSTI=6.0% & Re=100000.....	66
Figure 4.37 : Pressure Coefficient Comparison for FSTI=6.0% & Re=75000.....	66
Figure 4.38 : Velocity Profile for FSTI=6.0% & Re=75000.....	67
Figure 4.39 : Pressure Coefficient Comparison for FSTI=6.0% & Re=50000.....	67

Figure 4.40 : Velocity Profile for FSTI=6.0% & Re=50000.....	68
Figure 4.41 : Pressure Coefficient Comparison for FSTI=2.35% & Re=100000.....	68
Figure 4.42 : Pressure Coefficient Comparison for FSTI=2.35% & Re=75000.....	69
Figure 4.43 : Pressure Coefficient Comparison for FSTI=2.35% & Re=50000.....	69
Figure 4.44 : Pressure Coefficient Comparison for Experiments of Huang et al. (2003).....	70
Figure 4.45 : Effect of Varying s_1 for Low Freestream Turbulence and Low Reynolds Number Case.....	71
Figure 4.46 : Parametric Study I for Low Freestream Turbulence and Low Reynolds Number Case.....	71
Figure 4.47 : Parametric Study II for Low Freestream Turbulence and Low Reynolds Number Case.....	72
Figure 4.48 : Parametric Study III for Low Freestream Turbulence and Low Reynolds Number Case.....	72
Figure 4.49 : Computational Grid for Compressor Cascade Experiments of Zierke and Deutsch (1989).....	73
Figure 4.50 : Pressure Coefficient Comparison for Zierke and Deutsch Compressor Cascade, $i = -1.5^\circ$	73
Figure 4.51 : Pressure Coefficient Comparison for Zierke and Deutsch Compressor Cascade, $i = 5.0^\circ$	74
Figure 4.52 : Intermittency Contours for Zierke and Deutsch Compressor Cascade, $i = 5.0^\circ$	74
Figure 4.53 : Turbulent Kinetic Energy Contours for Zierke and Deutsch Compressor Cascade, $i = 5.0^\circ$	75
Figure 4.54 : Eddy Viscosity Contours for Zierke and Deutsch Compressor Cascade, $i = 5.0^\circ$	75
Figure 4.55 : Computational Grid for Turbine Cascade Experiments of Ubaldi et al. (1996).....	76
Figure 4.56 : Normalized Friction Velocity for Genoa Turbine Cascade.....	76
Figure 4.57 : Computational Grid for T106 Experiments of Stieger et al. (2003).....	77
Figure 4.58 : Velocity Profile at $x / C = -0.04$ for T106 Cascade.....	77
Figure 4.59 : Comparison of Computed and Experimental Pressure Coefficient Distributions for T106 Cascade.....	78
Figure 4.60 : Computed Phase Averaged Skin Friction Coefficient Distribution on the Suction Surface of T106 Blade.....	78

Figure 4.61 : Comparison of Computed and Experimental Pressure Coefficient Contours for T106 Cascade.....	79
Figure 4.62 : Mean Velocity Profiles for T106 Cascade.....	80
Figure 4.63 : Comparison of Computed and Experimental Velocity Distributions at Various Streamwise Stations on Suction Surface of the Blade for T106 Cascade.....	81
Figure 4.64 : Comparison of Computed and Experimental Isocontours of Turbulent Kinetic Energy at Different Time Levels for T106 Cascade.....	83

LIST OF FILES

Filename	File size
1. Likkthes.pdf.....	11.9 MB

Chapter One

Introduction

1.1 Introduction to Transition

Transition plays an important role in various turbomachinery applications. Flow transition is affected by large disturbances in the external flow such as pressure gradient and free stream turbulence intensity. Flow transition is also affected by Reynolds number variations, flow separation, unsteady wake/blade interactions, surface roughness, surface temperature, and curvature. The location of the onset and the extension of transition are of major importance in various turbomachinery applications. Throughout the transitional region, heat transfer and skin friction increase dramatically from their low laminar values at the onset of transition to their corresponding high fully turbulent values at the end of transition. In order to calculate heat transfer and skin friction in the transition region, accurate prediction of the onset of transition, extent of transition and its interaction with the boundary layer development is required. In addition the transition behavior has a dominant effect on the separation behavior of boundary layers and stall. As a consequence accurate prediction of transition plays an important role in the design of efficient turbomachinery components, particularly low-pressure turbines. Due to low density and low speeds the Reynolds numbers may drop to very low values. At these low Reynolds numbers, the flow remains laminar and may separate on the suction surface of the blades before it becomes turbulent. This flow separation is the main cause of losses in low-pressure turbines. Low-pressure turbines operate at low values of Reynolds number, especially at high-altitude cruise conditions. If the flow transition takes place, the separation bubble is suppressed and the losses are reduced. Therefore it is crucial to predict under what conditions and at what location the flow transition takes place in order to accurately predict losses. As a result, the ability to predict transition accurately is of great importance for the design of future, highly-loaded efficient turbines for gas turbine engines.

There are a number of different transition mechanisms depending on the turbulence level of the external flow, the pressure gradient along the laminar boundary layer, the geometrical details and the surface roughness. Flows in turbomachines are affected by free stream turbulence intensity,

pressure gradient and unsteady wake/blade interactions. Due to the above effects the main transition mechanism in turbomachines is bypass transition (Morkovin, 1969). Bypass transition takes place on the boundary layer by high levels of turbulence in the free stream that is generated by the upstream blade rows.

1.2 Motivation

Bypass transition is a complex phenomenon that depends mainly on the turbulence intensity and the status of the boundary layer due to pressure gradients and separation. There is also some empirical evidence that suggests the structure of the turbulence (length scale) can have an impact on the transition location (Mayle, 1991). As linear methods cannot be applied to bypass transition, there is only a limited range of engineering tools, most of which are highly empirical (Savill, 1993a, Savill, 1996).

It became apparent within the TRANSPRETURB European network on transition prediction (<http://transition.imse.unige.it/>) that there are mainly two concepts used to model bypass transition in industry (Menter et al., 2004). The first is the application of low Reynolds number turbulence models. However the ability of a low-Re turbulence model to predict transition seems to be coincidental. This is because the calibration of the damping functions is based on reproducing the viscous sublayer behavior, not on predicting transition from laminar to turbulent flow. The progress report of the TRANSPRETURB network states: *“The use of turbulence models without any coupling to an intermittency equation proves to be very delicate and often extremely unreliable in the prediction of transition.”*

The second approach, which is favored by industry over low-Re models, is the use of empirical correlations. The correlations usually relate the free stream turbulence intensity, Tu , to the transition Reynolds number where the length scale is based on the momentum thickness. There are a number of transition models based on empirical correlations. Considerable progress has been made in the development of transition models, but existing models are still not always robust, because they do not capture all the physics of the transition process well. Transitional boundary layers are intermittent, that is at a fixed position in the boundary layer, the flow is continuously switching between turbulent like state and non turbulent state as the turbulent spots

are convected past. Most existing transition models do not treat these two zones separately. Intermittency based models, such as those proposed by Steelant and Dick (1996), Suzen and Huang (2000), and Solomon et al. (1995) represent an attempt to model the transition region by treating the zones separately. More recently, a new transition model is developed by Menter et al. (2004). The new model is based on two transport equations, one for intermittency and one for transition onset. The model uses the concept of vorticity Reynolds number to link transition onset correlations with intermittency and is based only on local variables. The new model can be used for unstructured grids and parallel processing and is a significant improvement over the existing transition models.

Model validation is equally important as model development. Transition models can be calibrated for a particular test case. By doing so, the model gives good results for that particular case and may not perform well for other cases. What we really need is a transition model which gives good results for all the cases and performs well under the effects of freestream turbulence intensity, pressure gradient, flow separation, Reynolds number, and unsteadiness. Using the validation technique developed in this thesis, transition model is extensively tested for different test cases which investigate the predicting capability of the model under various effects like freestream turbulence intensity, pressure gradient, flow separation, Reynolds number, and unsteadiness. So there is a need to validate all the existing transition models. In this research an approach is developed to test and validate transition models using a wide range of test cases and efficient computational tools. Using this approach the predicting capability of the transition model under the effects of free stream turbulence intensity, pressure gradient, flow separation, Reynolds number, and unsteadiness is investigated. Efficient computational tools which include boundary layer code, single zone Navier Stokes solver, and multi block Navier Stokes solver are used. First the transition model is implemented in boundary layer code and tested for simple flat plate cases. Then the transition model is implemented in single zone Navier Stokes solver and tested for hysteresis effects for simple flat plate cases. Then the model is implemented in multi zone Navier Stokes solver and tested for compressor and turbine cascade experiments and finally for unsteady wake/blade interaction experiments. This thesis details the testing and validation of a new correlation based transition model using the systematic approach.

The new transition model is the result of a joint collaboration between ANSYS CFX, GE GRC and University of Kentucky as shown in figure 1.1. ANSYS CFX played the main role in development of the new transition model. University of Kentucky CFD group is responsible for testing and validation of the new transition model and also for assisting ANSYS CFX and GE GRC in rapid testing of the new model and setting up the test cases. GE GRC is responsible for the application of the new transition model for various industrial test cases. The new model is implemented in GE's TACOMA code, CFX code of ANSYS, and GHOST code of University of Kentucky. As a result, the new transition model is developed and tested for various turbomachinery applications, such as compressor and turbine cascade cases and also for industrial wind turbine cases.

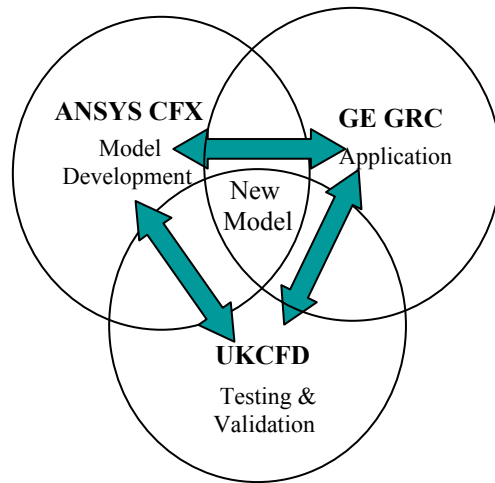


Figure 1.1 : Details of Project Collaboration

Chapter Two

Transition Review

2.1 Flow Transition

In general, there are three important modes of transition. The natural transition process is described by Schlichting (1979), and is based on the formation of a weak instability in the laminar boundary layer. This instability amplifies and proceeds through various stages until it forms fully turbulent flow. Bypass transition described by Morkovin (1969) is caused due to the disturbances in external flow such as free stream turbulence and pressure gradient and is dominant in gas turbine engines. Separated flow transition occurs in the free shear layer and may not involve T-S waves. Separated flow transition is common in low pressure turbines and compressors.

2.2 Modes of Transition

The different modes of transition are natural transition, bypass transition, separated-flow transition, periodic-unsteady transition and reverse transition. Bypass transition and periodic-unsteady transition are observed in majority of the turbomachinery applications. Separated-flow transition is observed in compressors and reverse transition is observed in nozzles with highly accelerating flows. The different modes of transition are detailed in the next sections.

2.2.1 Natural Transition

Natural transition is first described by Tollmien and Schlichting (Mayle, 1991). This type of transition begins with a weak instability in the laminar boundary layer at a critical value of the momentum thickness Reynolds number. These instabilities are one dimensional. These weak instabilities proceed through various stages of amplifications and amplifies into two dimensional instabilities and finally into three dimensional instabilities. These instabilities further grow and form loop vortices and then develop into turbulent spots. These turbulent spots convect downstream and coalesce to form a fully turbulent boundary layer.

2.2.2 Bypass Transition

Due to high turbulence intensity, pressure gradient and unsteady wake/blade interaction, the first two stages of the natural transition process are bypassed and formation of turbulent spots occur directly. As the first two stages of the transition process are bypassed, this type of transition is named Bypass transition. Morkovin (1969) introduced the term bypass transition to describe the transition process, which occurs in high disturbance flows, such as those present in turbomachinery. Kachanov (1994) noted that the bypass transition is connected to direct non-linear laminar flow breakdown under the influence of external disturbances. This is observed when high levels of environmental perturbations (free stream disturbances, surface roughness etc.) are present (Kyriakides et al., 1999). This type of transition is common in gas turbine engines.

2.2.3 Separated - Flow Transition

In low pressure turbines and compressors, transition may occur in the separated shear layer (Mayle, 1991). The laminar flow separates at low Reynolds number due to strong adverse pressure gradients. The flow may reattach as turbulent forming a laminar-separation/ turbulent reattachment bubble on the surface. The transition occurs within the separation bubble and this type of transition occurs due to adverse pressure gradients. The separation bubble length depends on the transition process within the shear layer. This type of transition may involve all the stages of natural transition. For low free stream turbulence levels the flow in the bubble is laminar and instabilities of the T-S type are observed.

2.2.4 Periodic - Unsteady Transition

This type of transition is caused by the periodic passage of wake structures from upstream airfoils or obstructions (cylinders) and is referred to as wake induced or periodic unsteady transition (Kyriakides et al., 1999). Transition induced by wakes or shocks, compared to the above mentioned stages, appear to bypass the first stage of natural transition. The turbulent spots are formed and convect downstream. Turbulent spots immediately coalesce after formation and immediately grow and propagate downstream to form fully turbulent layer. This type of transition is found in majority of the turbomachinery applications. In turbomachines, viscous wakes from the proceeding stator or rotor blade row pass through the succeeding rotor or stator

blade row, generating unsteady pressure, surface heat transfer and boundary layers. This is called unsteady wake/blade interaction (Fan and Lakshminarayana, 1996).

2.2.5 Reverse Transition or Relaminarization

Transition from turbulent to laminar flow also exists and is called reverse transition or relaminarization. This type of transition is noticed in flows through nozzles with strong acceleration (Mayle, 1991). This is because the acceleration on the pressure side of most airfoils near the trailing edge, in the exit ducts of combustors and on the suction side of turbine airfoils near the leading edge are generally higher than that for which reverse transition occurs. Reverse transition involves a balance between convection, production and dissipation of the turbulent kinetic energy within the boundary layer.

2.3 Factors Affecting Flow Transition

Transition phenomenon is affected by various factors such as free stream turbulence, pressure gradient, surface roughness, curvature, compressibility, heat transfer, film cooling, and acoustic disturbances. Although the transition phenomenon is affected due to various other secondary factors, the above mentioned factors play a significant role in affecting transition phenomenon. The effect of above mentioned factors on transition is detailed in the following section.

2.3.1 Free Stream Turbulence

Free stream turbulence does increase the dynamics and heat transfer in the turbulent boundary layer and the heat transfer seems to be more sensitive to free stream turbulence. Increasing the free stream turbulence reduces the Reynolds number at which transition onset occurs. Increasing the free stream turbulence, the production of turbulent spots increases and thus the transition length decreases. At higher turbulence levels, transition occurs in a bypass mode and is completely independent of the Tollmien-Schlichting instability (Mayle, 1991).

2.3.2 Pressure Gradient

The acceleration parameter is an appropriate measurement of the pressure gradient for favorable pressure gradient flows. With an increase in acceleration transition Reynolds number increases

thus delaying transition. For low turbulence levels the effect of acceleration is significant, while for flows in gas turbines where the turbulence level is high, effect of acceleration is negligible as the onset of transition is controlled by free stream turbulence. For adverse pressure gradient cases, increase in negative acceleration increases the transition Reynolds number, delaying transition onset. Effect of turbulence on transition is much less for adverse pressure gradient flows when compared to favorable pressure gradients (Mayle, 1991).

2.3.3 Surface Roughness

Surface Roughness plays a dominant role on transition behavior over an airfoil. Increasing the surface roughness decreases the transition Reynolds number and thus the transition occurs much earlier on a rough airfoil when compared to a smooth airfoil. For a high free stream turbulence level, a highly rough airfoil decreases the transition length by 60% when compared to a smooth airfoil. For a smaller roughness, a smaller effect can be observed (Mayle, 1991).

2.3.4 Curvature

Surface curvature plays an important role in the prediction of transition behavior. A concave curvature can either decrease or increase the transition Reynolds number depending on the strength of curvature and turbulence level. For a low free stream turbulence case, concave curvature can move the transition upstream when Gortler vortices form and break down to turbulence. For a high free stream turbulence case, a concave curvature does have a significant effect, moving the transition location upstream thereby increasing the turbulent transport and causing skin friction to rise by as much as 40%. Transition on a convex surface is only slightly delayed and an increase of around 10% in the transition length is observed (Mayle, 1991).

2.3.5 Compressibility

Majority of the flows in gas turbines are compressible. Compressibility has only very slight influence on stability and transition at subsonic speeds. However at higher supersonic speeds it has complicated effects. Thus the effect of Mach number on transition onset and production rate have to be taken into account along with the effect of shock waves. As Mach number increases the onset of transition is delayed and the spot production rate is decreased thus increasing the transition length roughly by 8-30%. A passing shock wave from an upstream airfoil induces a

small concentrated vortex on the pressure side of the airfoil near the leading edge and thus can cause transition as the shock moves along the surface (Mayle, 1991).

2.3.6 Heat Transfer

Heating or cooling the flow affects the transition at low free stream turbulence intensity. Wall heat transfer influences the stability and transition because viscosity depends on temperature. Heated or cooled wall also heats/cool the fluid in its vicinity and thus changes the viscosity. Reduced near wall viscosity stabilizes the flow owing to increased velocity gradient and decreased shape factor thus effecting flow transition. At high free stream turbulence levels it was observed that heat transfer has negligible effect on spot production rate and thus on the transition length (Mayle, 1991).

2.3.7 Film Cooling

Film cooling effects the state of the boundary layer and thus causes the flow to undergo transition to turbulent flow. Injection of coolant from the film holes along the turbine airfoil disrupts the laminar flow and acts as a source of turbulence. Thus the flow transition takes place. Even though injection causes transition, a strong acceleration can make the flow laminar again as observed during the first stages of film cooled turbine airfoils (Mayle, 1991).

2.3.8 Acoustic Disturbances

The external flow may contain disturbances, either fluctuations of decaying background turbulence (wind tunnels) or atmospheric turbulence (flight conditions). Acoustic noise may be present in both situations. Such disturbances especially if they are within a suitable frequency band and are large in amplitude, can accelerate the transition process. Thus acoustic disturbances can act as a source of turbulence and thus allows transition to take place.

2.4 Transition - Turbomachinery Applications

Transition plays an important role in various turbomachinery applications such as flows in compressors, combustors, high pressure and low pressure turbines. To calculate the heat transfer on various components of the turbomachine, transition and its interaction with boundary layer

development has to be predicted accurately. In the following section the transition phenomena in compressors, combustors, high pressure and low pressure turbines is explained.

2.4.1 Transition Phenomena in Compressors

In compressors the transition process is interlinked with separation process and thus the interplay between separation and transition has to be clearly understood to predict the transition phenomena in compressors. Transition in adverse pressure gradients, separated flows and wake induced transition has to be clearly studied to understand the transition process in compressors. On pressure side of the compressor, transition begins before the point of maximum pressure and near the trailing edge we encounter relaminarization. The transition phenomena on the pressure side can be calculated accurately but it is insignificant as the losses incurred on the pressure side are much less than on the suction side. On suction side transition usually begins near the point of minimum pressure and occurs either by bypass mode or separated flow mode depending on the Reynolds number of the flow (Mayle, 1991).

2.4.2 Transition Phenomena in Combustors

Laminar boundary layers exist in combustors for flows with high turbulence and favorable pressure gradient. In the exit ducts of combustors, where large favorable pressure gradients exist, flow transition occurs in either direction. Transition in combustors have no effect on the aerodynamic performance of the combustor unless, as possible in reverse curved exit ducts, the duct is so poorly designed that it separates. Transition in combustors mainly affects the heat transfer and thus understanding the transition phenomena benefits the prediction of heat transfer in combustors (Mayle, 1991).

2.4.3 Transition Phenomena in Turbines

Predicting flows in turbines is in much advanced stage compared to the flows in any other components of the engine. The main reason for this is because the flows in compressor and combustor involve large separated regions compared to turbines and thus are much more complicated to determine (Mayle, 1991). Also the heat transfer prediction on various parts of the turbine is in much advanced stage to provide adequate cooling in face of the ever increasing

turbine temperature. Since the flows in a turbine are transitional and as the turbulent heat transfer is much larger compared to the heat transfer in laminar flows, prediction of transition is important in turbines.

In high pressure turbines, transition mainly affects the heat transfer on various components. Since aerodynamic losses are mainly due to the turbulent flow after transition, the effect of transition on losses is less significant in high pressure turbines. In low pressure turbine, the flow has low Reynolds number. Understanding the transition behavior is particularly important to efficiently design the turbine both aerodynamically and thermally.

2.5 Transition Prediction Methods

Prediction of flow transition plays an important role in the analysis and performance of various components of turbomachinery. There are mainly four ways to determine flow transition (Suzen et al., 2001). One of the methods is to use the stability theory. In this method, stability equations are solved at streamwise stations to predict the onset of transition. This method requires prior solution of the mean flow field and does not give any information of the turbulent flow apart from onset of transition. Another method is using empirical correlations in the form of e^n . This method also requires prior solution of the mean flow field and these two methods are not compatible with current CFD approaches. Another method to predict flow transition is the use of low-Reynolds number turbulence models. Savill (1993a), Westin and Henkes (1997) showed that none of the existing low-Reynolds number models were adequate to predict the onset and length of transition accurately for a wide range of flow conditions.

An alternative to this approach is to use the concept of intermittency to blend the flow from laminar to turbulent regions. The intermittency concept was originally proposed by Emmons (1951). He defined the intermittency function γ as the probability of the flow being turbulent at a given position. With a constant turbulent spot propagation parameter σ the intermittency function can be written as (Narasimha, 1957):

$$\gamma = 1 - \exp\left[-\frac{n\sigma}{u} \left| (x - x_{tr})^2 \right| \right] \quad (2.1)$$

where u is the free stream velocity and n is the spot generation rate. The number of turbulent spots produced per unit length and time at the position of transition onset x_{tr} is given by n . The value of n is computed by transition models that correlate it to characteristic flow properties.

Chen and Thyson (1971) introduced an intermittency function taking into account the effect of changing freestream velocities on the spot convection velocity:

$$\gamma = 1 - \exp \left[-n_{tr} (x - x_{tr}) \int_{x_{tr}}^x \frac{1}{u} dx \right] \quad (2.2)$$

Solomon et al. (1995) extended this model by defining the spot spreading half-angle α and the spot propagation parameter σ as a function of the local pressure gradient parameter λ_θ .

$$\gamma = 1 - \exp \left[-n_{tr} \int_{x_{tr}}^x \frac{\sigma}{\tan \alpha u} dx \int_{x_{tr}}^x \tan \alpha dx \right] \quad (2.3)$$

The intermittency function is used to modify the turbulent viscosity as calculated by the Prandtl-Kolmogorov relation yielding:

$$\mu_t^* = \gamma \cdot \mu_t \quad (2.4)$$

As the flow in the freestream is turbulent the modification of μ_t is performed only within the boundary layer. At the interface a switching function is applied and γ is set to unity outside the boundary layer.

Steelant and Dick (1996) proposed a transport equation for intermittency, in which the source term of the equation is developed such that the γ distribution of Dhawan and Narasimha across the transition region can be reproduced. Steelant and Dick used their model to predict the transition flow under zero, favorable, and adverse pressure gradients. Since their method requires solution of two sets of conditioned Navier Stokes equations this method is not compatible with the current CFD approaches.

Cho and Chung (1992) developed a $\kappa - \varepsilon - \gamma$ turbulence model for free shear flows. This model explicitly incorporates the intermittency into the $\kappa - \varepsilon$ turbulence model by introducing an

additional transport equation for intermittency. Cho and Chung used this model to accurately calculate spreading rates for free shear flows. This model provided a realistic profile of γ in the cross stream direction.

Suzen and Huang (1999) improved the intermittency transport equation by combining the best properties of Steelant and Dick's model and Cho and Chung's model. Their model reproduces the streamwise intermittency distribution of Dhawan and Narasimha and also produces a realistic variation of intermittency in the cross stream direction. For attached flows the onset of transition is calculated using the new correlation developed by Suzen et al. (2001). For separated flows, the onset of transition is calculated using correlation developed by either Davis et al. (1987) or Suzen et al. (2001). This model has been validated for a wide range of flows and predicted good results for all the cases (Suzen and Huang, 2004). This model requires calculation of momentum thickness Reynolds number and running length of the boundary layer. As this model requires calculation of integral quantities, it is applicable only for 2-D flows and is difficult to use in parallel environment.

Langtry and Sjolander (2002) developed a new transition model which can predict flow transition under the influence of free stream turbulence intensity, pressure gradient and flow separation. The model is based on Van Driest and Blumer's (1963) concept of vorticity Reynolds number and has been calibrated for use with the Menter (1994) SST turbulence model. This new model is validated for T3 test cases and Pak-B low-pressure turbine cases and predicted good results. The new model is compatible with unstructured codes, compatible with various widely-accepted turbulence models, and is computationally inexpensive. This new model is relatively a simple transition model which is compatible with current Navier-Stokes codes and appears to predict with good accuracy the transition in both attached and separated shear layers.

Menter et al. (2004) developed a new transition model based on local variables. The model is based on two transport equations, one for intermittency and the other for transition onset. The proposed transport equations do not attempt to model the physics of the transition process (unlike e.g. turbulence models), but form a framework for the implementation of correlation based models into general purpose CFD methods. The intermittency obtained from the transport

equation is used to modify the production and destruction term of the SST turbulence model of Menter (1994). The details of the model formulation is given in Appendix A2. For prediction of separated flow transition a modification is introduced to the model which is called separated flow modification. This modification is implemented to predict good results for low free stream turbulence and low Reynolds number cases. However the new model predicted good results for high free stream turbulence and high Reynolds number cases and satisfactory results for low free stream turbulence and low Reynolds number cases. The new model uses the concept of vorticity Reynolds number to link the correlation and the intermittency equation. As the new model is based only on local variables, it is compatible with modern CFD methods using unstructured grids and massive parallel execution. The new transition model is a significant improvement over the existing transition models.

2.6 Transition Model Validation

There are a number of transition models which are developed and are under development. Testing and validation of transition model is as important as model development. Transition models can be calibrated for a particular test case. By doing so, the model gives good results for that particular case and may not perform well for other cases. What we really need is a transition model which gives good results for all the cases and can be used for the design of efficient turbines for gas turbine engines. So there is a need to validate all the existing transition models. In this thesis a technique to test and validate transition models is developed using a wide range of test cases and efficient computational tools. Test cases include simple flat plate experiments used for investigating the predicting capability of the transition model under the effects of free stream turbulence intensity and pressure gradient, compressor and turbine cascade experiments used for investigating the predicting capability of the transition model under the effects of free stream turbulence intensity, pressure gradient, flow separation, and Reynolds number, and finally unsteady wake/blade interaction experiments used for investigating the predicting capability of the transition model under the effect of unsteadiness. Computational tools include boundary layer code, single zone Navier Stokes solver, and multi-zone Navier Stokes solver. Using the above test cases and testing tools an approach is developed to validate transition models systematically. First the transition model is implemented in boundary layer code and tested for simple flat plate cases. Then the transition model is implemented in single zone Navier Stokes

solver to check for hysteresis effects for simple flat plate cases. Finally the transition model is implemented in multi-zone Navier Stokes solver and tested for compressor and turbine cascade experiments followed by unsteady wake/blade interaction experiments.

Chapter Three

Method of Testing and Validation

A systematic method of testing and validating transition models is developed using a wide range of test cases and efficient computational tools. Test cases include simple flat plate experiments, compressor and turbine cascade experiments, and unsteady wake/blade interaction experiments. These test cases investigate the predicting capabilities of the transition model under various effects like free stream turbulence, pressure gradient, Reynolds number, flow separation, and unsteady wake/blade interaction. The efficient computational tools include boundary layer code, single zone Navier Stokes solver, and multi block Navier Stokes solver. Using the above test cases and computational tools a validation algorithm is developed to test and validate transition models. The following section details the test cases, computational tools and the validation algorithm.

3.1 Test Cases

In order to investigate the predicting capability of the transition model under the effects of Reynolds number, free stream turbulence intensity, pressure gradient, flow separation, and unsteady wake/blade interaction the test cases are setup. The test cases are chosen to investigate the capability of the transition models under a wide range of flow conditions which include zero, favorable and adverse pressure gradients for different free stream turbulence intensities and Reynolds numbers. The test cases assembled form a complete set which simulate realistic turbomachinery flow conditions. The test cases are tabulated in table 3.1 along with the effects investigated.

Simple flat plate experiments are assembled to investigate the predicting capability of the transition model under the effects of free stream turbulence intensity and pressure gradient. Compressor and turbine cascade experiments are assembled to investigate the predicting capability of the model under the effects of free stream turbulence intensity, pressure gradient, Reynolds number, and flow separation. Unsteady wake/blade interaction experiments are

assembled to investigate the capability of the model under the effect of unsteadiness. The test cases are described in detail in the following sections.

3.1.1 T3 Flat Plate Experiments of Savill (1993a, 1993b)

The ERCOFTAC T3 benchmark test cases are assembled by Savill (1993a, 1993b) to test the ability of transition and turbulence models to predict the effects of free stream turbulence intensity and Reynolds number on the development and subsequent transition of a laminar boundary layer under zero and variable pressure gradient conditions. For the testing and validation of transition models some of the T3 flat plate test cases used include T3A, T3B, T3A-, T3C1, and T3C2. Cases T3A, T3B, and T3A- are zero pressure gradient cases for three different free stream turbulence intensities. Cases T3C1 and T3C2 are cases with continuous change in pressure gradient representing an aft-loaded turbine blade for two different turbulence intensities. The schematic diagram of the flat plate used for the experiments is shown in figure 3.1. The variation of the pressure coefficient distribution along the flat plate for variable pressure gradient cases is shown in figure 3.2. Table 3.2 gives the details of the inlet velocity, turbulence intensity, and pressure gradient for each of the flat plate cases. T3 flat plate test cases are used for initial model testing and validation.

3.1.2 Pak-B Low-Pressure Turbine Blade Experiments of Huang et al. (2003)

Huang et al. (2003) conducted experiments on PAK-B blade cascade for a wide range of Reynolds numbers and turbulence intensities. These experiments are assembled to investigate the effect of free stream turbulence, pressure gradient, Reynolds number, and separation on flow transition. The Reynolds number range from 50,000 to 100,000 based on inlet velocity and axial chord. In their experiments the blades has an axial chord length of 6.28 inches. The Pak-B cascade details are shown in figure 3.3. The experimental pressure coefficient values and velocity profiles are measured using surface mounted hot films along the suction side of the Pak-B blade cascade. The freestream turbulence intensity in the tunnel was measured as 0.08%. In order to increase the turbulence intensity, two grids with different mesh sizes are used. One of the grids had the mesh size of 2.54cm (denoted as Grid 0) and the other had 0.80cm (denoted as Grid 3). The decay of turbulence after the grids was measured using crosswire. The grids were movable in the tunnel so that the turbulence level of the flow that reaches the blades could be

controlled by moving the grid that is, by increasing or decreasing the distance between the grid and the blade. Experiments were performed for Reynolds numbers 50,000, 75,000 and 100,000 with grids placed 30 inches away from the blade leading edge, corresponding to turbulence intensities of 2.85% and 1.6% at the leading edge for Grid 0 and Grid 3 respectively. Pressure coefficient data is available for all cases and velocity profiles are available for $Re=50,000$, 75,000, and 100,000 with $FSTI=0.08\%$ and 2.85% cases. Table 3.3 gives the details of the free stream turbulence intensities for all the cases.

Experiments of Huang et al. (2003) on Pak-B cascade are used to investigate the effect of free stream turbulence intensity, pressure gradient, Reynolds number, and separation on flow transition. These experiments form a good case as it tests the ability of transition model to predict flow separation and its interaction with transition for a wide range of free stream turbulence intensities and Reynolds numbers.

3.1.3 Highly Loaded Compressor Cascade Experiments of Zierke and Deutsch (1989)

Comparisons of viscous computations are most needed under flow conditions typical of modern compressor blades, especially under off-design conditions (Zierke and Deutsch, 1989). Therefore, measurements of boundary layers and near wakes have been acquired on a highly loaded compressor cascade blade at two incidence angles near a chord Reynolds number of 500,000. The incidence angles of 5.0° and -1.5° yield boundary layers with a wide variety of characteristics. In order to provide the experimental data, a cascade facility with a one-component laser Doppler Velocimeter to measure the periodic, two-dimensional flow field about a double-circular-arc, compressor blade in cascade is developed. These measurements provide some physical insight into the very complex flows in the turbomachinery. The transitional separation bubbles in compressors play an important role in the development of most of the boundary layers and wakes measured in the cascade and thus computing these bubbles prove to be a key aspect in computing the entire cascade flow field. The blade section used in the tests is a compressor blade designed at the NASA Lewis Research Center. The blade section is a double-circular-arc blade with 65° of camber, a 20.5° stagger angle, a solidity of 2.14 and 228.6 mm

chord length. Available data from the experiments include skin friction coefficient on both the pressure side and suction side of the cascade measured using laser Doppler velocimetry.

The experiments of Zierke and Deutsch on a compressor cascade are conducted to predict the transitional separation bubbles in the compressor which prove to be a key aspect in computing the much complex flow field in a compressor cascade. This experiment forms a good case as it provides physical insight into the very complex flows in a compressor.

3.1.4 Large Scale Turbine Cascade Experiments of Ubaldi et al. (1996)

Wakes from turbine blades are unsteady in character, because of the formation of large organized vertical structures, known as Von Karman vortex sheet. This phenomenon is well known in cylinders, especially at moderate Reynolds numbers. Vortex shedding is a cause of energy losses, periodic mechanical loading, vibrations and noise (Ubaldi et al., 1996). The current experiment is a technique on large scale cascades of a turbine blade profile designed at VKI. The details of the VKI blade are summarized in table 3.4. The VKI cascade details are shown in figure 3.4. The blade boundary layer development was noted on the suction and pressure sides of the central blade of a three-blade large scale turbine linear cascade. The blade profile, designed at VKI, is representative of a high efficiency gas turbine nozzle blade. During the experiment, the cascade was operating at an isentropic downstream Mach number of 0.24 and the Reynolds number based on the outlet flow conditions and chord length was 1.6×10^6 . Experimental data include normalized friction velocity on the suction side of the blade measured using fiber optic laser Doppler velocimeter.

3.1.5 Unsteady Wake/blade Interaction Experiments of Stieger et al. (2003)

An experimental investigation of the effects of unsteady wake/blade interaction on transition and separation in low pressure turbines is performed by Stieger et al. (2003). These experiments were conducted in order to investigate the effects of periodically passing wakes on laminar to turbulent transition and separation in low pressure turbines. The test section was designed to simulate unsteady wakes in turbine engines in order to study their effects on boundary layers and separated flow regions on blade suction surface. The test section involved a T106 turbine blade cascade subjected to wake passing from a moving bar wake generator. The flow conditions

correspond to $Re_x=91,077$ based on chord and inlet velocity and $FSTI = 0.1\%$. Table 3.5 shows the details of T106 cascade. Figure 3.5 shows the experimental setup of the bar passing cascade with T106 profile and figure 3.6 shows the cascade arrangement for the experiment. The experimental data include velocity profiles of the wake at different locations, pressure coefficient distribution, turbulent kinetic energy contours, and phase averaged and mean velocity distributions along the suction side of the blade measured together with hot wire boundary layer traverses and PIV.

Unsteady wake/blade interaction experiments of Stieger et al. (2003) on T106 cascade are used to investigate the effect of periodically passing wakes on laminar turbulent transition and separation in low pressure turbines.

3.2 Computational Tools

The computational tools used for testing and validation of transition models consists of a boundary layer code which solves the boundary layer equations and a single zone Navier Stokes solver and a multi zone Navier Stokes solver. All the codes use finite volume approach to solve the flow field equations, turbulence model equations, and the transition model equations. Boundary layer code is used for initial testing and validation of transition models and also for the development of new correlations, grid dependence, and parametric studies. During the validation process of the transition model, boundary layer code is used in the initial stages as it takes comparatively less time computationally to obtain a solution compared to the Navier Stokes solvers. The single zone Navier Stokes solver is used to validate the transition model for T3 flat plate test cases to check the hysteresis effects. Multi zone Navier Stokes solver is used for the validation of the transition model for compressor and turbine cascade experiments and also for unsteady wake/blade interaction experiments. Multi zone Navier Stokes solver “GHOST” uses MPI to allow different computational zones to be executed on different processors at the same time reducing the computational time. All the codes are developed at University of Kentucky by Dr. P. G. Huang. The details of the codes are given in the following sections.

3.2.1 Boundary Layer Code

The boundary layer code solves the mean flow equations using second order finite volume method. The boundary layer code has SST, $\kappa - \varepsilon$ and $\kappa - \omega$ turbulence models implemented in it. Boundary layer code solves the turbulence model and the transport equations for intermittency and transition onset using second order finite volume method. The code is used for validation of the new transition model for T3 flat plate test cases. Boundary layer code is used during the first stages of testing as it is computationally efficient and takes less time to obtain a solution compared to Navier Stokes solver. Boundary layer code is used for grid dependency check and parametric study of the transition model. Also the boundary layer code is used for development of various correlations for transition onset and transition length and also for the development of new transition model.

3.2.2 Single Zone Navier Stokes Solver

The single zone Navier Stokes solver calculates the flow field equations, turbulence model and the transport equations for intermittency and transition onset using second order finite volume method. The code has SST, $\kappa - \varepsilon$ and $\kappa - \omega$ turbulence models implemented in it. The code is used in the second stage of the validation process described in the next section to check the model for hysteresis effects for zero pressure gradient T3 cases. Single zone Navier Stokes code is used to test and validate the transition model for simple flat plate cases, investigating the predicting capability of the model under the effects of Reynolds number, free stream turbulence and pressure gradient.

3.2.3 Navier Stokes Solver “GHOST”

GHOST is a multi-zone Navier Stokes solver developed at University of Kentucky by Dr. P. G. Huang. This code is based on a finite volume formulation with chimera overset grids. GHOST code is implemented with Menter’s SST two-equation model, which has been found to provide good predictive capability for flows with separation. QUICK and TVD schemes are applied to discretize the convective terms in the momentum, turbulence and transition model equations. Central difference scheme is used for the diffusive terms and the second order upwind time discretization is employed for the temporal terms. GHOST code employs MPI parallelization to

allow different computational zones to be executed on different processors thus decreasing the effective computation time. GHOST code has been tested extensively and is currently being used for a variety of CFD studies. GHOST code is used to validate the transition model for turbine and compressor cascade cases.

3.3 Method of Validation

A systematic approach of testing and validating transition models is developed using the wide range of test cases and the available testing tools. The validation approach is given below in the form of an algorithm.

Algorithm for testing and validation of transition models

Step 1 : The transition model is implemented in the boundary layer code and tested for T3 flat plate test cases of Savill (1993a,1993b). The boundary layer code is used at this level as it is computationally efficient and takes less time to obtain the solution. Also T3 flat plate cases are so chosen because they are the simplest of all the cases used to investigate the effect of Reynolds number, free stream turbulence intensity, and pressure gradient on flow transition. T3 flat plate experiments employed consist of three zero pressure gradient cases of varying free stream turbulence intensities and two variable pressure gradient cases for different turbulence intensities. T3 flat plate experiments are used for initial testing and validation of the transition model.

Step 2 : The transition model is then implemented in the single zone Navier Stokes solver and tested for T3 flat plate test cases. The solution obtained from Navier Stokes solver is checked against the solution obtained from boundary layer code for hysteresis effects. If the solutions obtained from step one and step two are different then the source of discrepancy is found and changes are made in the transition model and step one is repeated. The same procedure is repeated until solutions obtained from step one and two are the same. If the solutions obtained from both the codes are similar then step three is performed. At this step, the results obtained from step one are tested for hysteresis effects and verified.

Step 3 : The transition model is implemented in the multi block Navier Stokes solver “GHOST” and tested for turbine and compressor cascade experiments. This step consists of three substeps which were performed using a systematic approach. If any discrepancy from the results is found for the below steps, then the source of discrepancy is found and changes are made in the transition model and all the steps starting from step one are repeated until a satisfactory result is obtained.

Step 3.1 : The transition model is first tested for Pak-B cascade experiments of Huang et al. (2003). These experiments are used to investigate the predicting capability of the transition model under the effects of flow separation, Reynolds number variations, and freestream turbulence intensity. Using this case the transition model is tested for a wide range of free stream turbulence intensities and Reynolds numbers. The predicting capability of the transition model is investigated for three different turbulence intensities and for three different Reynolds numbers.

Step 3.2 : The transition model is then tested for PSU compressor cascade experiments of Zierke and Deutsch (1989) and Genoa large scale turbine cascade experiments of Ubaldi et al. (1996). Using these cases the predicting capability of the transition model is investigated under the effects of free stream turbulence intensity, Reynolds number, pressure gradient, and flow separation.

Step 3.3 : The transition model is finally tested for effects of unsteadiness using the unsteady wake/blade interaction experiments of Stieger et al. (2003). This experiment investigates the capability of the transition model under the effects of free stream turbulence, Reynolds number, pressure gradient, flow separation, and unsteady wake/blade interaction.

Conclusion : Using all the above stages of the algorithm the predicting capabilities of the transition model is extensively tested under the effects of various important parameters such as free stream turbulence intensity, Reynolds number, pressure gradient, flow separation, and unsteadiness.

Table 3.1 : List of Test Cases

Test Cases	Effects Investigated
T3 Flat plate cases of Savill (1993a, 1993b)	Re, FSTI, dp/ds
Pak-B cascade experiments of Huang et al. (2003)	Re, FSTI, dp/ds, separation
PSU compressor cascade experiments of Zierke and Deutsch (1989)	Re, FSTI, dp/ds, separation
Genoa large scale turbine cascade experiments of Ubaldi et al. (1996)	Re, FSTI, dp/ds, separation
Unsteady wake/blade interaction experiments of Stieger et al. (2003)	Re, FSTI, dp/ds, separation, unsteadiness

Table 3.2 : Details of T3 Flat Plate Experiments of Savill (1993a, 1993b)

Test Case	Inlet Velocity(m/s)	Turbulence Intensity(%)	Pressure Gradient
T3A	5.4	0.035	zero
T3B	9.4	0.065	zero
T3A-	19.8	0.00874	zero
T3C1	6.3	0.0911	variable
T3C2	5.3	0.0287	variable

Table 3.3 : Details of Experiments of Huang et al. (2003)

Reynolds Number ($Re = \rho u_{in} c_x / \mu$)	Turbulence Intensity(%)
50000	0.08
75000	0.08
100000	0.08
50000	2.35
75000	2.35
100000	2.35
50000	6.0
75000	6.0
100000	6.0

Table 3.4 : Cascade Geometry for Genoa Cascade Experiments of Ubaldi et al. (1996)

Chord Length	$C = 300$ mm
Pitch to chord ratio	$g/c = 0.7$
Aspect ratio	$h/c = 1.0$
Inlet blade angle	$\beta_1 = 0$ deg
Number of blades	$N = 3$

Table 3.5 : Details of T106 Cascade for Experiments of Stieger et al. (2003)

Chord	198mm
Blade stagger	59.3°
Cascade pitch	158mm
Inlet flow angle	37.7°
Design exit flow angle	63.2°
Bar diameter	2.05mm
Axial Distance: bars to LE	70mm
Flow Coefficient(U_{axial}/U_{bar})	0.83

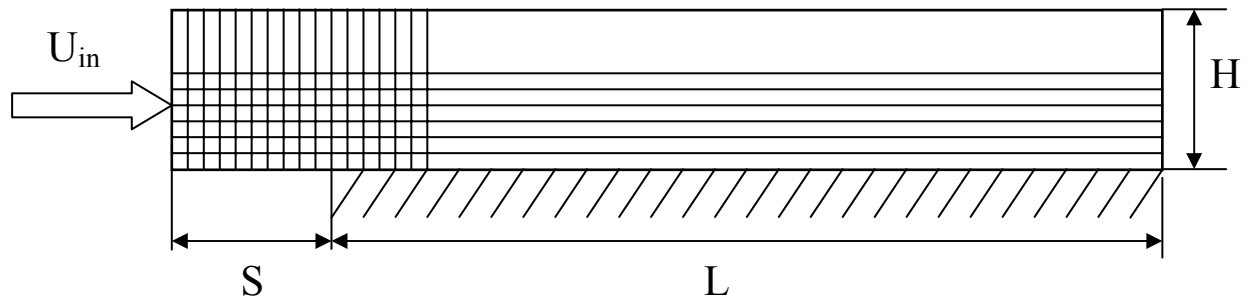


Figure 3.1 : Schematic Diagram of Computational Grid for Flat Plate Experiments of Savill (1993a, 1993b)

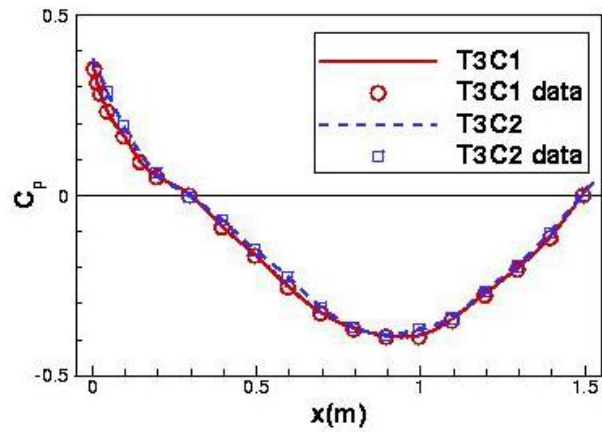


Figure 3.2 : Pressure Coefficient Profile for Variable Pressure Gradient Flat Plate Experiments of Savill (1993a, 1993b)

Chord length, L
 Axial chord length, L_x
 Axial chord to chord ratio, $L_x/L = 0.906$
 Pitch to chord ratio, $P/L = 0.8$
 Blade inlet angle, $\beta_1 = 35^\circ$
 Blade outlet angle, $\beta_2 = -60^\circ$

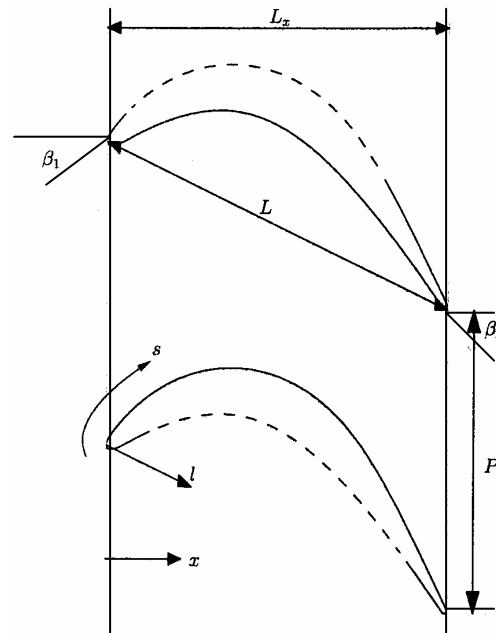


Figure 3.3 : Details of P&W PAK-B Blade Cascade (Huang et al., 2003)

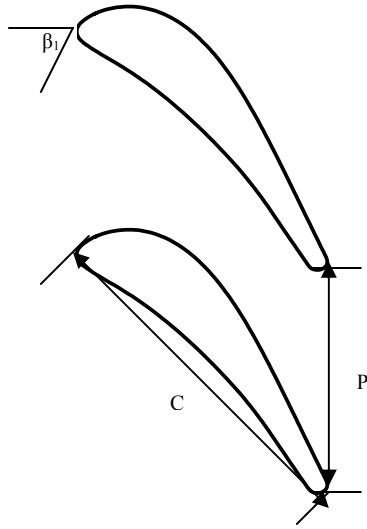


Figure 3.4 : Details of Genoa Blade Cascade (Ubaldi et al., 1996)

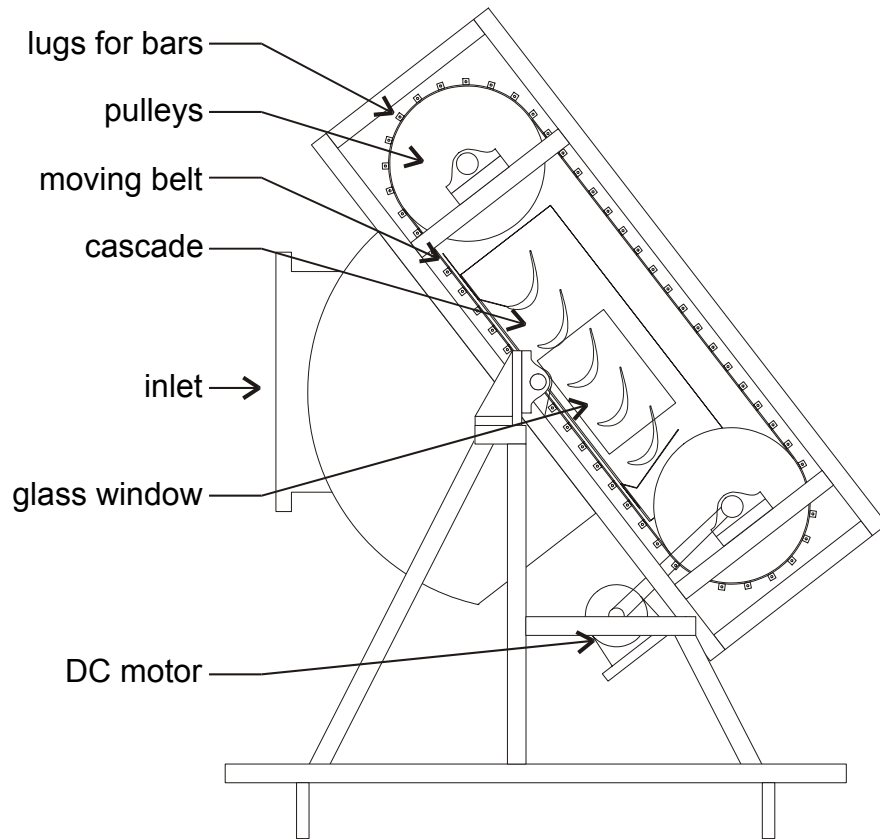


Figure 3.5 : Bar Passing Cascade With T106 Profile (Stieger et al., 2003)

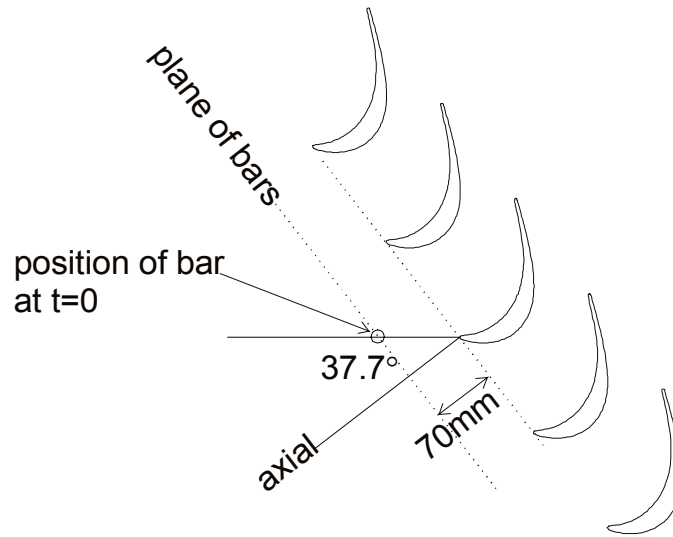


Figure 3.6 : T106 Cascade Arrangement for Unsteady Transition due to Wake Impingement
(Stieger et al., 2003)

Chapter Four

Results and Discussion

The new transition model developed by Menter et al. (2004) is tested and validated using the algorithm outlined in the previous chapter. The transition model consists of two transport equations, one for intermittency and one for transition onset. To predict good results for low free stream turbulence intensity and low Reynolds number flows, a separated flow modification is made to the model. Details of the model formulation is given in appendix A2. The model is validated for simple flat plate experiments, compressor and turbine cascade experiments and unsteady wake/blade interaction experiments. The transition model is validated using the boundary layer code, single zone Navier Stokes code, and multi zone Navier Stokes code. The transition model is first tested using simple flat plate experiments, then tested using compressor and turbine cascade experiments and finally using unsteady wake/blade interaction experiments as per the validation algorithm given in previous chapter. The results obtained for all the test cases are described in the following sections.

4.1 T3 Flat Plate Experiments of Savill (1993a, 1993b)

The new transition model is first tested for the simple flat plate experiments as mentioned in step one of the validation algorithm. T3 flat plate test experiments assembled by Savill (1993a, 1993b) investigate the predicting capability of the transition model under the effect of free stream turbulence intensity, Reynolds number and pressure gradient. Cases T3A, T3B, and T3A- are zero pressure gradient cases and T3C1 and T3C2 are cases with continuous change in pressure gradient representing an aft-loaded turbine blade. The length before the flat plate at which free stream conditions are mentioned is called the starting length. The starting length for all the cases is 0.05m. The height of the grid is 0.08m. The schematic diagram of the computational grid used for flat plate cases is shown in figure 3.1 in the previous chapter. The length of the grid and inflow conditions for all the T3 cases is given in Table 4.1. In the computations, 100 grid points, expanding from wall to the freestream, were used in the cross stream direction for all the T3 cases. The y^+ values for the first point away from the wall is 0.1 for all the cases. The solutions were obtained by using 2000 streamwise points for T3A test

case. For T3B, T3A-, T3C1, and T3C2 test cases 1000 streamwise points are used. These step sizes and cross stream grid points were found satisfactory by performing a careful grid-independency check, in which the step sizes and grid spacing were both decreased by half and no effect on the solutions was found. Inlet turbulent kinetic energy is fixed according to the freestream turbulence levels and the energy dissipation rate is adjusted according to the decay of the freestream turbulence. The Reynolds number (Re_x) for all the T3 test cases is based on the freestream velocity at the flat plate leading edge.

T3A experiment of Savill corresponds to a zero-pressure-gradient flow over a flat plate at $Re = 6.48 \times 10^5$ per meter. The inlet free stream turbulence intensity is 3.5%. The decay of freestream turbulence intensity is matched with experimental data by specifying $\mu_t / \mu = 13.3$ at the inlet and is shown in figure 4.1.

The computed skin-friction coefficient distribution is compared to the experimental data in figure 4.2. The new transition model predicted the length of the transition well. The onset of transition is slightly delayed in the computations when compared to the experiments. The comparison of the Reynolds number based on momentum thickness, Re_θ , is shown in figure 4.3. The Reynolds number based on momentum thickness obtained from the computation is under predicted compared to the experimental values as seen in figure 4.3. Also the predicted shape factor variations were compared with the experimental data in figure 4.4. We can observe premature decline of the shape factor in the computations when compared to the experiments.

T3B experiment of Savill corresponds to a zero-pressure-gradient flow over a flat plate at $Re = 12.53 \times 10^5$ per meter. The inlet free stream turbulence intensity is 6.5%. The decay of freestream turbulence intensity is matched with experimental data by specifying $\mu_t / \mu = 100.0$ at the inlet as shown in figure 4.5.

The computed skin-friction coefficient distribution is compared to the experimental data as shown in figure 4.6. The skin friction plot shows that the new model predicted slightly early transition to turbulent flow when compared to the experiment. The comparison of the Reynolds number based on momentum thickness, Re_θ , and shape factor variation are shown in figures 4.7

and 4.8 respectively. We can observe that the shape factor is under predicted in the computations when compared to experiments from figure 4.8.

T3A- experiment of Savill corresponds to a zero-pressure-gradient flow over a flat plate at $Re = 26.4 * 10^5$ per meter. The inlet free stream turbulence intensity is 0.874%. The decay of freestream turbulence intensity is matched with experimental data by specifying $\mu_t / \mu = 8.72$ at the inlet as shown in figure 4.9.

The computed skin-friction coefficient distribution is compared to the experimental data and shown in figure 4.10. The onset of transition from the computations is much earlier compared to the experimental value as seen in figure 4.10. The comparison of the Reynolds number based on momentum thickness, Re_θ , and shape factor variation are shown in figures 4.11 and 4.12 respectively. Shape factor variation from the computational results does not match well with the experimental data.

The next cases are the T3C1 and T3C2 experiments of Savill (1993a, 1993b). These cases are variable pressure gradient flows representing actual turbine characteristics. Both cases have similar pressure variations, but with different Reynolds numbers and free stream turbulence intensities.

T3C1 case has an inlet Reynolds number of $6.72 * 10^5$ per meter. The inlet free stream turbulence intensity is 9.11%. The decay of freestream turbulence intensity is matched with experimental data by specifying $\mu_t / \mu = 48.702$ at the inlet and is shown in figure 4.13.

The computed skin-friction coefficient distribution is compared to the experimental data in figure 4.14. The length of the transition mode predicted according to the computations is short compared to the experiments. The flow transitions to turbulent flow earlier in the computations when compared to the experiments. The comparison of the Reynolds number based on momentum thickness, Re_θ , is shown in figure 4.15 along with the shape factor variation in figure 4.16. The calculated value of Reynolds number based on momentum thickness, Re_θ , agrees well

with the experiment as seen from figure 4.15. However the shape factor is under predicted according to the computations when compared to the experiment as seen in figure 4.16.

T3C2 case has an inlet Reynolds number of 5.65×10^5 per meter. The inlet free stream turbulence intensity is 2.87%. The decay of freestream turbulence intensity is matched with experimental data by specifying $\mu_t / \mu = 8.9335$ at the inlet, as shown in figure 4.17.

The computed skin-friction coefficient distribution is compared to the experimental data and is shown in figure 4.18. The onset of transition is delayed according to the computations when compared to the experiments. The length of transition is small from the computation compared to the experiment. The comparison of Reynolds number based on momentum thickness, Re_θ , with the experimental data and the shape factor variations are shown in figures 4.19 and 4.20 respectively. From figure 4.19, we can observe that the Reynolds number based on momentum thickness is under predicted according to the computations when compared to the experiments. The shape factor variation does not match well with the experimental data.

4.1.1 Grid Dependence Study

In order to study the effect of grid dependence on flow transition a comprehensive study of the effect of grid density on the skin friction variation is made for zero pressure gradient T3 test cases. The dimensions of the computational grid for T3A case is 3.3m*0.08m. First T3A case is computed using 1000 points in the streamwise direction and 100 points in the cross stream direction as shown in figure 4.21. Then the points in the streamwise direction are doubled to 2000. We can observe from the figure that the solution obtained using 2000*100 points is the grid independent solution. To further study the effect of grid dependence the number of points both in the streamwise and cross stream direction were doubled to 4000*200. We can observe that the solution obtained using 4000*200 points is same as the solution obtained using 2000*100 points. Finally the points in both streamwise and cross stream direction are increased to 8000*400 points and it is observed that increasing the points does not affect the solution. T3A case is then computed using Navier Stokes code which is the second step in the validation algorithm. The size of the computational domain for T3A case using Navier Stokes code is 3.3m*0.08m with 400 and 200 points in the streamwise and cross stream direction respectively.

The solution obtained from the Navier Stokes solver is same as the solution obtained using 2000*100 points for boundary layer code. Then the effect of grid dependence is studied for T3B and T3A- cases. The dimensions of the computational grid for T3B and T3A- cases are 2.0m*0.08m. The skin friction variation for T3B and T3A- cases are shown in figures 4.22 and 4.23 respectively. First the boundary layer code is run using 1000 points in the streamwise direction and 100 points in the cross stream direction. Then the points in the streamwise direction are increased to 2000. The solution obtained using 1000*100 points is the grid independent solution. Finally the grid points are increased to 4000*200 and 8000*400 for both T3B and T3A- case and no effect on the skin friction variation is observed. Then T3B and T3A- cases are computed using Navier Stokes code. The size of the computational domain for T3B and T3A- cases using Navier Stokes code is 2.0m*0.08m with 400 and 200 points in the streamwise and cross stream direction respectively. The solution obtained using the Navier Stokes code is same as the solution obtained using 1000*100 points for the boundary layer code.

The grid independent solutions for all the zero pressure gradient T3 test cases are established and the effect of grid density on the solution is studied. Also the transition model is tested for hysteresis effects for the flat plate experiments using the single Navier Stokes code which is the second stage of the validation algorithm.

4.1.2 Study on Effect of y^+

In order to investigate the effect of first grid point spacing on the predicting capability of the transition model, a study on the skin friction variation is made for flat plate T3A experiment. The skin friction variation for T3A experiment for different values of y^+ is shown in figure 4.24. First the solution is computed using a y^+ value of 1.0. Then the y^+ value is decreased to 0.5. The skin friction prediction does not change as the y^+ value is decreased from 1.0 to 0.5. Next computations are performed using y^+ values of 0.1, 0.01, and 0.001. Decreasing the y^+ all the way down from 0.5 to 0.001 does not affect the solution. Finally, the y^+ value is decreased to a value of 0.0001. Decreasing the y^+ value to such a low value affects the solution and it can be observed from the figure that the onset of transition is delayed. This might be due to the adverse effect of the SST blending function. From the figure it can be said that choosing a value from 1.0

to 0.001 for y^+ does not affect the solution for flat plate test cases. However a value of around 1.0 is suggested based on the results for all the test cases.

The new transition model predicted satisfactory results for all T3 cases. The computations were performed using boundary layer code. Then the transition model is tested for hysteresis using single zone Navier Stokes code. The results obtained from the single zone Navier Stokes code are similar to the results obtained from boundary layer code. Having completed both the steps of the validation algorithm successfully, the model is then tested for Pak-B cascade experiments of Huang et al. (2003) which is the next step of the validation algorithm.

4.2 Pak-B Low-Pressure Turbine Blade Experiments of Huang et al. (2003)

Next step in the testing and validation process is testing the transition model for Pak-B low-pressure turbine blade experiments of Huang et al. (2003). Huang et al. (2003) conducted experiments on PAK-B blade cascade for a range of Reynolds numbers and turbulence intensities. The Reynolds numbers range from 50,000 to 100,000 based on inlet velocity and axial chord, coupled with FSTI's of 0.08%, 2.35%, and 6.0% as listed in Table 4.2.

The computations for FSTI=0.08% case were performed using the grid shown in figure 4.25. The multiblock grid has five zones. The four zones on which the blade grid is superposed each have 125*225 grid points and the O-type grid around the blade has 401*101 points with first y^+ less than 0.5. Further refinement of the grid has negligible effect on the solution.

The computations for high FSTI cases are computed using the six zone multiblock grid system shown in figure 4.26. The background zones each have 125*225 grid points and the O-type grid around the blade has 401*101 points. The computational domain is extended upstream of the blade in order to specify the correct turbulence intensity at the inlet and to match the decay of turbulence that reaches the blade.

First the cases with no grid in the tunnel corresponding to FSTI=0.08% are computed. The comparisons of computed and the experimental pressure coefficient distribution along with the velocity profiles for Re=100,000, 75,000, and 50,000 are shown in figures 4.27 through 4.32.

Velocity profiles are computed at seven axial stations on the suction side of the blade and the computed results are compared with the experimental data.

For $Re=100,000$ the computed pressure coefficient distribution is compared with the experimental data as shown in figure 4.27. The experimental data is shown by solid dots, the fully turbulent solution is given by dotted line and the result from the transition model is given by solid line. The pressure coefficient distribution shown is along the suction and pressure side of the Pak-B cascade. The pressure plateau apparent in the figure on the suction side of the blade characterizes the separation bubble. We can observe a small separation bubble on the second half of the suction side of the blade. From the pressure coefficient distribution we can observe that the flow separates around $x/C_x = 0.725$ and reattachment takes place around $x/C_x = 0.85$. The velocity profile is shown in figure 4.28. The velocity profiles compare well with the experimental data as shown in figure 4.28. At the first three stations, the flow is laminar and attached. The flow separation takes place at $x/C_x = 0.725$ according to both computations and experiments. Reattachment of the flow takes place around $x/C_x = 0.85$ according to the computation and experiment.

When the Reynolds number is reduced to 75,000, the size of the separation bubble increases as seen from the plateau on the suction side of the Pak-B blade as shown in figure 4.29. The velocity profile is shown in figure 4.30. The flow separates around $x/C_x = 0.725$ and the flow reattaches around 0.85 according to the computation, whereas the flow reattaches around 0.875 according to the experiment.

Finally, the computations are performed for a Reynolds number of 50,000. The size of the separation bubble is much larger as seen from the plateau on the suction side of the blade in figure 4.31. The velocity profile is shown in figure 4.32. The flow separates around $x/C_x = 0.725$ and the flow reattaches earlier compared to the experiments at $x/C_x = 0.90$ and seen in figure 4.32. According to the computation the flow reattaches earlier compared to the experiment. Figures 4.33 shows the effective intermittency contours and the streamlines for a freestream turbulence intensity of 0.08% and Reynolds number of 50000. The figure on the left shows the intermittency contours on a Pak-B cascade and the figure on the right shows the zoomed portion

of the cascade near the trailing edge. From the streamlines in the right figure we can observe the flow separation and reattachment clearly. Figure 4.34 shows the turbulent kinetic energy contours along with the streamlines for a freestream turbulence intensity of 0.08% and Reynolds number of 50000. The figure on the left shows the turbulent kinetic energy contours along the Pak-B cascade and the figure on the right shows the zoomed portion near the trailing edge on the suction side of the blade. From the figure on the right the separation bubble can be observed.

Next the high FSTI cases are computed and a comparison of computed and experimental pressure coefficient distributions along with the velocity profiles is made for $Re = 50,000$, $75,000$, and $100,000$ for freestream turbulence intensity of 6.0%.

For $Re=100,000$ case, the computed velocity profiles compare well with the experiment as shown in figure 4.36. The flow is laminar and attached at the first three measurement stations. The flow starts to separate at $x/C_x = 0.74$ and the flow reattached around $x/C_x = 0.85$. We can observe a small separation bubble from the plateau in figure 4.35. The size of the separation bubble is in good agreement with the experiment as seen from figure 4.35.

For $Re=75,000$ case, the pressure coefficient distribution is shown in figure 4.37. We observe a separation bubble from the plateau on the suction side of the blade and also the reattachment can be observed from the figure. The velocity profile is shown in figure 4.38. The flow is attached at the first three measurement stations as shown in figure 4.38. The flow starts to separate around $x/C_x = 0.74$ and the flow reattaches around $x/C_x = 0.85$ according to the computation, whereas the flow reattaches around $x/C_x = 0.87$ according to the experiment.

For $Re=50,000$ case, the pressure coefficient distribution is shown in figure 4.39. We can observe a larger separation bubble in this case and the size of the separation bubble from the computation is small compared to the experiment. The velocity profile is shown in figure 4.40. The flow starts to separate around $x/C_x = 0.725$ and the flow reattaches much earlier than the experiment around $x/C_x = 0.85$ compared to $x/C_x = 0.89$ according to the experiment.

Finally computations are performed for Reynolds number of 100,000, 75,000 and 50,000 for a freestream turbulence intensity of 2.35%. The computed and experimental pressure coefficient distributions for FSTI = 2.35% for $Re = 100,000$, 75,000, and 50,000 are shown in figures 4.41, 4.42 and 4.43 respectively. The computed pressure coefficient distributions are in well agreement with the experiments.

The pressure coefficient distribution for all nine experiments on Pak-B cascade is shown in figure 4.44. The Reynolds number increases from 50,000 to 75,000 and finally to 100,000 from left to right. The freestream turbulence intensity increases from 0.08% to 2.35% and finally to 6.0% from bottom to top. Each plot shows the experimental results, fully turbulent solution and the results from transition model. We can observe separation from the plateau on the suction side of the blade in all the nine cases. From the figure, we can observe that as the FSTI increases from bottom to top, the size of the separation bubble decreases. Also as the Reynolds number increases from left to right, the size of the separation bubble decreases. The figures on the top right hand side have small separation bubble from both the computations and experiments. The size of the separation bubble predicted is in well agreement with the experiments. The figures on the bottom left hand side have large separation bubble according to both the computations and experiments. The size of the separation bubble is small from the computations compared with the experiments. As the transition model does not predict the size of the separation bubble correctly and also the reattachment length is not in well agreement with the experiments for low freestream turbulence and low Reynolds number cases, a parametric study on the separation modification is made to improve the results for low freestream turbulence and low Reynolds number cases.

4.2.1 Parametric Study for Low Freestream Turbulence and Low Reynolds Number Case

In order to study the effect of separated flow modification for low freestream turbulence and low Reynolds number cases, a parametric study on the separated flow modification is made. The computations were performed for a freestream turbulence of 0.08% and for a Reynolds number of 50000. The modification for separation-induced transition is shown in appendix A2. Using this modification the intermittency obtained from the transport equation is modified to obtain

effective intermittency. First the separated flow modification is switched off and the computation is performed. Figure 4.45 shows the pressure coefficient distribution along the suction and pressure side of the Pak-B cascade from the experiment, fully turbulent solution, transition model without separated flow modification and also from transition model for various values of s_1 . The size of the separation bubble is controlled by the constant s_1 . The solution obtained by switching off the separation modification is considered as baseline solution. A large separation bubble is observed for the baseline solution.

Next the value of s_1 in the separation modification term is changed. The original value for the new transition model is 8.0. When the value of s_1 is decreased to 0.1 and 0.001, the separation bubble size increases and the solution is similar to the baseline solution. Then the s_1 value is increased to 5.0. Increasing the value of s_1 to 5.0 the solution obtained is similar to the solution obtained from the original transition model which has a value of 8.0 for s_1 . Further increasing the value of s_1 to 10, 15, 50, 150, and finally 500 does not seem to affect the solution. The solution obtained using these values is similar to the original solution. We observed the size of the separation bubble increases as the value of s_1 is decreased to 0.1 and 0.001. This is due to the presence of the limiting factor in the calculation of the effective intermittency. The results show that it is not possible to match the experimental data only by changing s_1 (i.e. transition length). We observe that the transition length can be changed by varying the value of s_1 . However we can match the experimental data only if we predicted the onset of transition accurately. The onset of transition correlation we are using is predicting transition onset earlier. Once the transition onset is offset it is not possible to match the experimental data changing alone the transition length. There are a number of correlations for separated flows in literature. Two such correlations are the correlation developed by Davis et al. (1987) and the correlation developed by Suzen et al. (2001). In order to predict the onset of transition correctly, the present correlation used in the transition model has to be improved or replaced by one of the above correlation. Once the onset of transition is predicted accurately, then we can vary the value of s_1 such that the reattachment length matches the experimental data. However the effect of other parameters on the solution is studied and described below.

Table 4.3 gives the details of the modifications for all the computations made here after for the parametric study for low freestream turbulence and low Reynolds number cases. Runs 1 through 7 are made for different values of the constants in the term $F_{reattach}$. The formulation of the term $F_{reattach}$ can be seen from appendix A2. The constants used for the runs 1 through 7 are detailed in the table 4.3. Table 4.3 clearly shows the modification made for each run along with the original term. From figure 4.46, it can be observed clearly that the separation bubble size and the reattachment length cannot be changed changing the constants in $F_{reattach}$ term.

Next the value of the limiter in the calculation of the effective intermittency is changed. The original value of the limiter as seen from appendix A2 is 5. Runs 8 through 12 are computed for different values of the limiter and the values of the limiter are given in table 4.3. Decreasing the value of the limiter to 1.0 (run 9) and to 0.1 (run 8), a large separation bubble is observed and the solution is similar to the solution obtained without separation modification (baseline solution). When the value of the limiter is increased to 1.5 (run 10) the size of the separation bubble decreases. However the size of the separation bubble is large compared to the original solution. When the value of the limiter is increased to 3 (run 11) and to 10 (run 12) the solution obtained is similar to the original transition model solution. From the above study a value of 5.0 which is used for the limiter is highly recommended.

Finally, the effect of changing the blending function on the predicting capability of the transition model is studied. Figure 4.48 shows pressure coefficient distribution for the experiment, fully turbulent solution, original transition model, and the transition model for different values of the factor to the blending function. The values of the factor used for the computations are tabulated in table 4.3. Decreasing the blending function by a factor of 10 i.e. for a value of 0.1 (run 13), the separation bubble size increases and we observe a large separation bubble. Next the blending function is increased by a factor of 5.0 (run 14) and 10.0 (run 15). Multiplying the blending function by 5.0 and 10.0 does not affect the solution. The size of the separation bubble is same from run 14 and run 15 and are similar to the original transition model solution.

Based on the above parametric study it can be observed that the constants chosen in the final model formulation are the best values. Changing the constants increase the separation bubble

size. Also changing the transition length (s_1) only, the reattachment length does not match the experiment. The transition onset has to be predicted accurately for the reattachment length and separation bubble size to match the experimental data. Thus the correlation developed by Davis et al. (1987) or the correlation developed by Suzen et al. (2001) for separated flows has to be incorporated to predict the onset of transition accurately. Once the onset of transition is predicted correctly the reattachment length and the separation bubble size can be matched well with the experimental results.

4.3 Highly Loaded Compressor Cascade Experiments of Zierke and Deutsch (1989)

Then the next step in the validation algorithm is performed. In this step the transition model is tested using the compressor and turbine cascade experiments. First the transition model predictability is investigated using the experiments of Zierke and Deutsch (1989). Comparisons of viscous computations are most needed under flow conditions typical of modern compressor blades, especially under off-design conditions. Therefore, measurements of boundary layers and near wakes have been acquired on a highly loaded compressor cascade blade at two incidence angles near a chord Reynolds number of 500,000. Computational grid used for this case is shown in figure 4.49. Computational grid consists of 9 zones.

A comparison of computed pressure coefficient distribution against experiments are shown in figures 4.50 and 4.51 for two different incidence angles -1.5° and 5.0° respectively. Table 4.2 gives the inflow conditions for the computations. On the suction side transition occurs at the leading edge due to a small leading edge separation bubble. A separation bubble on the suction side trailing edge can be observed from figure 4.51. On the pressure side, transition occurs at mid chord and the prediction agrees well with the experimental data. Contours of intermittency, turbulent kinetic energy and eddy viscosity are shown in figures 4.52, 4.53, and 4.54 respectively. There is a discrepancy on the suction side trailing edge for -1.5° case, both in the experiments and in the computations. This might be due to the error in the incidence angle. As the Reynolds number is very high, there is not much difference between the solution obtained using transition model and fully turbulent solution.

4.4 Large Scale Turbine Cascade Experiments of Ubaldi et al. (1996)

Next the transition model is investigated using the large scale turbine cascade experiments of Ubaldi et al. (1996). Wakes from turbine blades are unsteady in character, because of the formation of large organized vertical structures, known as Von Karman vortex sheet. This phenomenon is well known in cylinders, especially at moderate Reynolds numbers. The current experiment is a technique on large scale cascades of a turbine blade profile designed at VKI. The grid used for the computations is shown in figure 4.55. The computational grid consists of six zones with blade grid overlapped on five background zones.

The Reynolds number based on the outlet flow conditions and chord length is 1.6×10^6 and table 4.2 gives the inflow conditions. The normalized friction velocity is computed on the suction side of the blade and is compared with the experimental data as shown in figure 4.56. From the figure we can observe that according to the computation, the onset of transition is predicted earlier compared to the experiment. Also the transition length is shorter from the computation when compared to the experiment. Having tested the transition model using the compressor and turbine cascade experiments for the effects of freestream turbulence intensity, Reynolds number, pressure gradient and separation, the transition model is finally investigated for the effects of unsteady wake/blade interaction.

4.5 Unsteady Wake/blade Interaction Experiments of Stieger et al. (2003)

A computational investigation on the effects of unsteady wake/blade interaction on transition and separation in low pressure turbines has been performed by numerical simulations of recent experiments of Stieger et al. (2003). These experiments were conducted in order to investigate the effects of periodically passing wakes on laminar to turbulent transition and separation in low pressure turbines. The flow conditions correspond to $Re_x = 91,077$ based on chord and inlet velocity and $FSTI = 0.1\%$. The grid used for the computations is shown in figure 4.57 along with the details of the rod grid.

The computed velocity profile of the wake at $x/C = -0.04$ before it enters the blade passage is compared to the experiment as shown in figure 4.58. The figure shows that the computation is in good agreement with the experiment illustrating that the wake from the moving bars is captured accurately. The computed time averaged pressure coefficient distribution for unsteady experiments and computations is shown in figure 4.59. Also shown in figure are the steady state results from the computation and the experiment. In steady state computations separation is predicted further downstream when compared to the experiment as evident from the comparison of the pressure coefficient distributions. We observe that in unsteady computations the separation bubble is completely suppressed according to the experiments whereas a small separation bubble is predicted according to the computation. However the size of the separation bubble is small from the unsteady computations when compared to the steady state computations. Time variation of the skin friction coefficient on the suction side of the blade is shown in figure 4.60. It can be observed that the flow is largely separated near the trailing edge of the blade for most of the time. We observe at a wake passing time (t/T) of 0.5 early transition appears at the 70 percent chord location, which is where the wake is located at that point in time. Also observed is the reverse flow in the turbulent part downstream of the transition location. Similar regions of the reverse flow in the turbulent patch were also observed by Stieger et al. (2003) in the experiment using a particle image velocimetry method. The computed and experimental pressure coefficient contours are shown in figure 4.61. From the figure it can be observed that the peaks in experiments were well captured in the computations. But we observe some unsteadiness in the computations. Figure 4.62 shows the mean velocity comparisons between the computations and experiment. The mean velocity comparisons are made at 25 different stations on the suction side of the T106 cascade. From the first twenty stations the computational results are in well agreement with the experiment. However for the last five stations, near the trailing edge of the T106 cascade, we observe a discrepancy and a separation bubble is predicted according to the computations. However in experiments no separation bubble is observed. Also comparison of computed and experimental phase averaged velocity distributions at various streamwise stations on the suction surface of the blade is shown in figures 4.63a through 4.63x. It can be observed from the figures that the movement of the wake is captured accurately according to the computations when compared to the experiments. The computed and experimental turbulent kinetic energy contours at various time levels are shown in figures 4.64a through 4.64h. In the figures the computed

results are shown on the right column and the experimental data are shown on the left. From the figure it can be observed that the location of the wake and the width of the wake is captured accurately according to the computations when compared to the experiments. However the magnitude of the turbulent kinetic energy is different from the computations when compared to the experiments.

Using the unsteady wake/blade interaction experiments of Stieger et al. (2003) the transition model is finally tested for the effect of unsteadiness. This experiment investigates the effect of periodically passing wakes on laminar to turbulent transition and separation in low pressure turbines. From the computational results it is observed that the wake is captured accurately compared to the experiments. From the pressure coefficient distribution it can be observed that the unsteadiness suppresses the separation bubble. However from the unsteady time averaged results it can be observed that flow separation is still predicted, whereas experimental results indicate attached flow. Also discrepancies are observed near the trailing edge of the T106 cascade in the mean velocity profile comparisons. From the results it is evident that a small separation bubble is predicted according to the computations. So the separation modification made to the transition model has to be further improved.

Table 4.1 : Inflow Conditions for T3 Flat Plate Experiments of Savill (1993a, 1993b)

Test Case	Inlet Velocity(m/s)	Turbulence Intensity(%)	μ_r/μ	Length of the Plate, L (m)	Starting Length, S (m)	Minimum Grid Size
T3A	5.4	0.035	13.3	3.3	0.05	2000*100
T3B	9.4	0.065	100.0	2.0	0.05	1000*100
T3A-	19.8	0.00874	8.72	2.0	0.05	1000*100
T3C1	6.3	0.0911	48.702	1.6	0.05	1000*100
T3C2	5.3	0.0287	8.9335	1.6	0.05	1000*100

Table 4.2 : Inflow Conditions for Cascade Cases

Test Case	Reynolds Number	Turbulence Intensity (%)	μ_t/μ
Huang FSTI = 0.08%	50000	0.08	10.0
Huang FSTI = 0.08%	75000	0.08	10.0
Huang FSTI = 0.08%	100000	0.08	10.0
Huang FSTI = 2.35%	50000	2.35	6.50
Huang FSTI = 2.35%	75000	2.35	9.75
Huang FSTI = 2.35%	100000	2.35	13.0
Huang FSTI = 6.0%	50000	6.0	15.0
Huang FSTI = 6.0%	75000	6.0	22.5
Huang FSTI = 6.0%	100000	6.0	30.0
Zierke(i=5°)	505000	0.18	10.0
Zierke(i=-1.5°)	501000	0.18	9.0
Genoa	593200	3.0	1.0

Table 4.3 : Modifications for the Parametric Study for Experiments of Huang et al. (2003)

Run	Original Term	Modified Term
Run 1	$F_{reattach} = e^{-\left(\frac{R_f}{15}\right)^4}$	$F_{reattach} = e^{-\left(\frac{R_f}{15}\right)^1}$
Run 2	$F_{reattach} = e^{-\left(\frac{R_f}{15}\right)^4}$	$F_{reattach} = e^{-\left(\frac{R_f}{15}\right)^8}$
Run 3	$F_{reattach} = e^{-\left(\frac{R_f}{15}\right)^4}$	$F_{reattach} = e^{-\left(\frac{R_f}{20}\right)^3}$
Run 4	$F_{reattach} = e^{-\left(\frac{R_f}{15}\right)^4}$	$F_{reattach} = e^{-\left(\frac{R_f}{4}\right)^4}$
Run 5	$F_{reattach} = e^{-\left(\frac{R_f}{15}\right)^4}$	$F_{reattach} = e^{-\left(\frac{R_f}{100}\right)^4}$
Run 6	$F_{reattach} = e^{-\left(\frac{R_f}{15}\right)^4}$	$F_{reattach} = e^{-\left(\frac{R_f}{4}\right)^8}$
Run 7	$F_{reattach} = e^{-\left(\frac{R_f}{15}\right)^4}$	$F_{reattach} = e^{-\left(\frac{R_f}{2}\right)^{20}}$
Run 8	$\gamma_{sep} = \min\left(s_1 \max\left[\left(\frac{Re_v}{2.193 Re_{\theta_c}}\right) - 1, 0\right] F_{reattach}, 5\right) F_{\theta}$	$\gamma_{sep} = \min\left(s_1 \max\left[\left(\frac{Re_v}{2.193 Re_{\theta_c}}\right) - 1, 0\right] F_{reattach}, 0.1\right) F_{\theta}$
Run 9	$\gamma_{sep} = \min\left(s_1 \max\left[\left(\frac{Re_v}{2.193 Re_{\theta_c}}\right) - 1, 0\right] F_{reattach}, 5\right) F_{\theta}$	$\gamma_{sep} = \min\left(s_1 \max\left[\left(\frac{Re_v}{2.193 Re_{\theta_c}}\right) - 1, 0\right] F_{reattach}, 1\right) F_{\theta}$
Run 10	$\gamma_{sep} = \min\left(s_1 \max\left[\left(\frac{Re_v}{2.193 Re_{\theta_c}}\right) - 1, 0\right] F_{reattach}, 5\right) F_{\theta}$	$\gamma_{sep} = \min\left(s_1 \max\left[\left(\frac{Re_v}{2.193 Re_{\theta_c}}\right) - 1, 0\right] F_{reattach}, 1.5\right) F_{\theta}$
Run 11	$\gamma_{sep} = \min\left(s_1 \max\left[\left(\frac{Re_v}{2.193 Re_{\theta_c}}\right) - 1, 0\right] F_{reattach}, 5\right) F_{\theta}$	$\gamma_{sep} = \min\left(s_1 \max\left[\left(\frac{Re_v}{2.193 Re_{\theta_c}}\right) - 1, 0\right] F_{reattach}, 3\right) F_{\theta}$
Run 12	$\gamma_{sep} = \min\left(s_1 \max\left[\left(\frac{Re_v}{2.193 Re_{\theta_c}}\right) - 1, 0\right] F_{reattach}, 5\right) F_{\theta}$	$\gamma_{sep} = \min\left(s_1 \max\left[\left(\frac{Re_v}{2.193 Re_{\theta_c}}\right) - 1, 0\right] F_{reattach}, 10\right) F_{\theta}$

Table 4.3 : continued

Run 13	$\gamma_{sep} = \min\left(s_1 \max\left[\left(\frac{Re_v}{2.193 Re_{\alpha}}\right) - 1, 0\right] F_{reattach}, 5\right) F_{\alpha}$	$\gamma_{sep} = \min\left(s_1 \max\left[\left(\frac{Re_v}{2.193 Re_{\alpha}}\right) - 1, 0\right] F_{reattach}, 5\right) 0.1 F_{\alpha}$
Run 14	$\gamma_{sep} = \min\left(s_1 \max\left[\left(\frac{Re_v}{2.193 Re_{\alpha}}\right) - 1, 0\right] F_{reattach}, 5\right) F_{\alpha}$	$\gamma_{sep} = \min\left(s_1 \max\left[\left(\frac{Re_v}{2.193 Re_{\alpha}}\right) - 1, 0\right] F_{reattach}, 5\right) 5 F_{\alpha}$
Run 15	$\gamma_{sep} = \min\left(s_1 \max\left[\left(\frac{Re_v}{2.193 Re_{\alpha}}\right) - 1, 0\right] F_{reattach}, 5\right) F_{\alpha}$	$\gamma_{sep} = \min\left(s_1 \max\left[\left(\frac{Re_v}{2.193 Re_{\alpha}}\right) - 1, 0\right] F_{reattach}, 5\right) 10 F_{\alpha}$

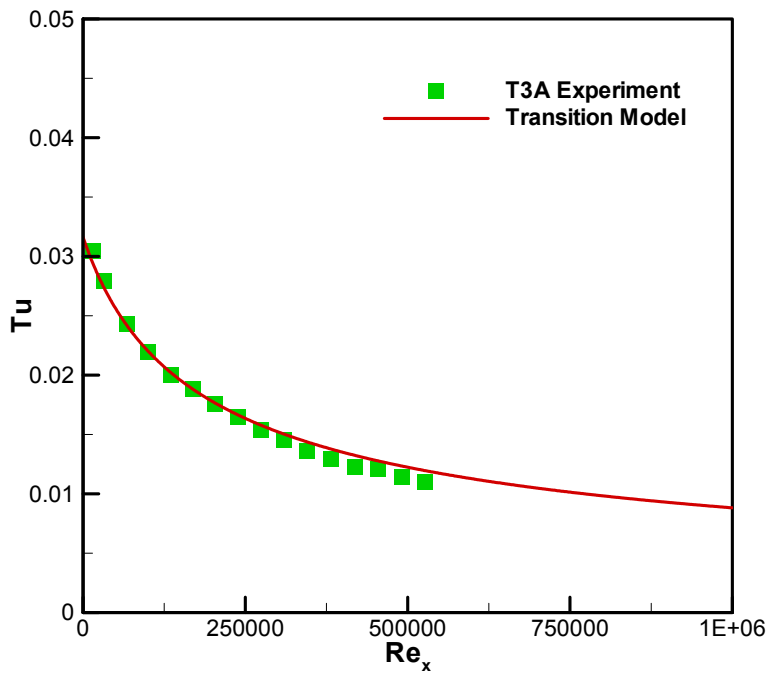


Figure 4.1 : Variation of Freestream Turbulence Intensity Along the Flat Plate for T3A Case

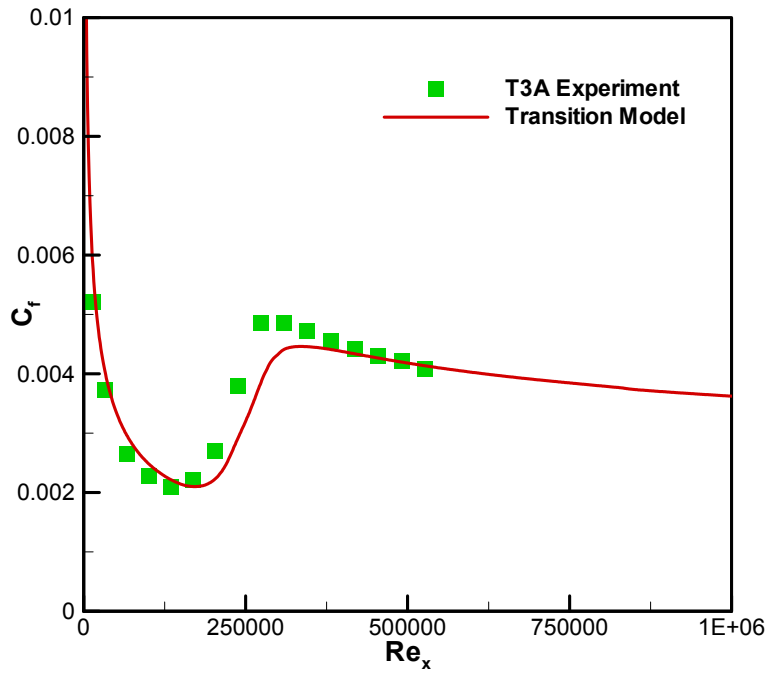


Figure 4.2 : Variation of Skin Friction Coefficient Along the Flat Plate for T3A Case

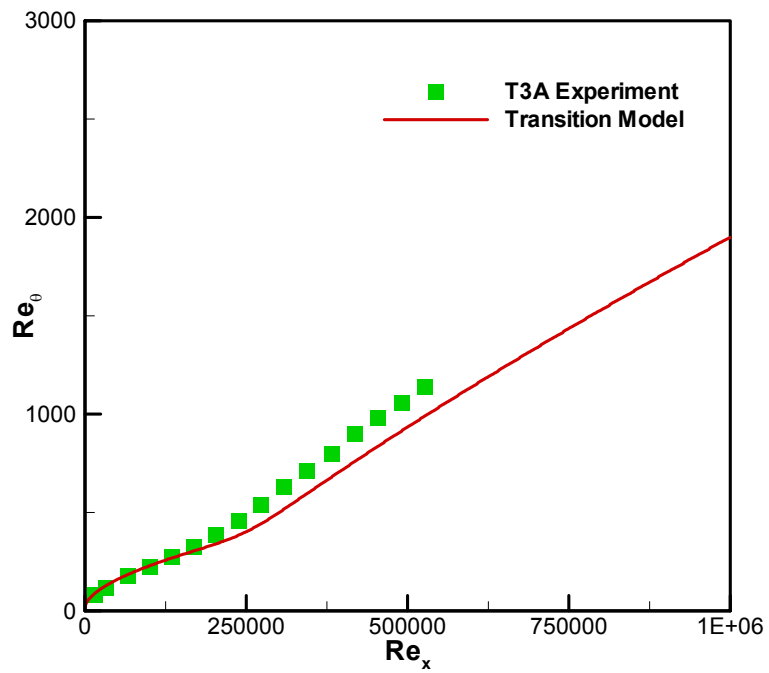


Figure 4.3 : Variation of Reynolds Number Based on Momentum Thickness Along the Flat Plate for T3A Case

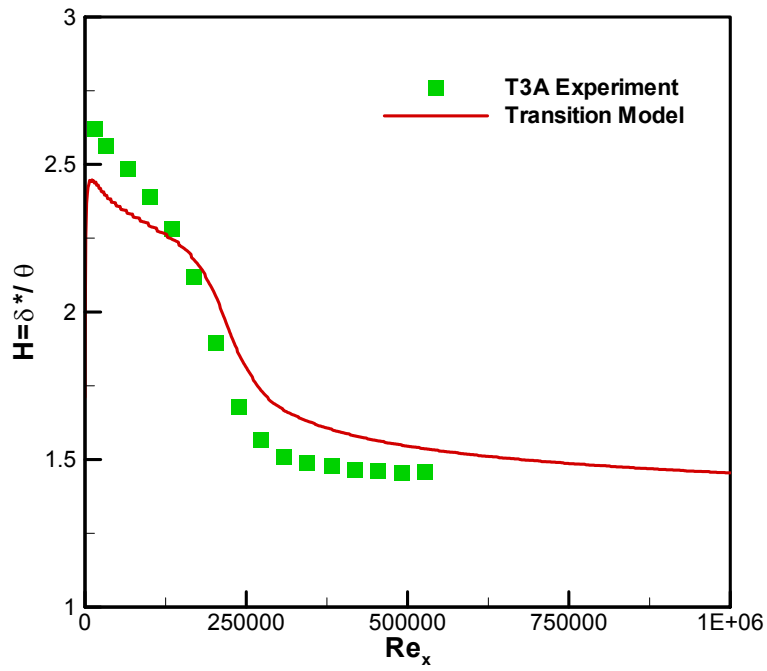


Figure 4.4 : Variation of Shape Factor Along the Flat Plate for T3A Case

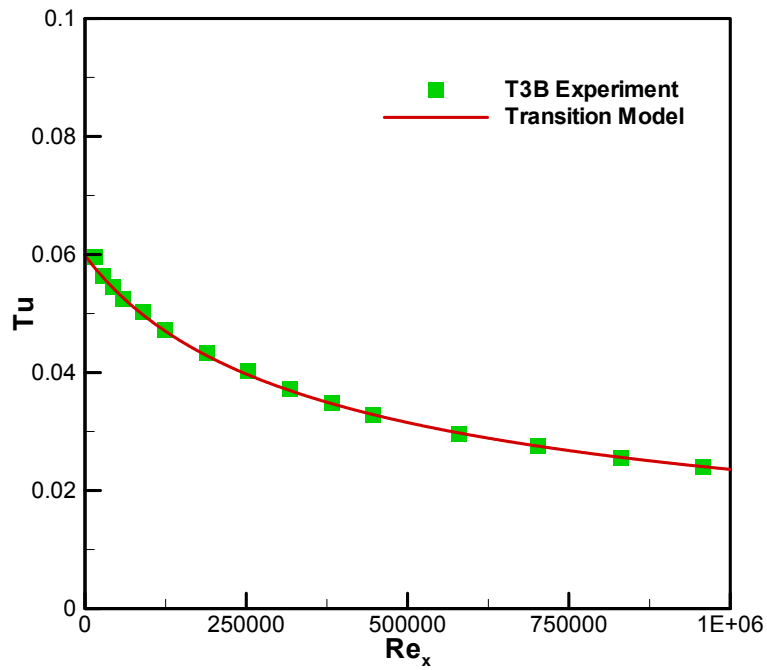


Figure 4.5 : Variation of Freestream Turbulence Intensity Along the Flat Plate for T3B Case

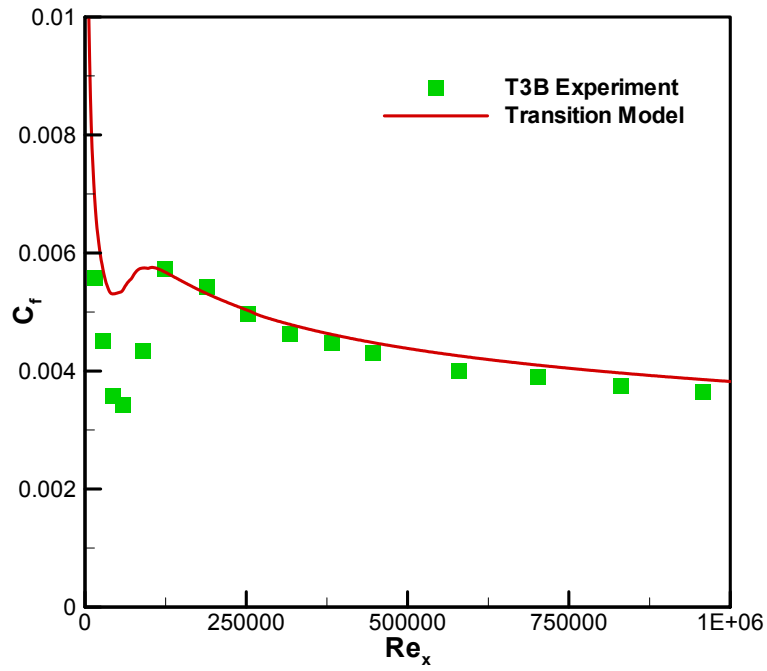


Figure 4.6 : Variation of Skin Friction Coefficient Along the Flat Plate for T3B Case

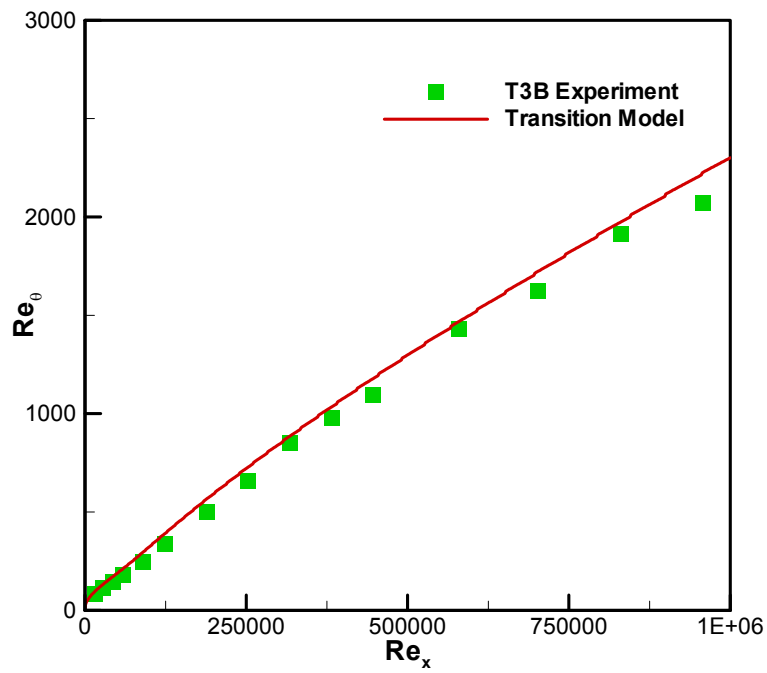


Figure 4.7 : Variation of Reynolds Number Based on Momentum Thickness Along the Flat Plate for T3B Case

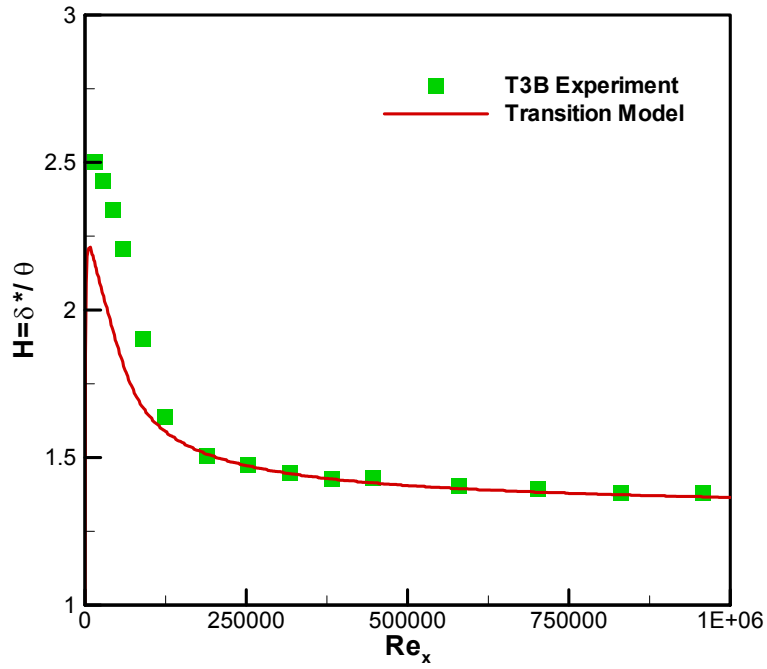


Figure 4.8 : Variation of Shape Factor Along the Flat Plate for T3B Case

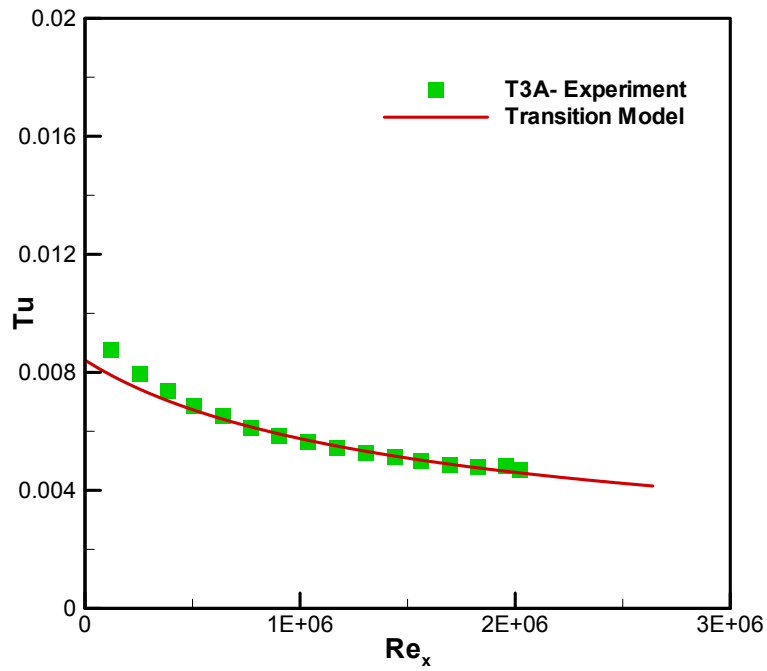


Figure 4.9 : Variation of Freestream Turbulence Intensity Along the Flat Plate for T3A- Case

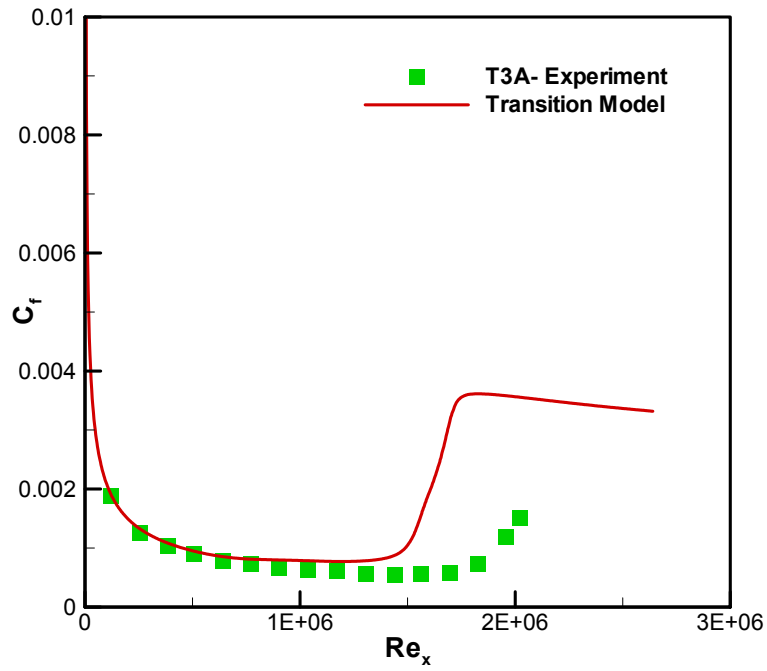


Figure 4.10 : Variation of Skin Friction Coefficient Along the Flat Plate for T3A- Case

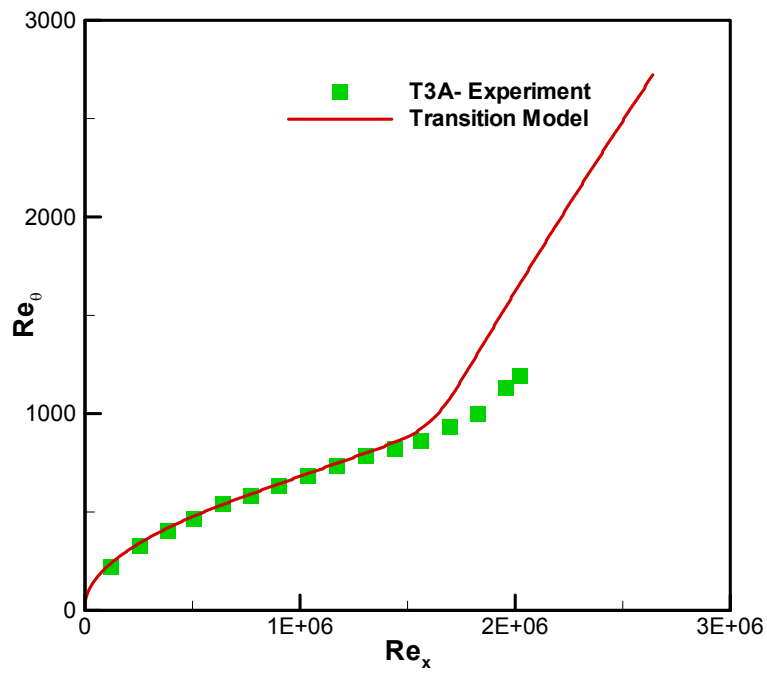


Figure 4.11 : Variation of Reynolds Number Based on Momentum Thickness Along the Flat Plate for T3A- Case

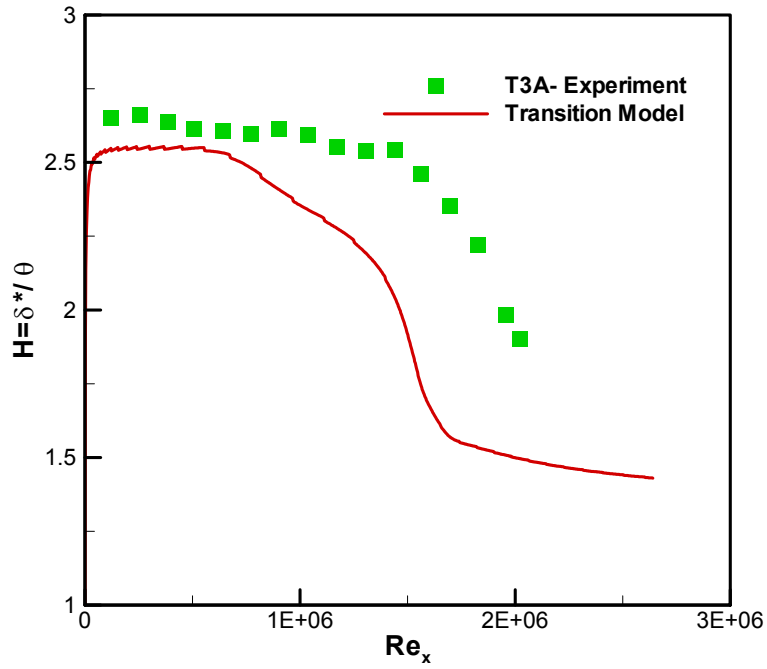


Figure 4.12 : Variation of Shape Factor Along the Flat Plate for T3A- Case

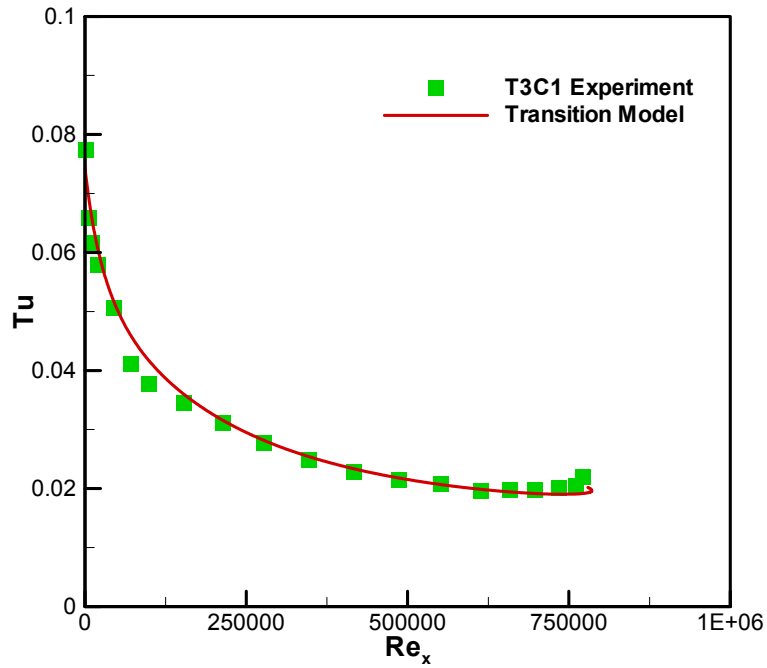


Figure 4.13 : Variation of Freestream Turbulence Intensity Along the Flat Plate for T3C1 Case

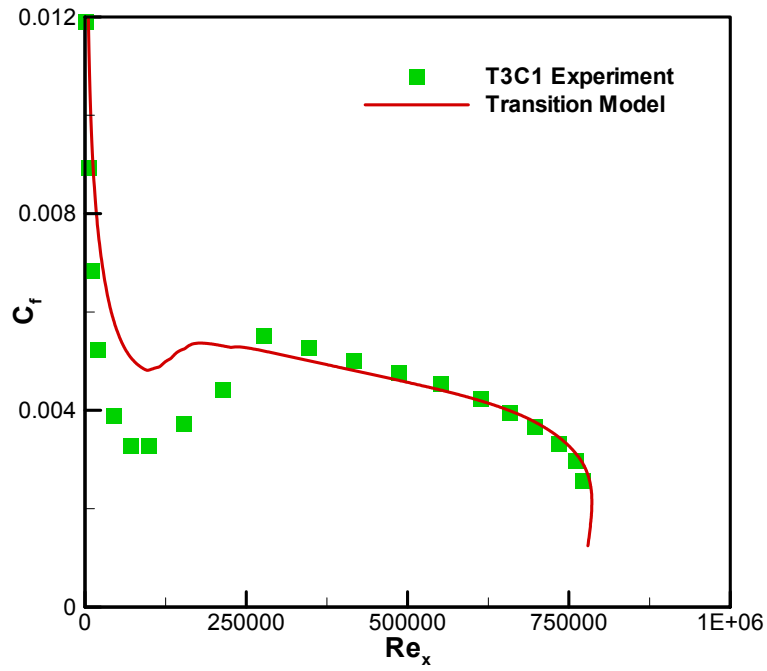


Figure 4.14 : Variation of Skin Friction Coefficient Along the Flat Plate for T3C1 Case

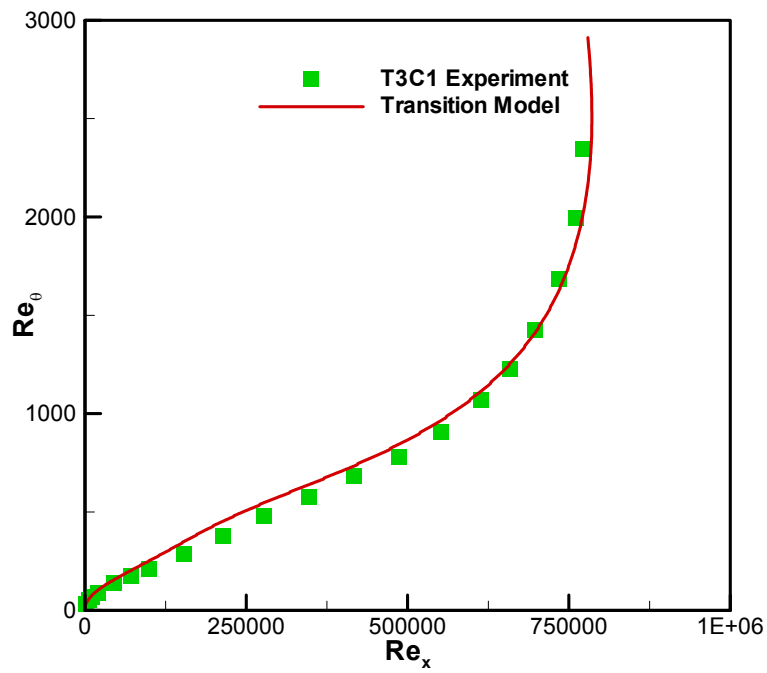


Figure 4.15 : Variation of Reynolds Number Based on Momentum Thickness Along the Flat Plate for T3C1 Case

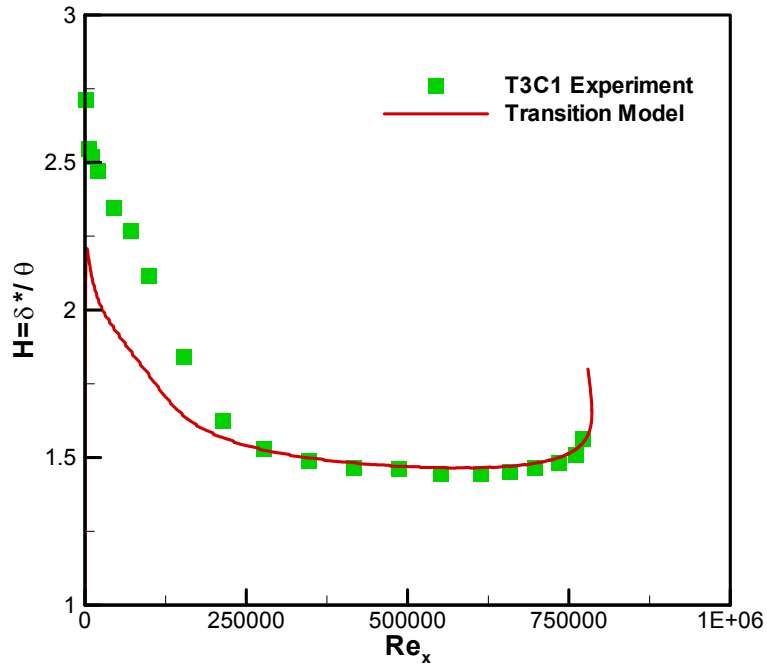


Figure 4.16 : Variation of Shape Factor Along the Flat Plate for T3C1 Case

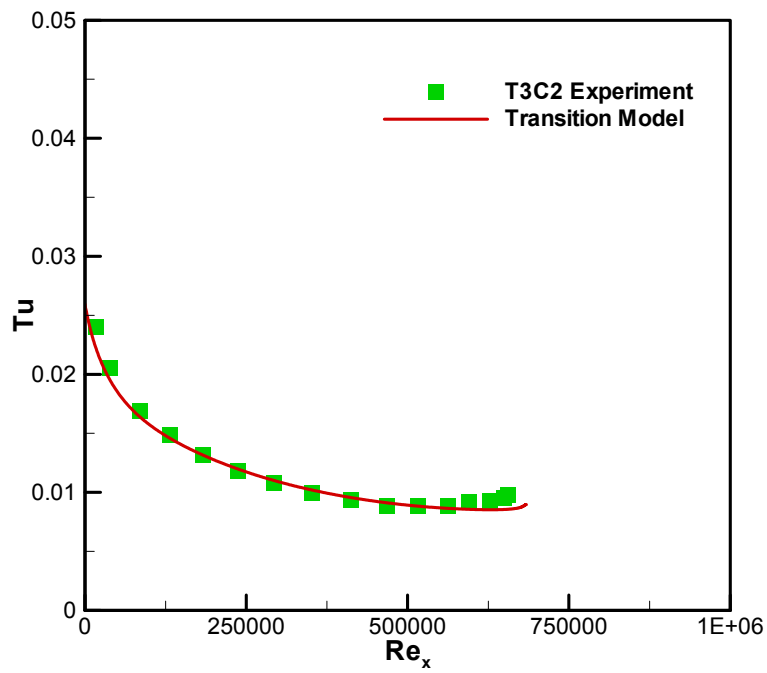


Figure 4.17 : Variation of Freestream Turbulence Intensity Along the Flat Plate for T3C2 Case

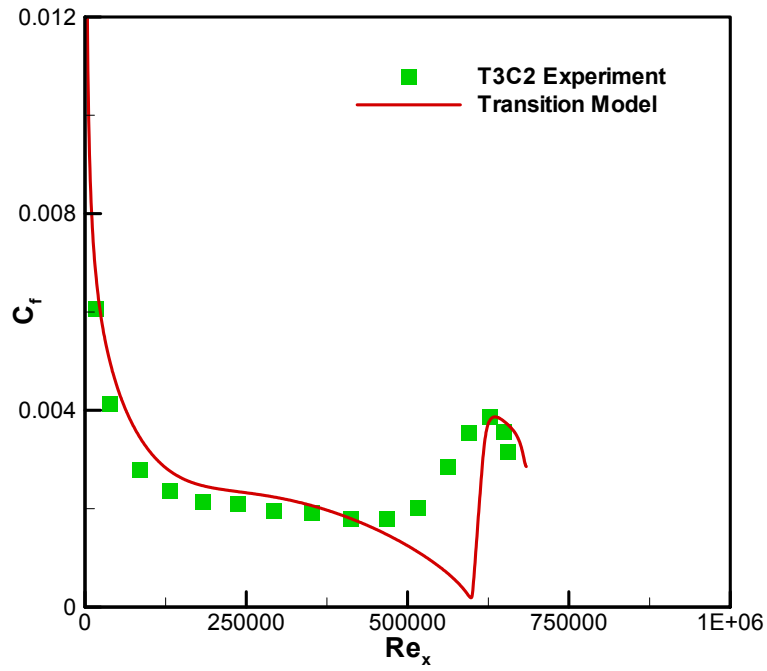


Figure 4.18 : Variation of Skin Friction Coefficient Along the Flat Plate for T3C2 Case

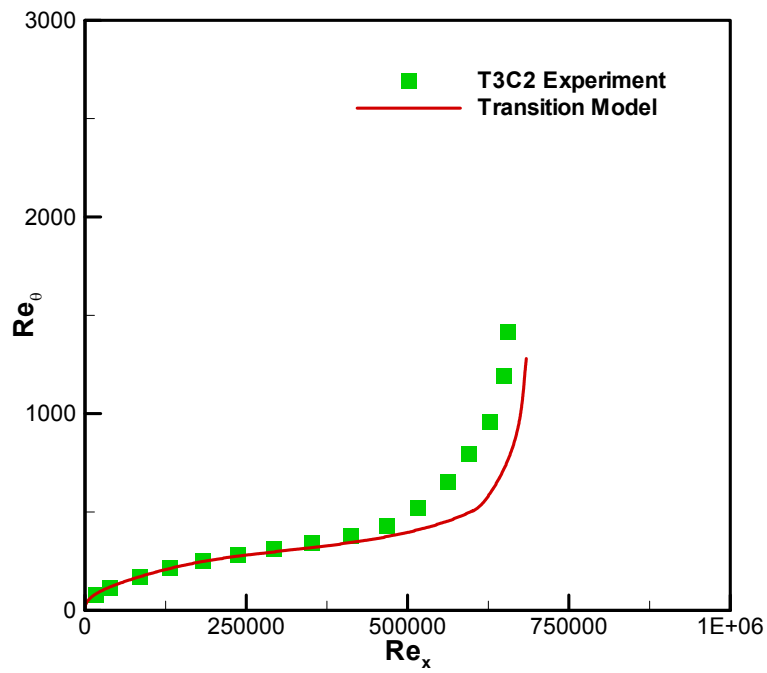


Figure 4.19 : Variation of Reynolds Number Based on Momentum Thickness Along the Flat Plate for T3C2 Case

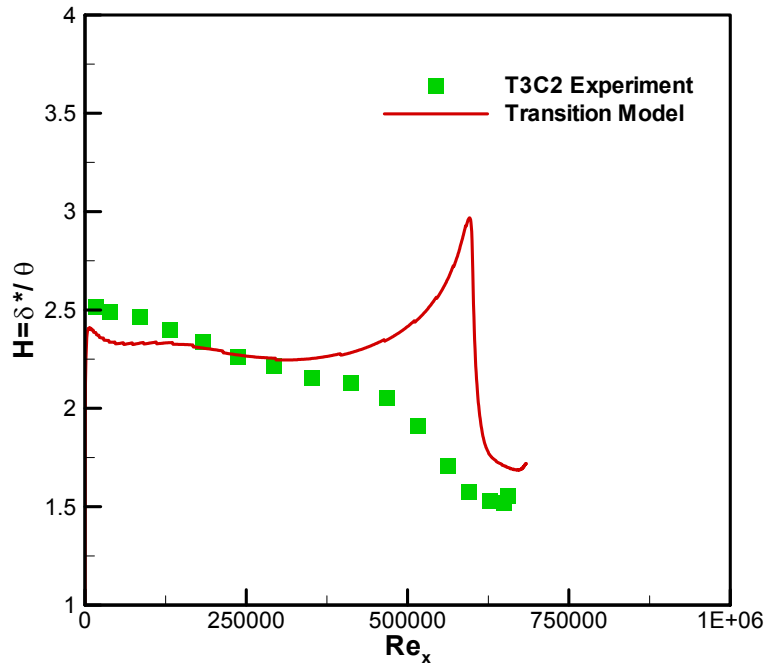


Figure 4.20 : Variation of Shape Factor Along the Flat Plate for T3C2 Case

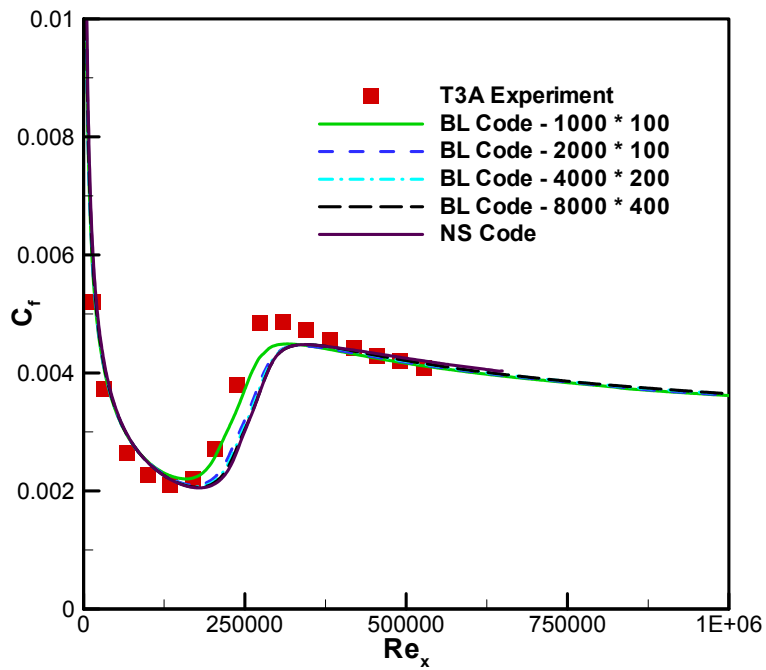


Figure 4.21 : Effect of Grid Dependence for T3A Case

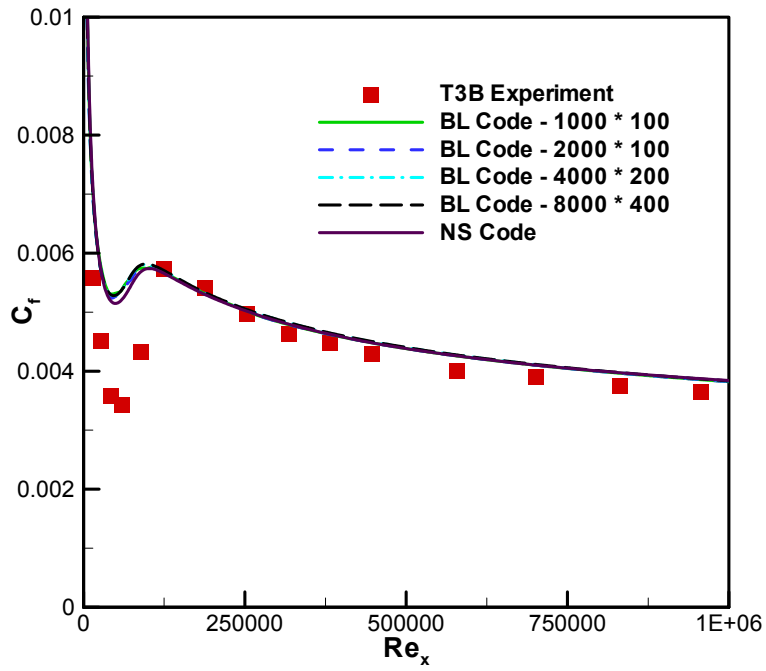


Figure 4.22 : Effect of Grid Dependence for T3B Case

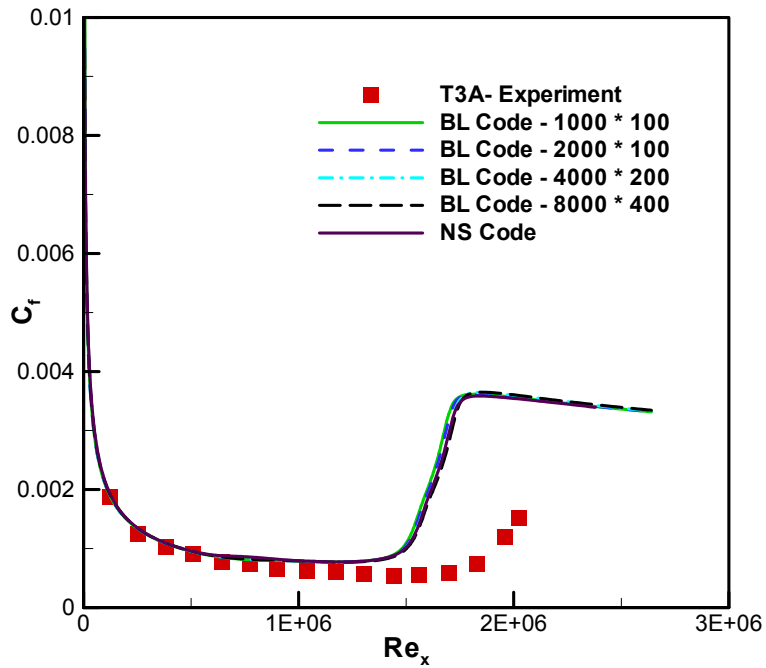


Figure 4.23 : Effect of Grid Dependence for T3A- Case

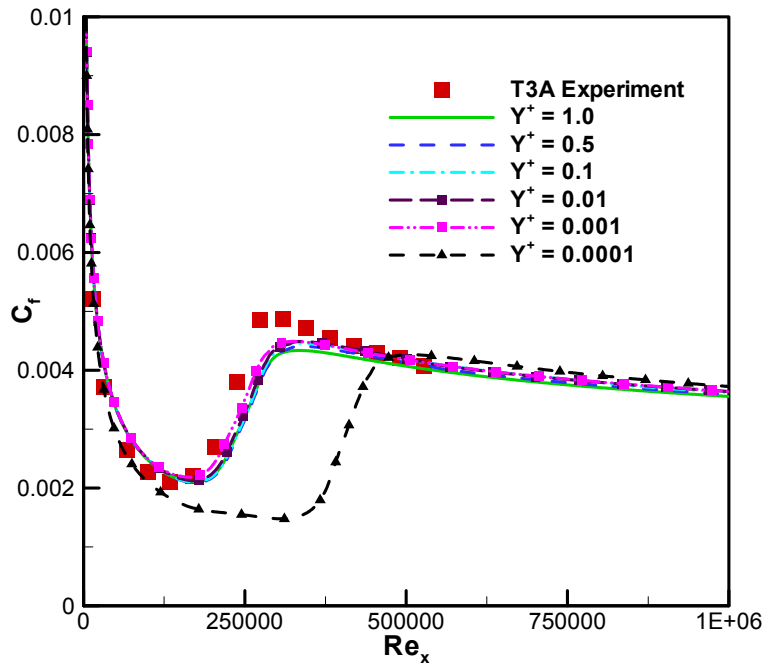


Figure 4.24 : Effect of y^+ for T3A Case

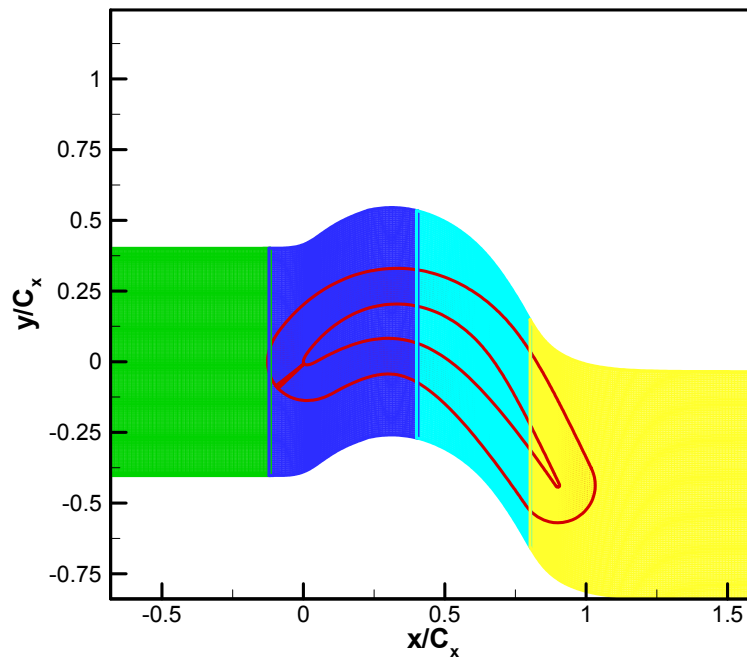


Figure 4.25 : Computational Grid for FSTI = 0.08% Case of Huang et al. (2003)

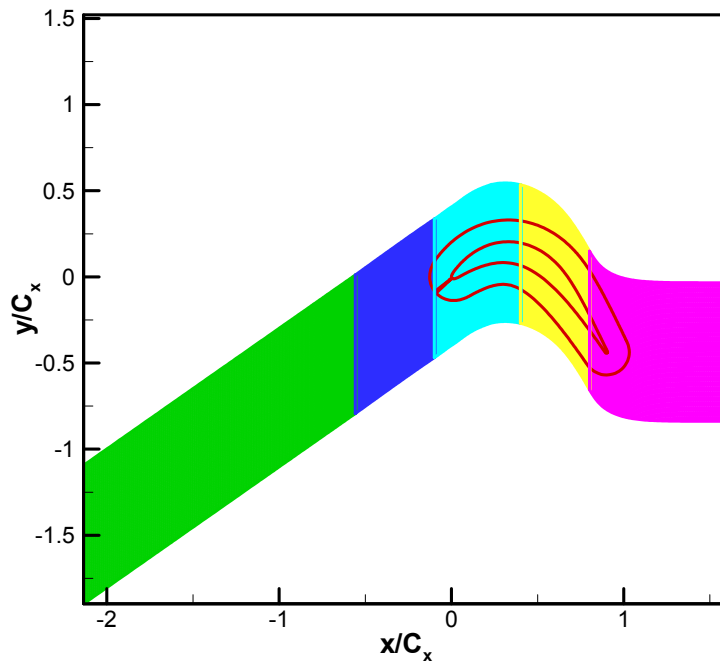


Figure 4.26 : Computational Grid for FSTI = 2.35% and FSTI = 6.0% Case of Huang et al. (2003)

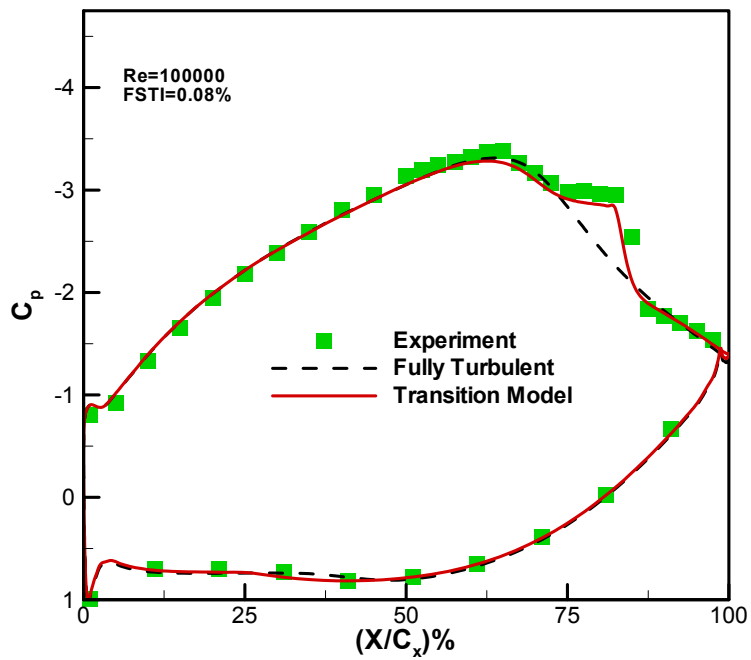


Figure 4.27 : Pressure Coefficient Comparison for FSTI=0.08% & Re=100000

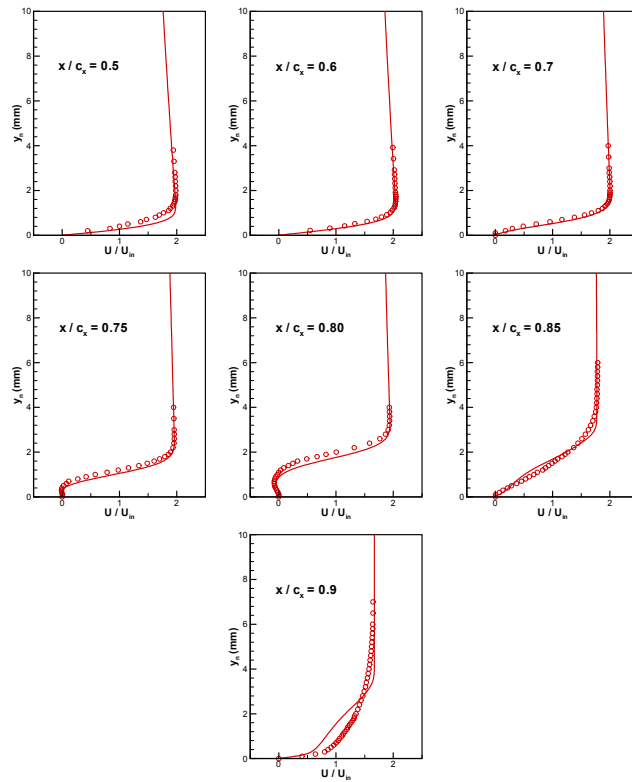


Figure 4.28 : Velocity Profile for FSTI=0.08% & Re=100000

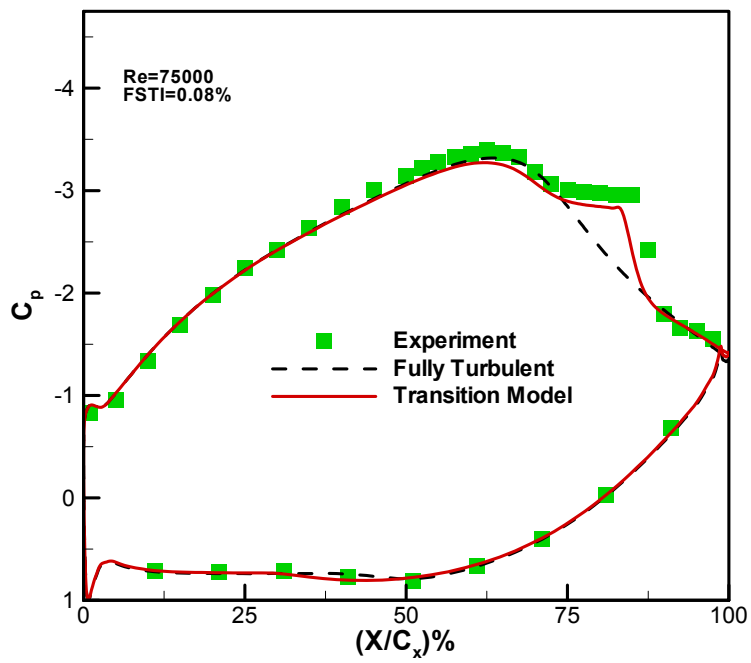


Figure 4.29 : Pressure Coefficient Comparison for FSTI=0.08% & Re=75000

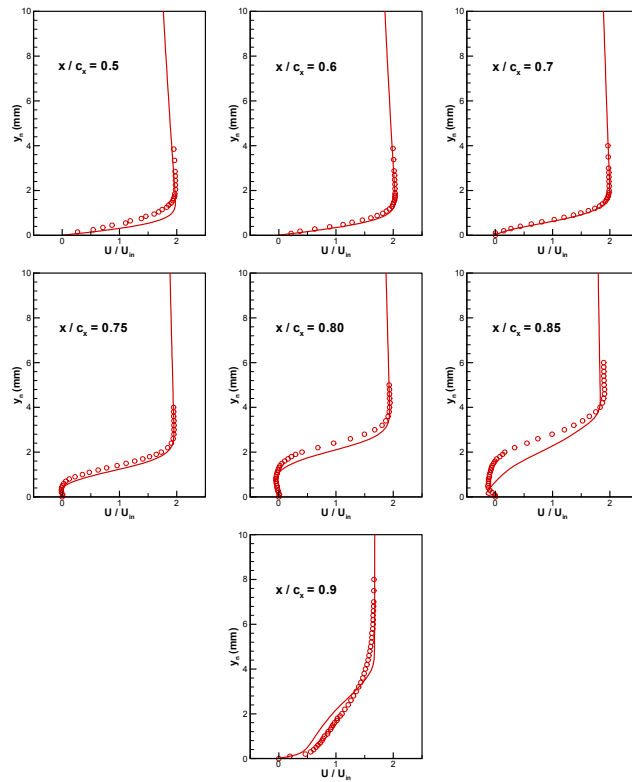


Figure 4.30 : Velocity Profile for FSTI=0.08% & Re=75000

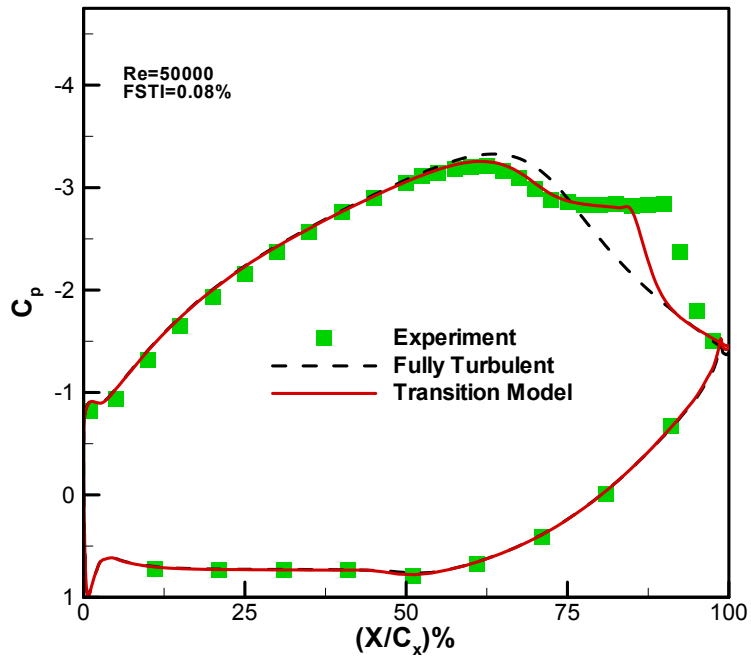


Figure 4.31 : Pressure Coefficient Comparison for FSTI=0.08% & Re=50000

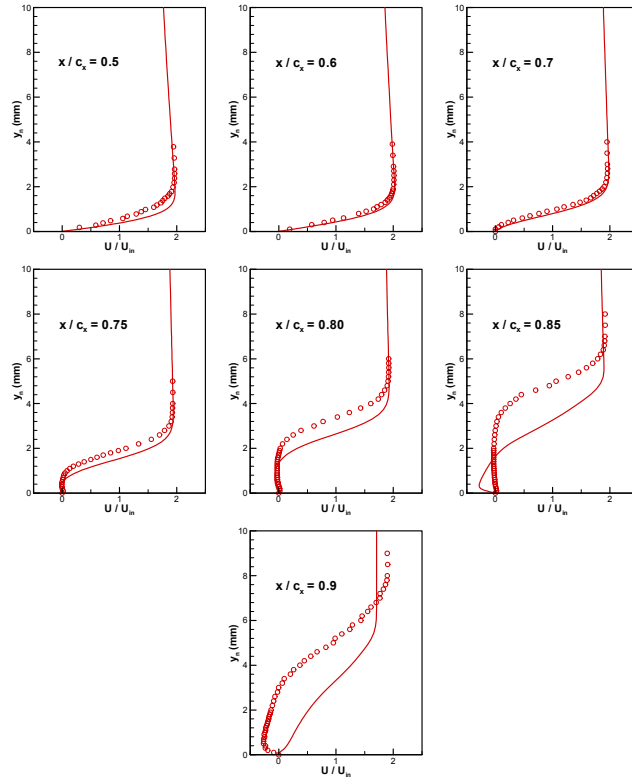


Figure 4.32 : Velocity Profile for FSTI=0.08% & Re=50000

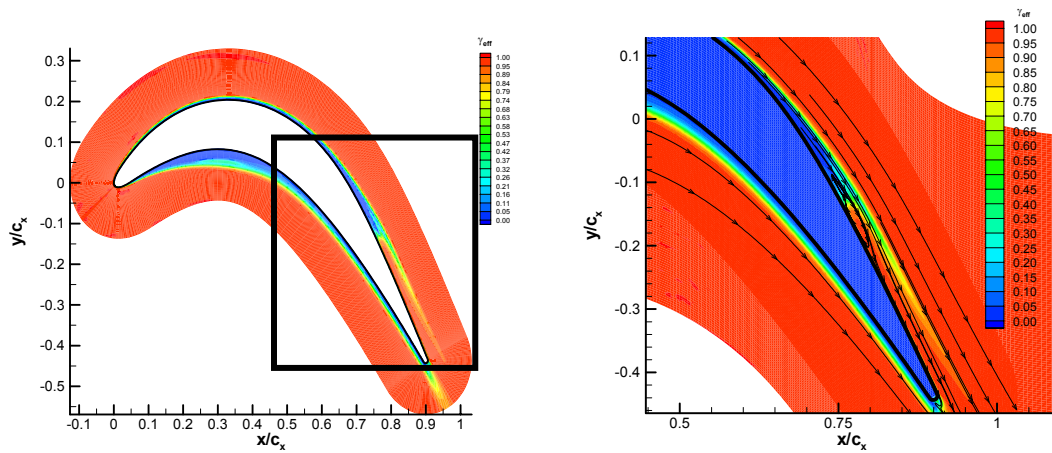


Figure 4.33 : Streamlines and Effective Intermittency Contours for PAK B Cascade
(FSTI = 0.08% & Re = 50000)

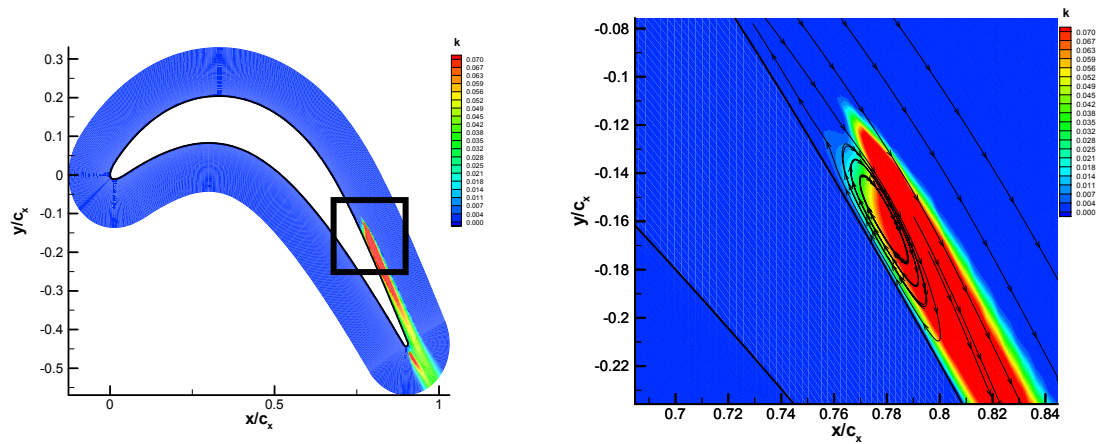


Figure 4.34 : Streamlines and Turbulent Kinetic Energy Contours for PAK B Cascade
(FSTI = 0.08% & Re = 50000)

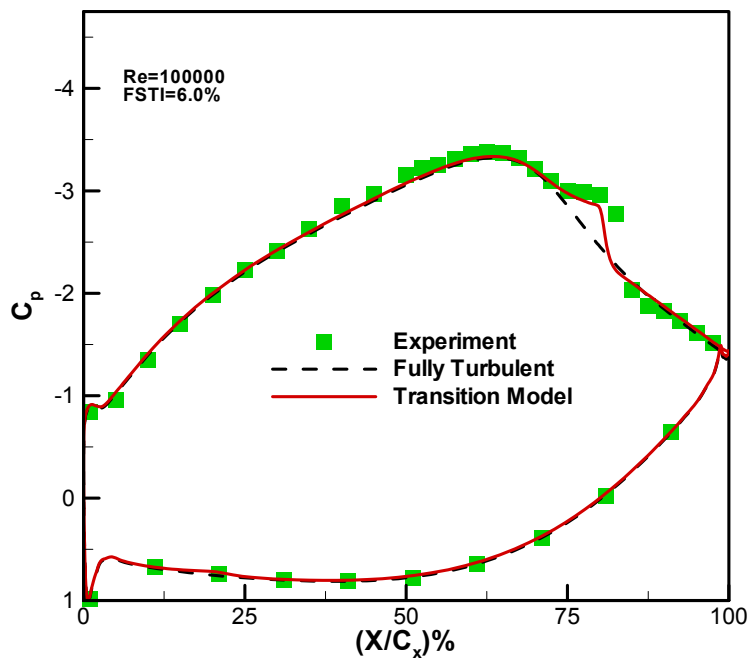


Figure 4.35 : Pressure Coefficient Comparison for FSTI=6.0% & Re=100000

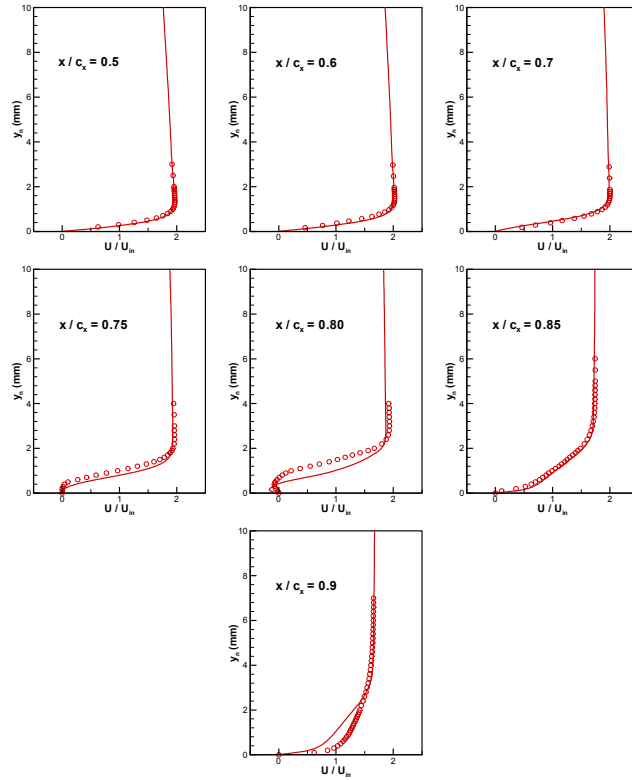


Figure 4.36 : Velocity Profile for FSTI=6.0% & Re=100000

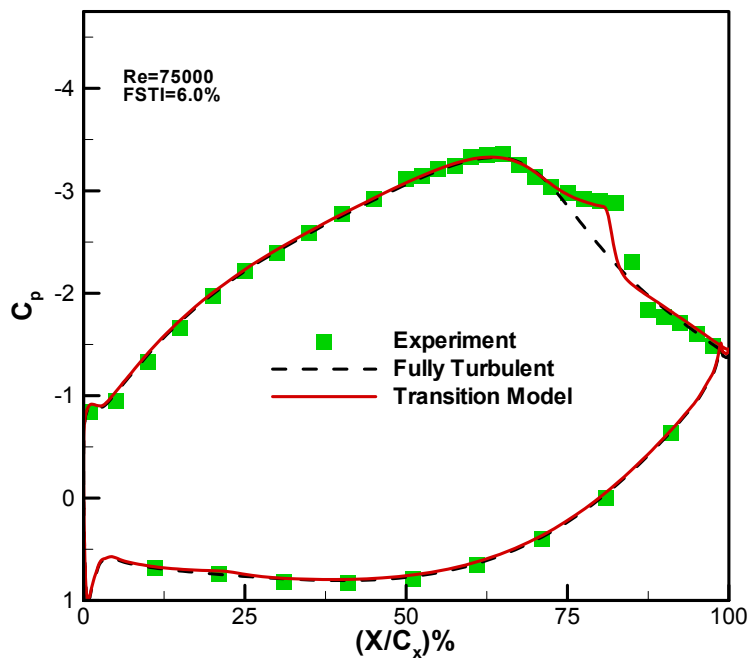


Figure 4.37 : Pressure Coefficient Comparison for FSTI=6.0% & Re=75000

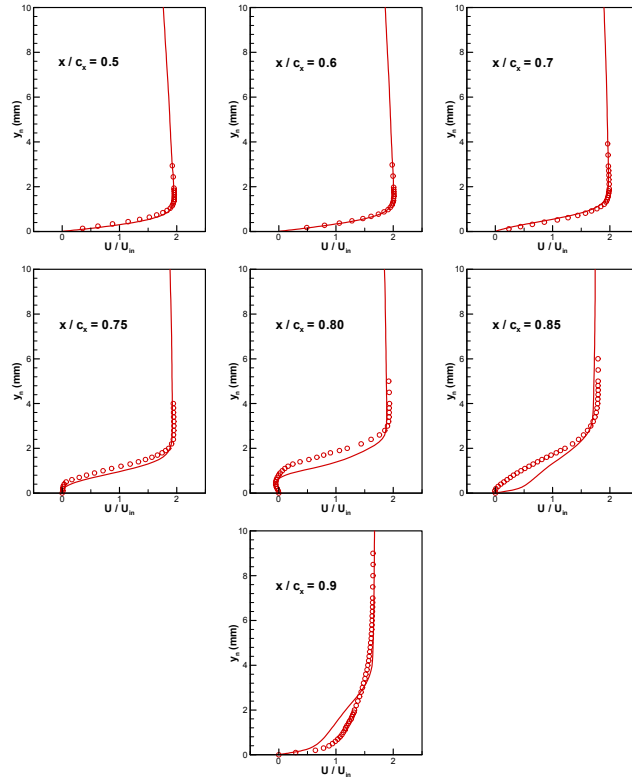


Figure 4.38 : Velocity Profile for FSTI=6.0% & Re=75000

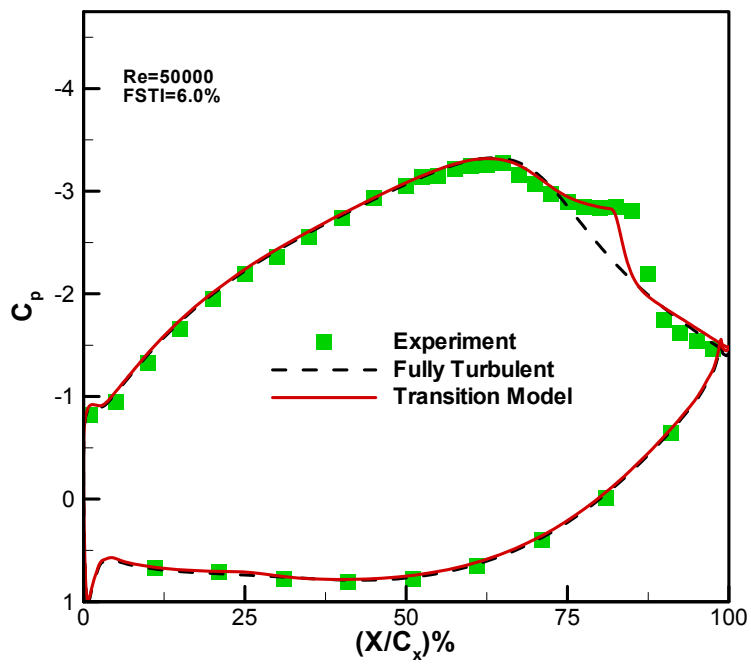


Figure 4.39 : Pressure Coefficient Comparison for FSTI=6.0% & Re=50000

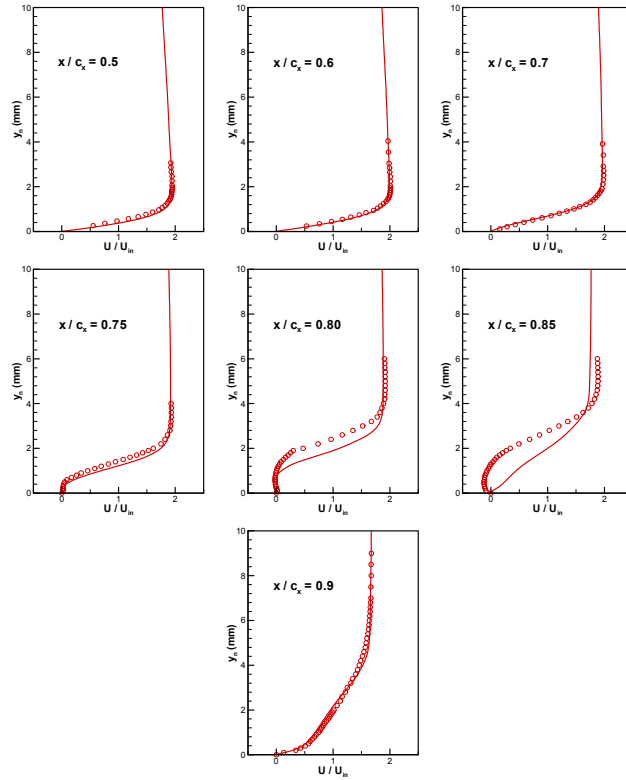


Figure 4.40 : Velocity Profile for FSTI=6.0% & Re=50000

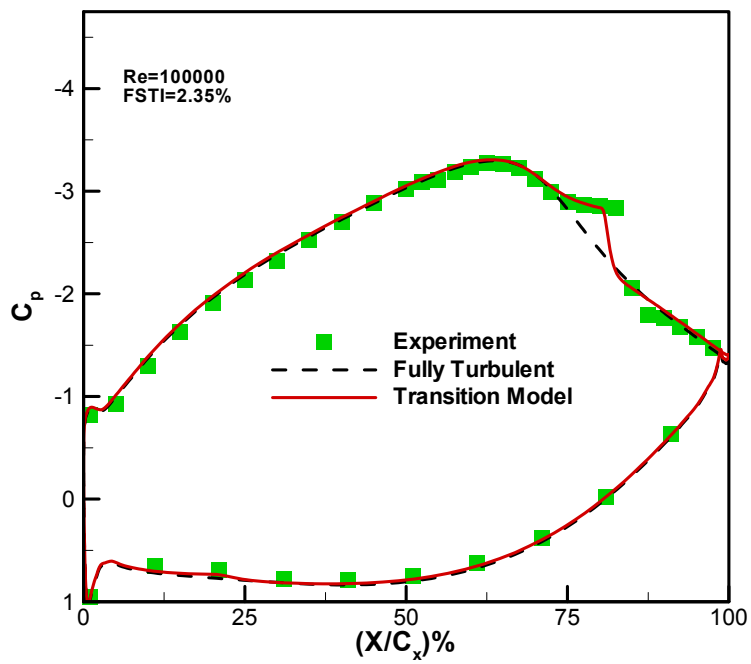


Figure 4.41 : Pressure Coefficient Comparison for FSTI=2.35% & Re=100000

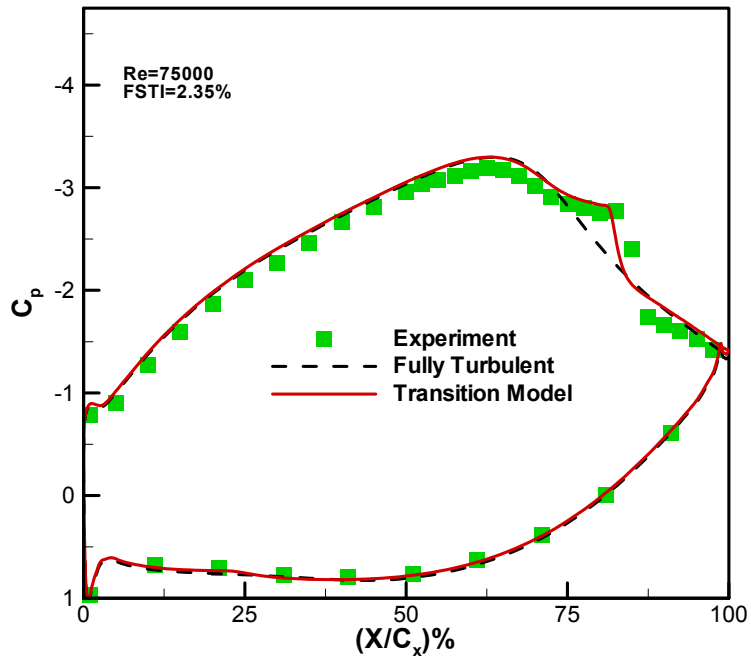


Figure 4.42 : Pressure Coefficient Comparison for FSTI=2.35% & Re=75000

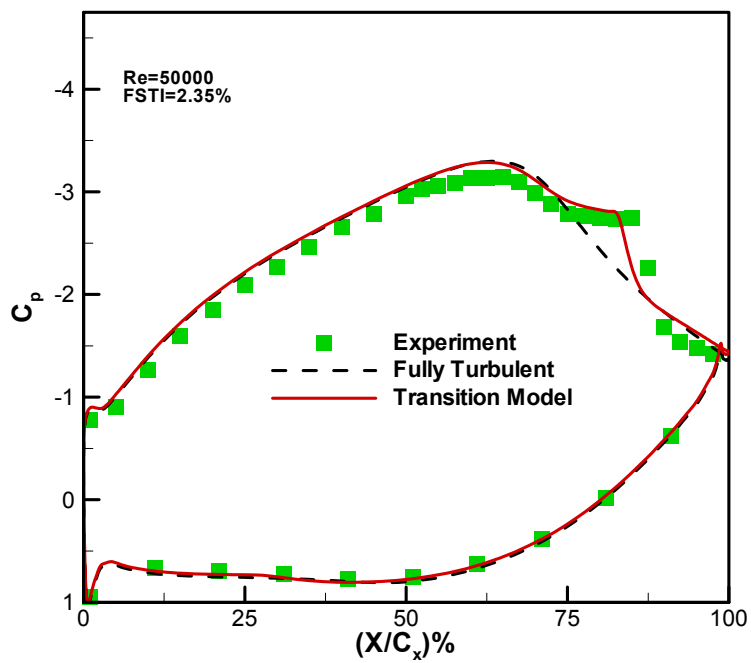


Figure 4.43 : Pressure Coefficient Comparison for FSTI=2.35% & Re=50000

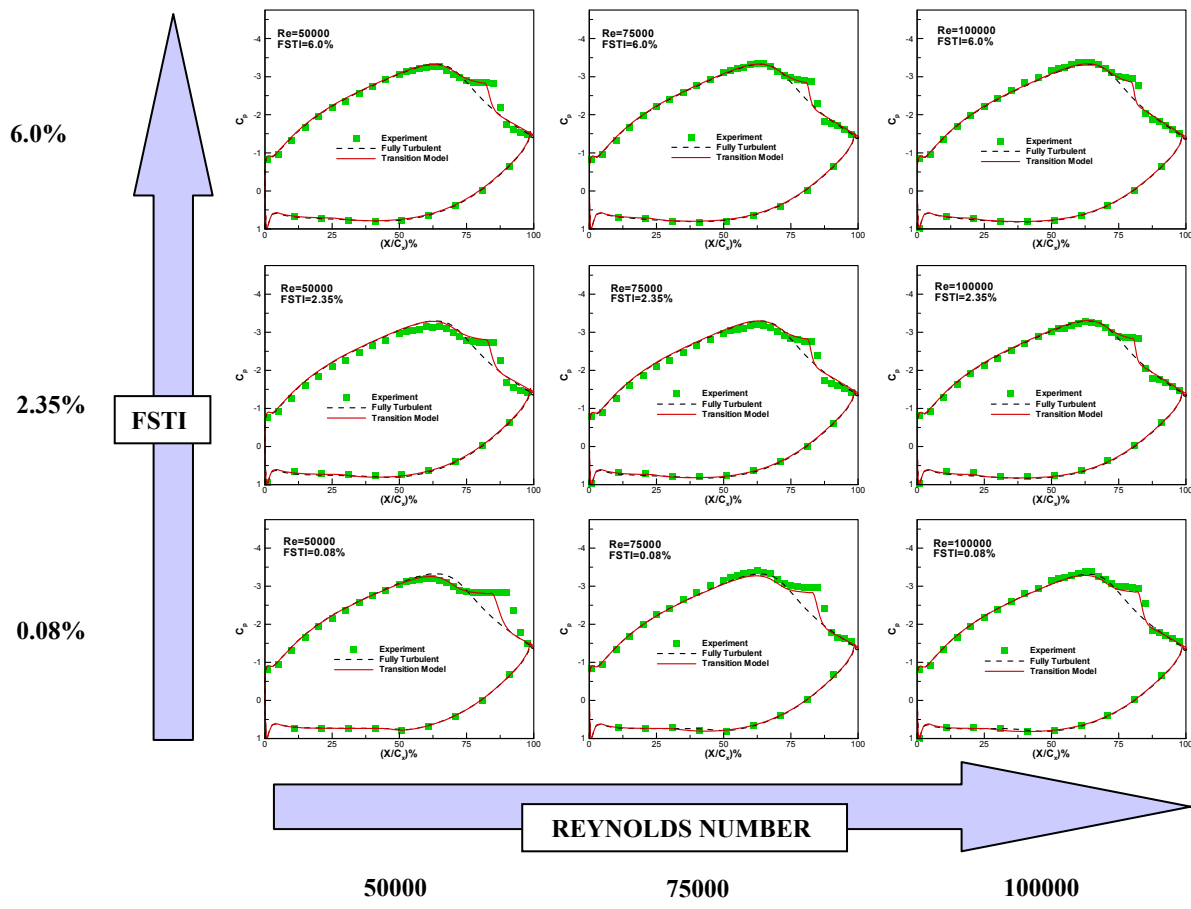


Figure 4.44 : Pressure Coefficient Comparison for Experiments of Huang et al. (2003)

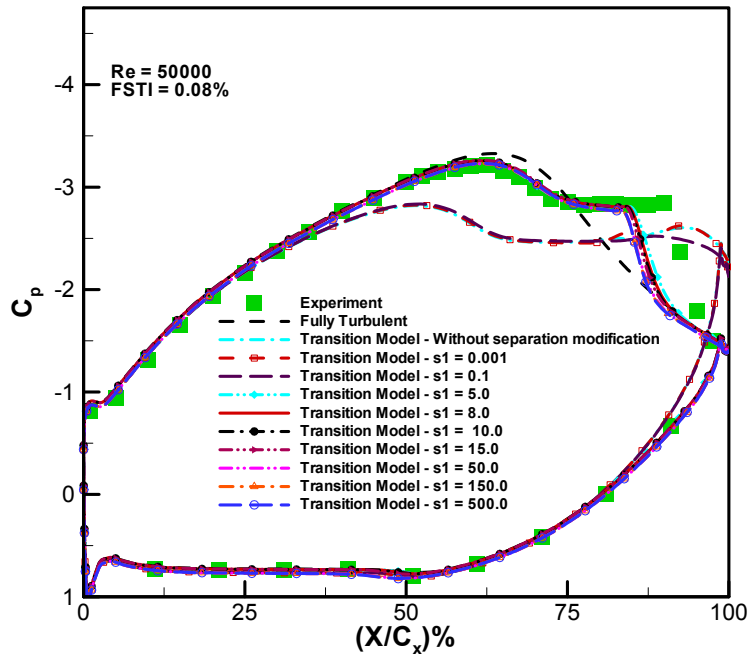


Figure 4.45 : Effect of Varying s_1 for Low Freestream Turbulence and Low Reynolds Number Case

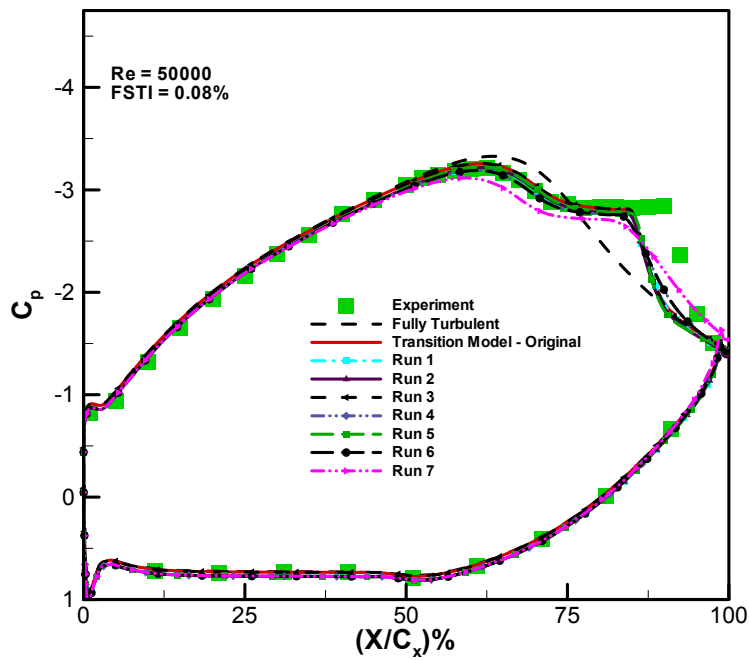


Figure 4.46 : Parametric Study I for Low Freestream Turbulence and Low Reynolds Number Case

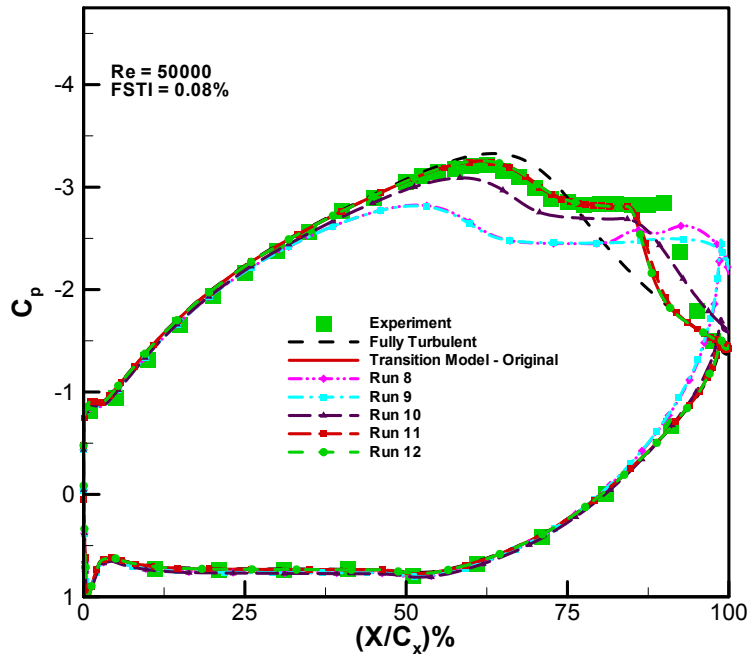


Figure 4.47 : Parametric Study II for Low Freestream Turbulence and Low Reynolds Number Case

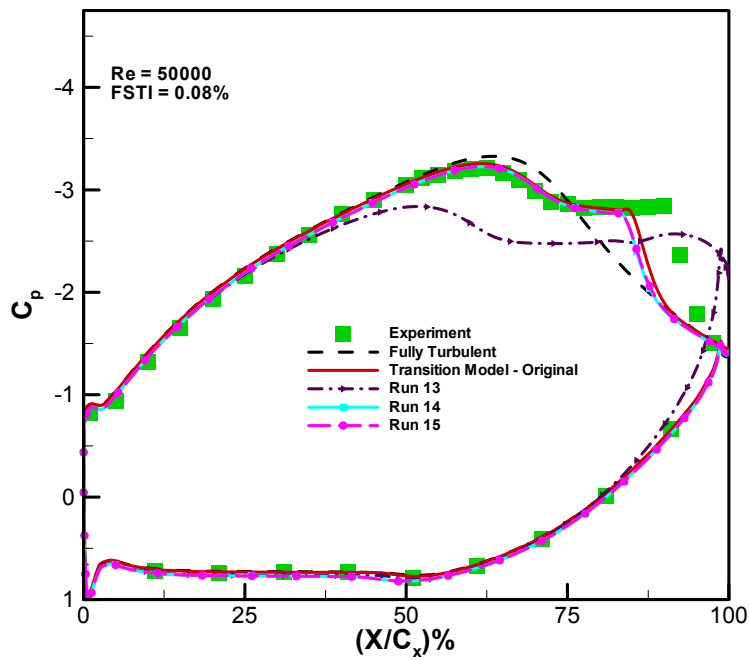


Figure 4.48 : Parametric Study III for Low Freestream Turbulence and Low Reynolds Number Case

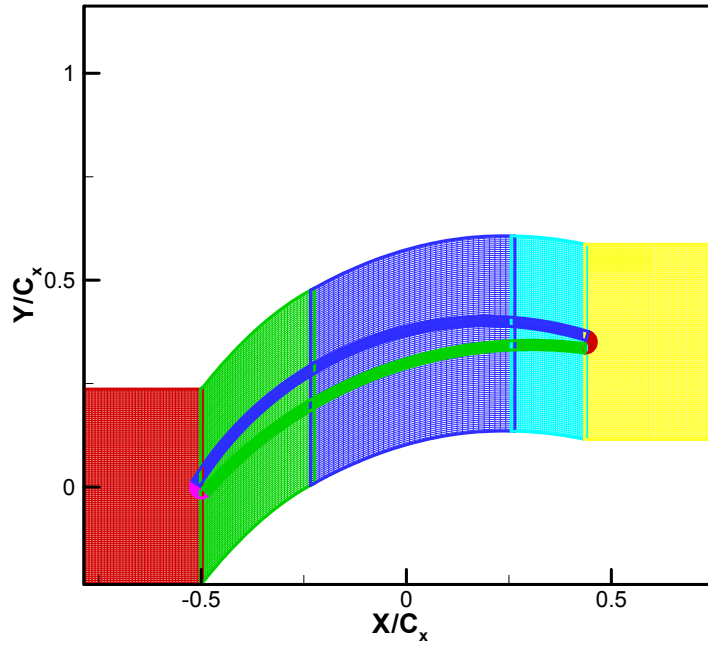


Figure 4.49 : Computational Grid for Compressor Cascade Experiment of Zierke and Deutsch (1989)

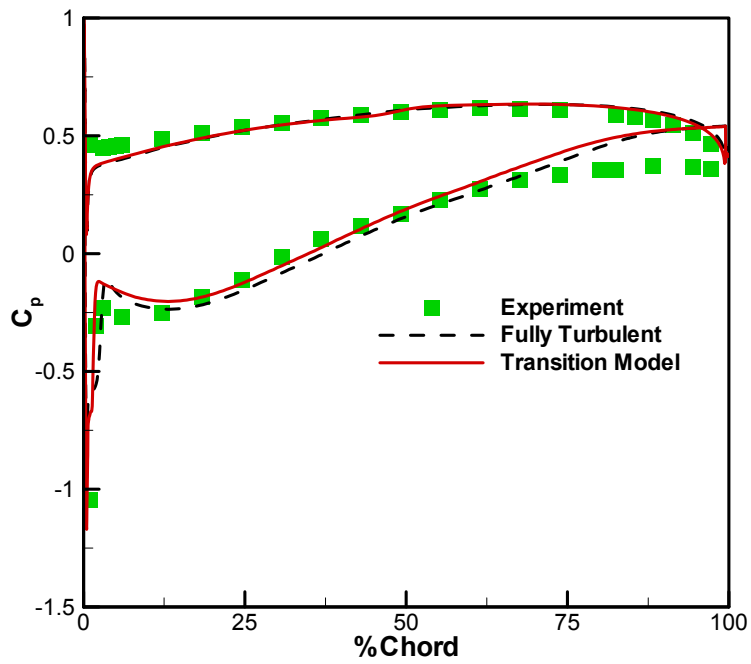


Figure 4.50 : Pressure Coefficient Comparison for Zierke and Deutsch Compressor Cascade, $i = -1.5^\circ$

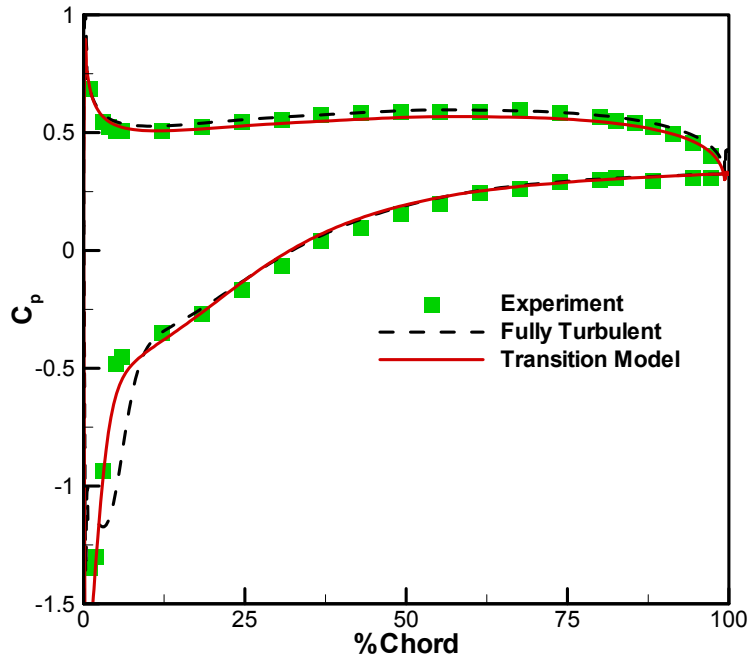


Figure 4.51 : Pressure Coefficient Comparison for Zierke and Deutsch Compressor Cascade, $i = 5.0^\circ$

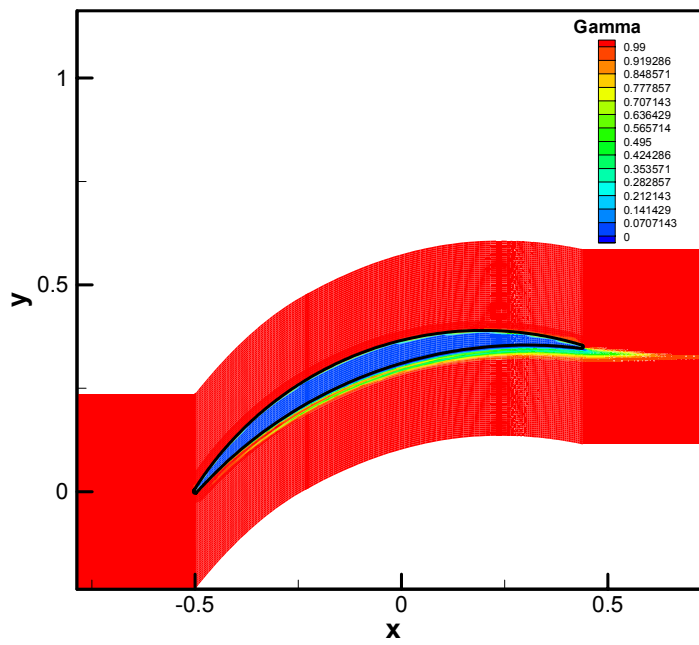


Figure 4.52 : Intermittency Contours for Zierke and Deutsch Compressor Cascade, $i = 5.0^\circ$

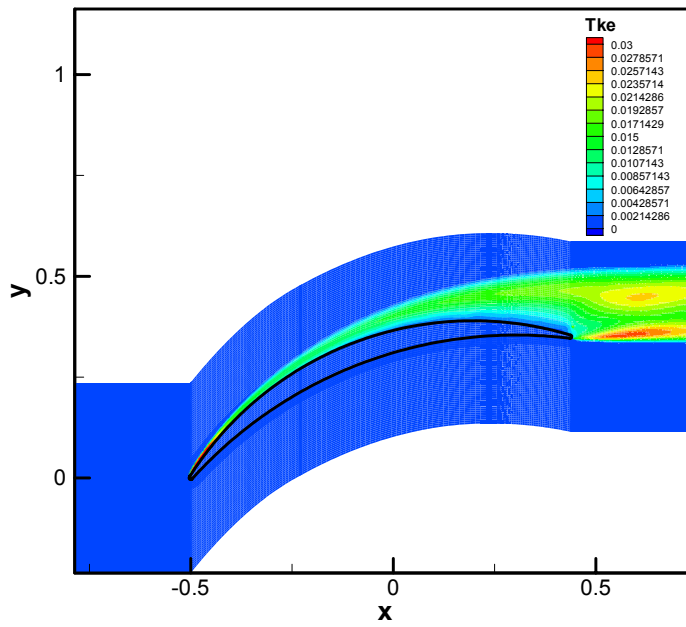


Figure 4.53 : Turbulent Kinetic Energy Contours for Zierke and Deutsch Compressor Cascade,
 $i = 5.0^\circ$

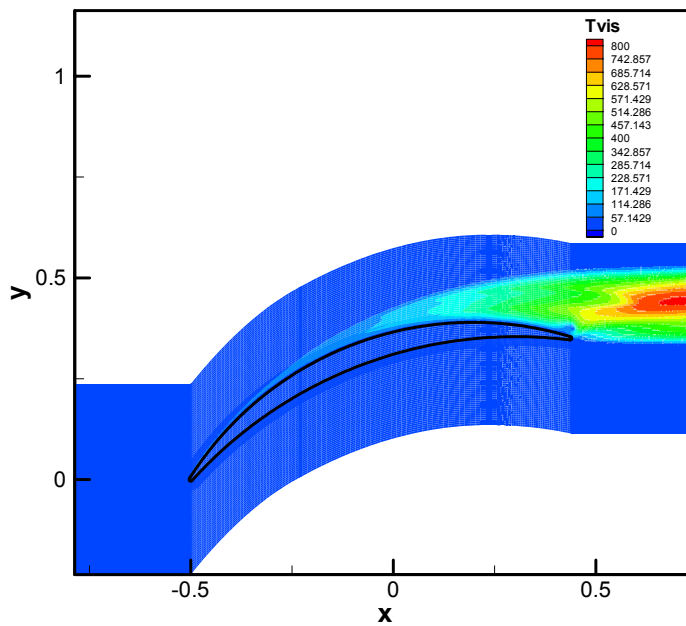


Figure 4.54 : Eddy Viscosity Contours for Zierke and Deutsch Compressor Cascade,
 $i = 5.0^\circ$

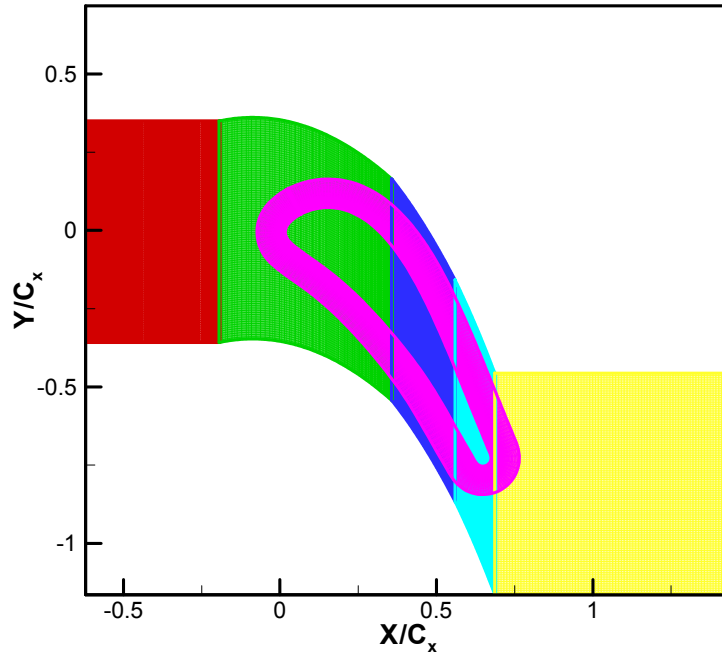


Figure 4.55 : Computational Grid for Turbine Cascade Experiment of Ubaldi et al. (1996)

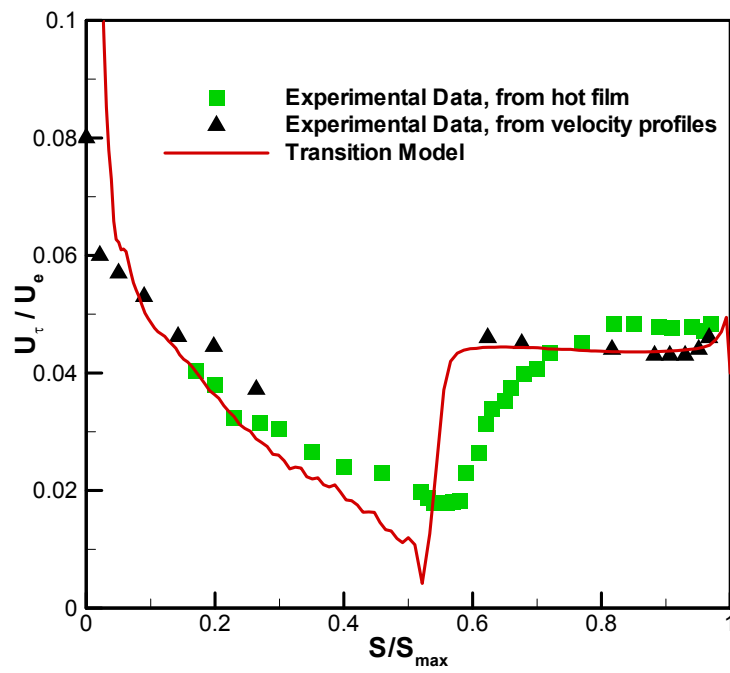


Figure 4.56 : Normalized Friction Velocity for Genoa Turbine Cascade

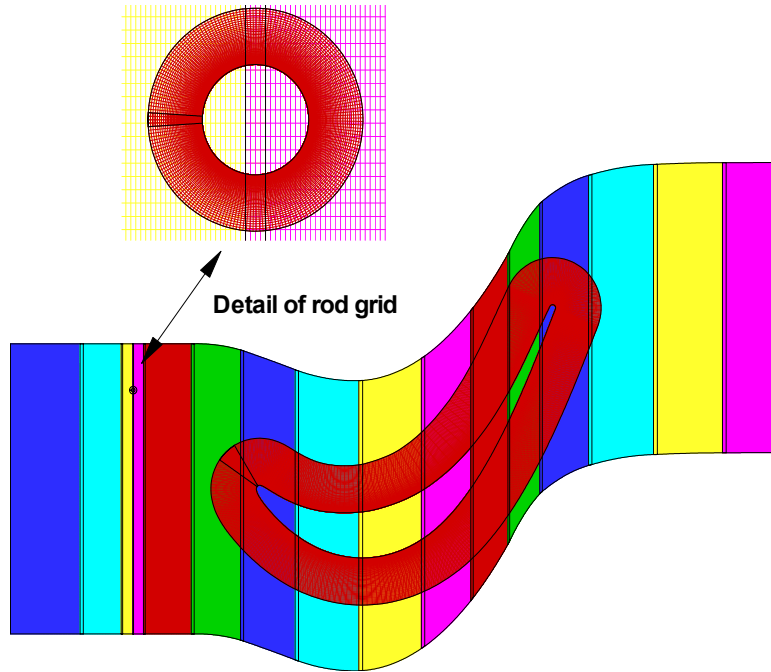


Figure 4.57 : Computational Grid for T106 Experiments of Stieger et al. (2003)

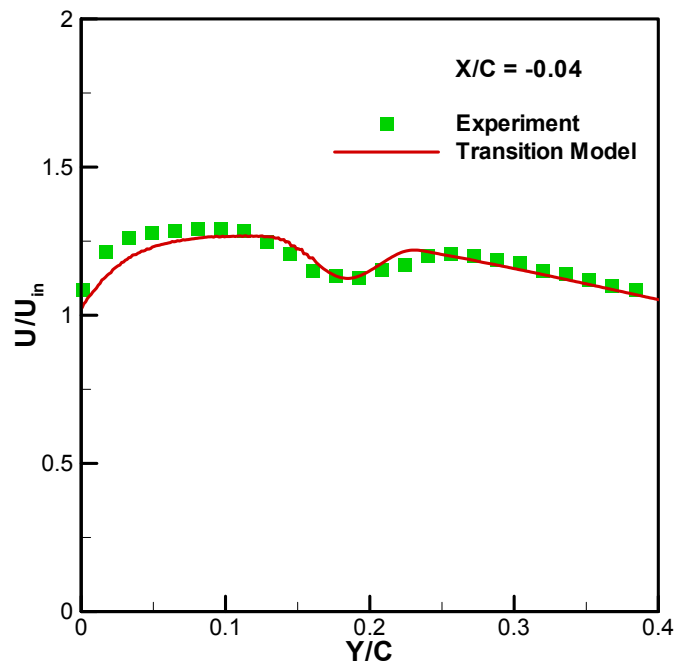


Figure 4.58 : Velocity Profile at $x / C = -0.04$ for T106 Cascade

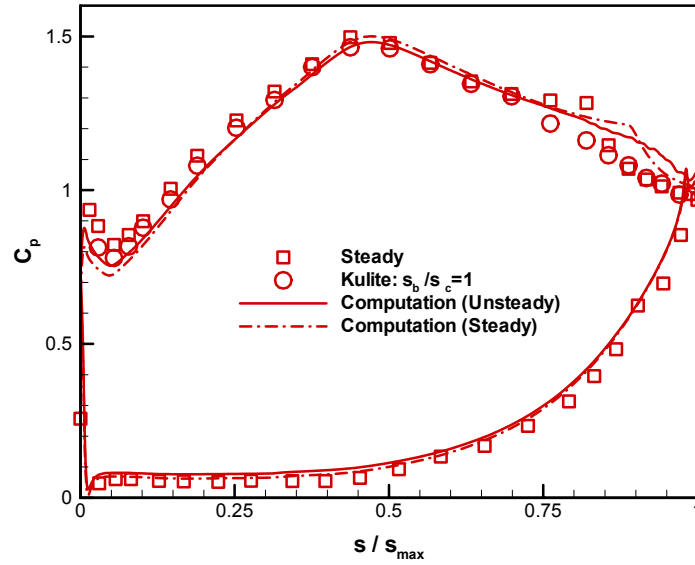


Figure 4.59 : Comparison of Computed and Experimental Pressure Coefficient Distributions for T106 Cascade

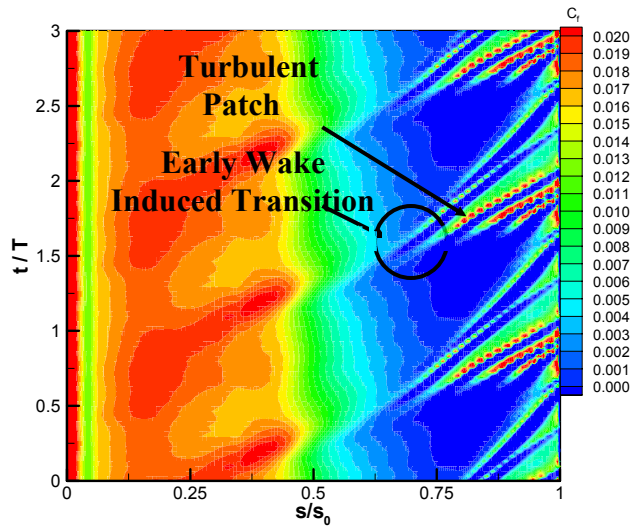


Figure 4.60 : Computed Phase Averaged Skin Friction Coefficient Distribution on the Suction Surface of T106 Blade

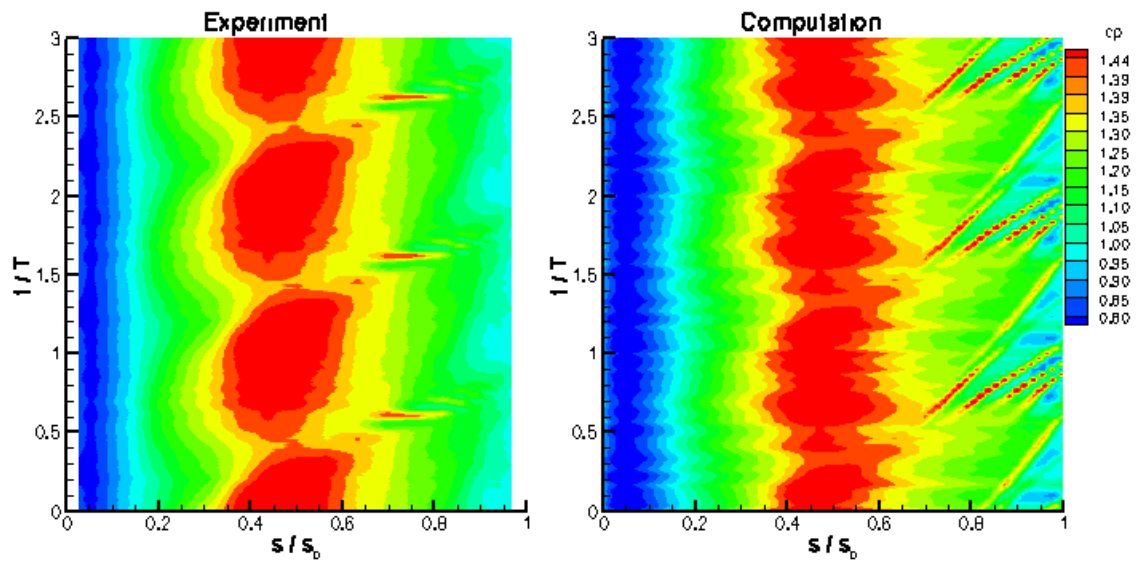


Figure 4.61 : Comparison of Computed and Experimental Pressure Coefficient Contours for T106 Cascade

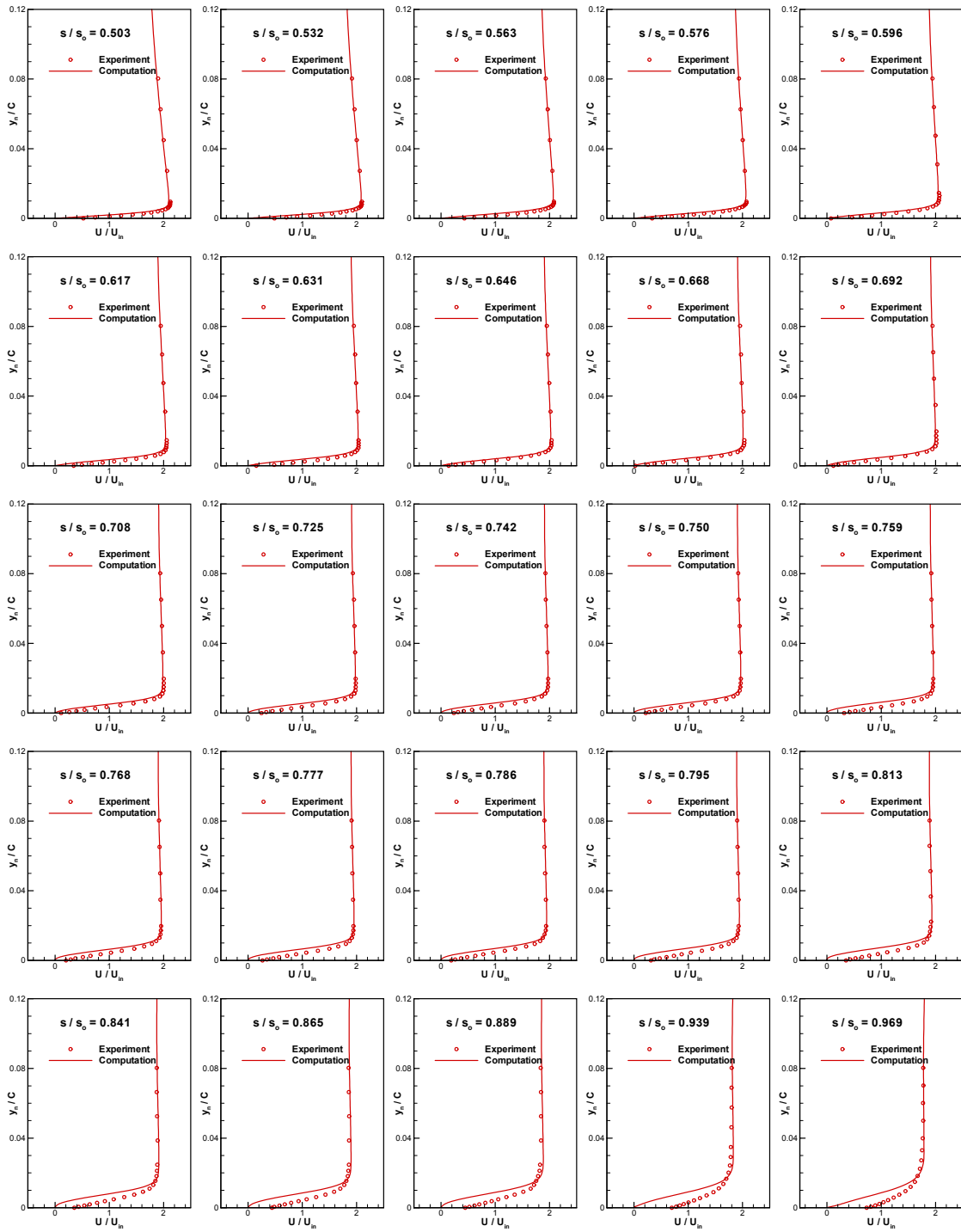


Figure 4.62 : Mean Velocity Profiles for T106 Cascade

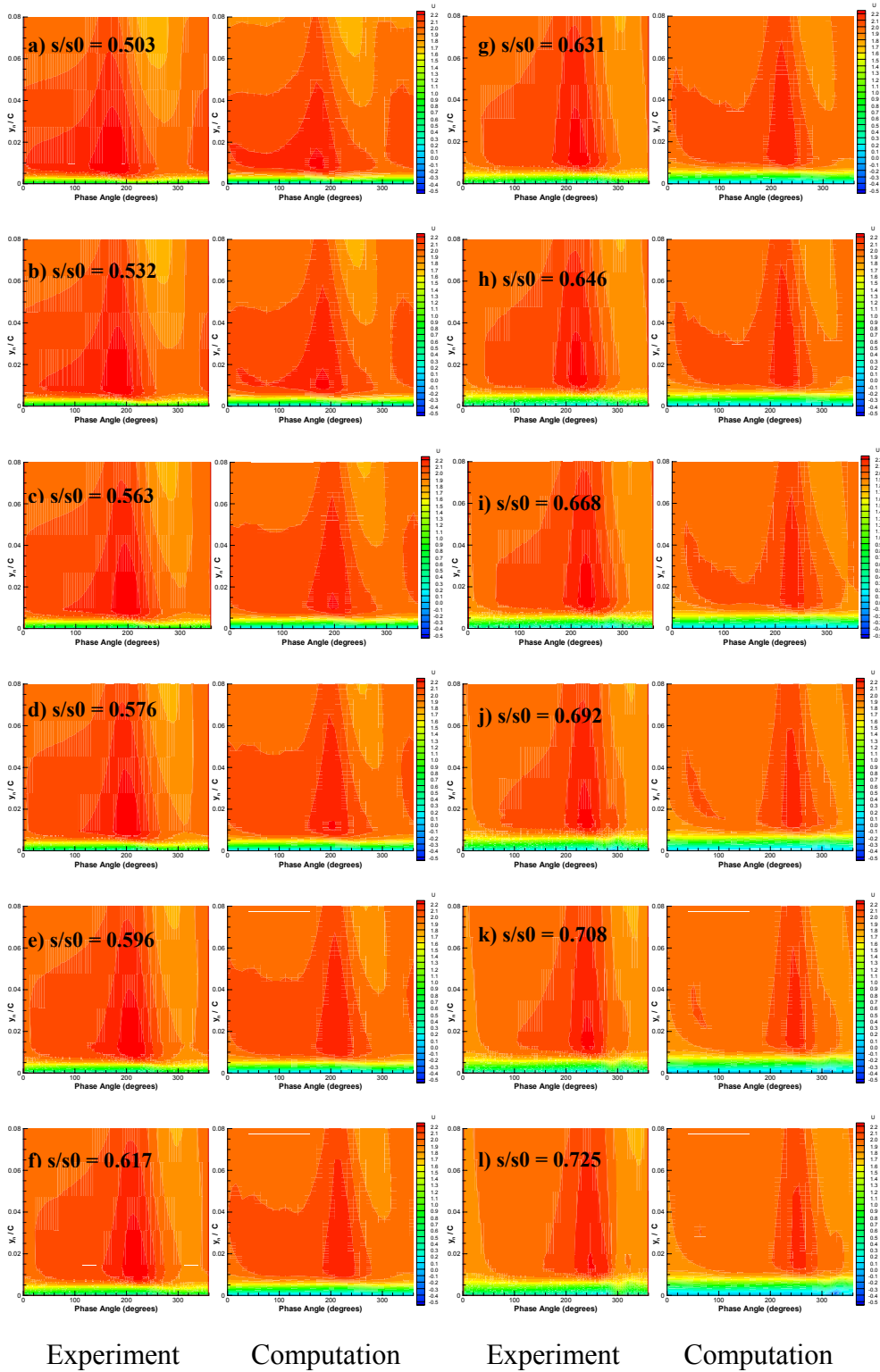


Figure 4.63 : Comparison of Computed and Experimental Velocity Distributions at Various Streamwise Stations on Suction Surface of the Blade for T106 Cascade

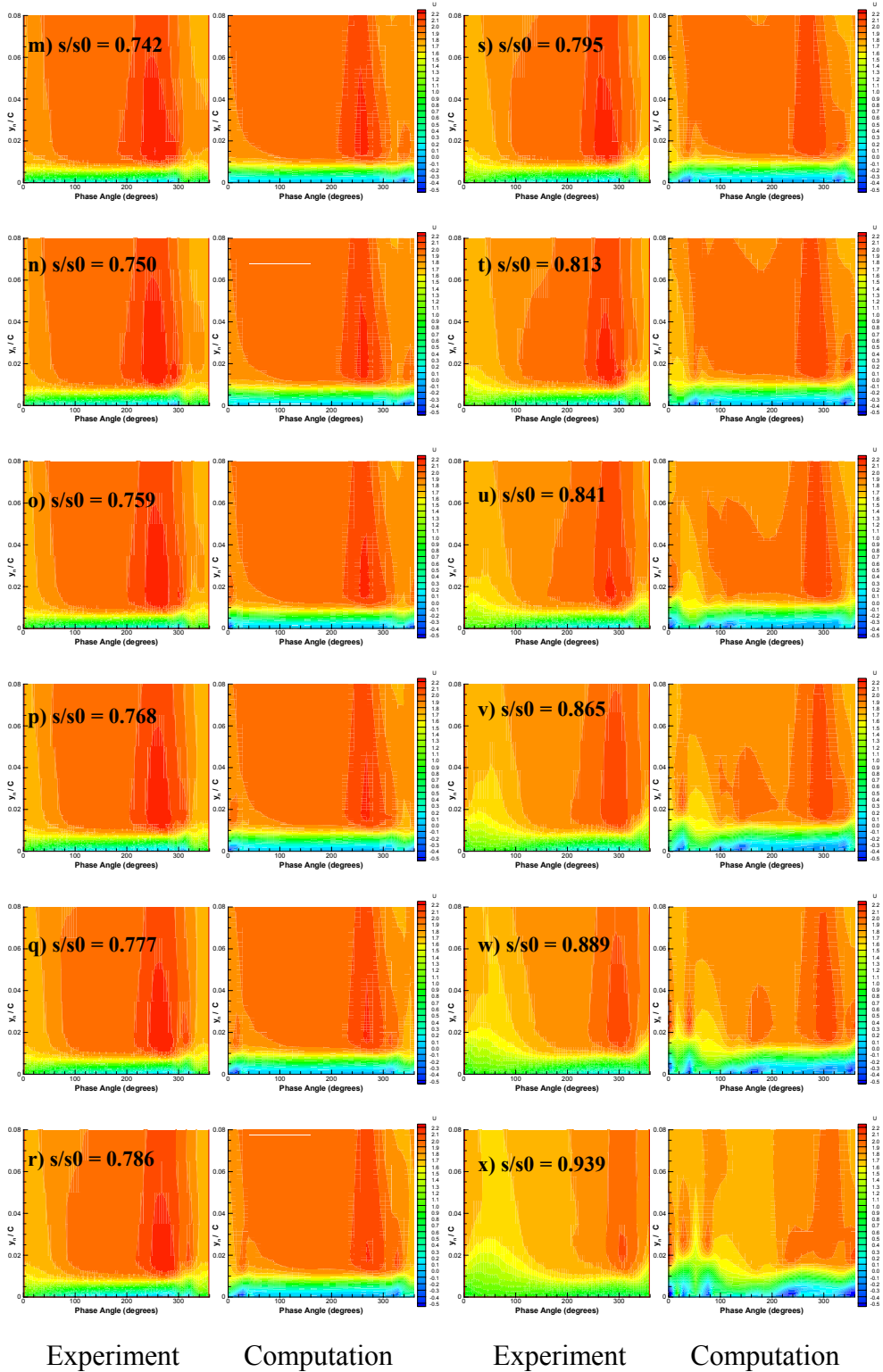
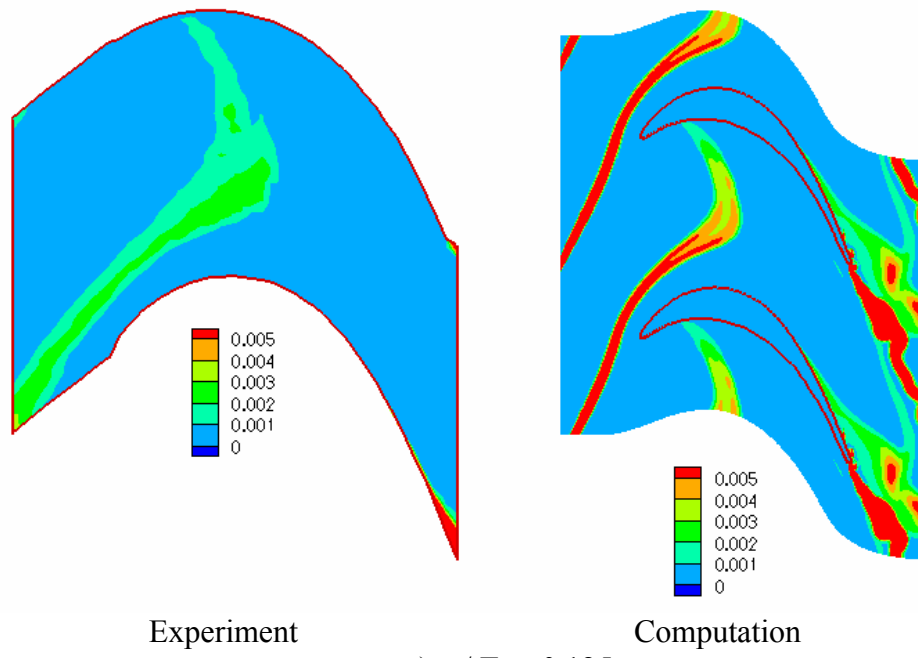
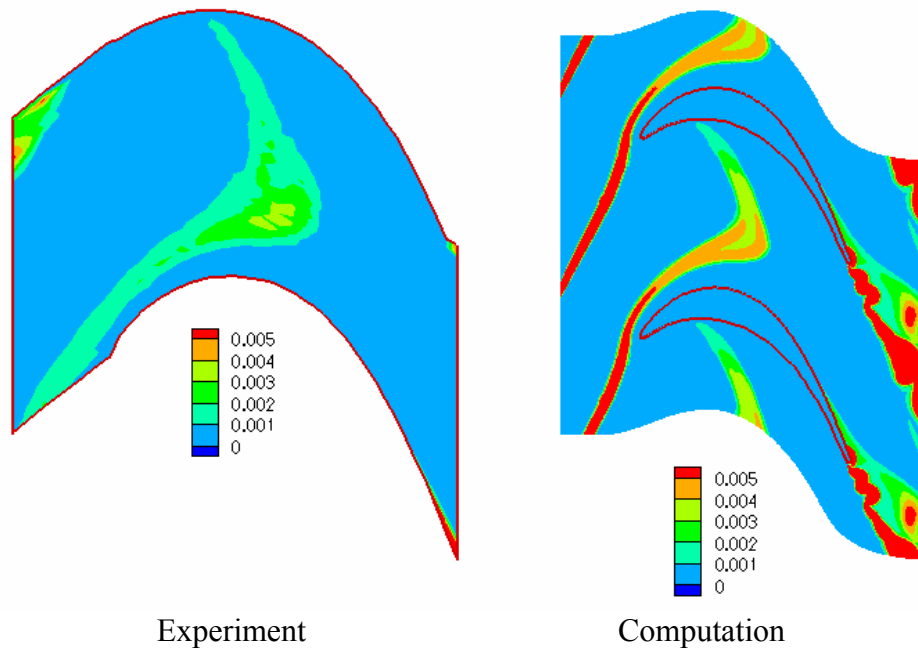


Figure 4.63 : continued



a) $t / T = 0.125$



b) $t / T = 0.250$

Figure 4.64 : Comparison of Computed and Experimental Isocontours of Turbulent Kinetic Energy at Different Time Levels for T106 Cascade, continued

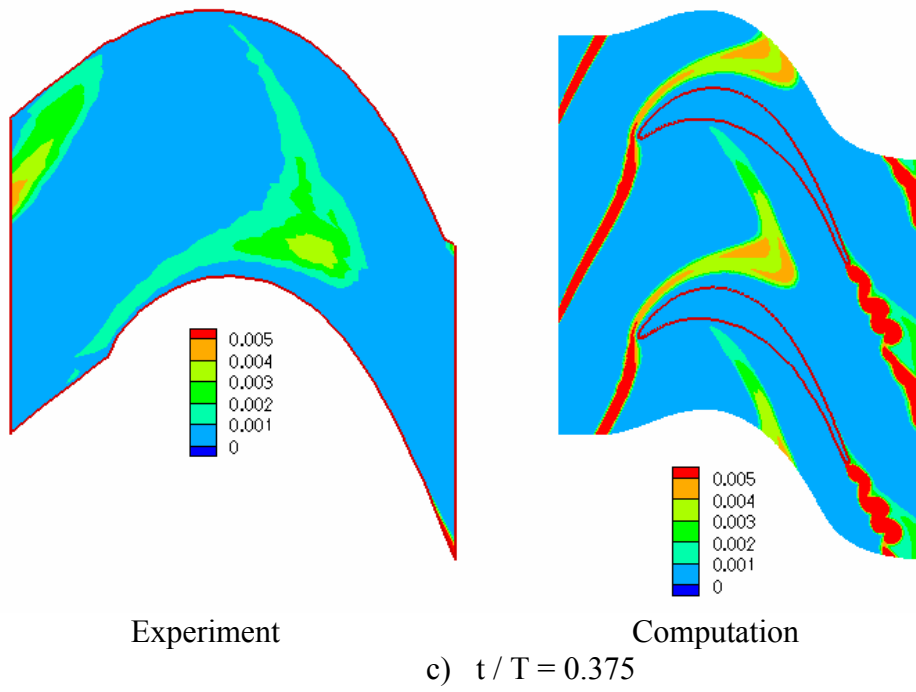


Figure 4.64 : continued

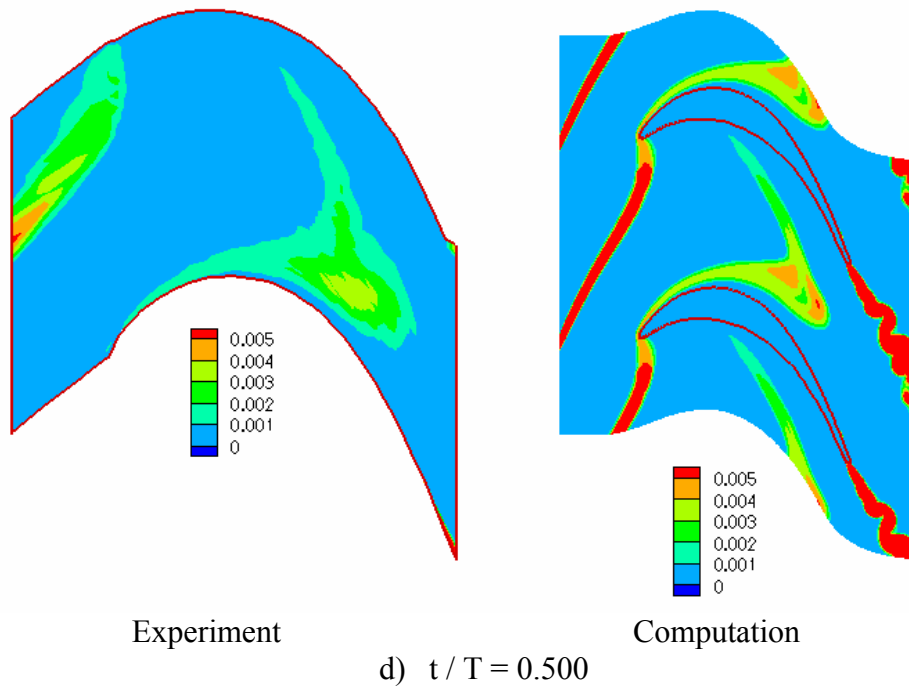


Figure 4.64 : continued

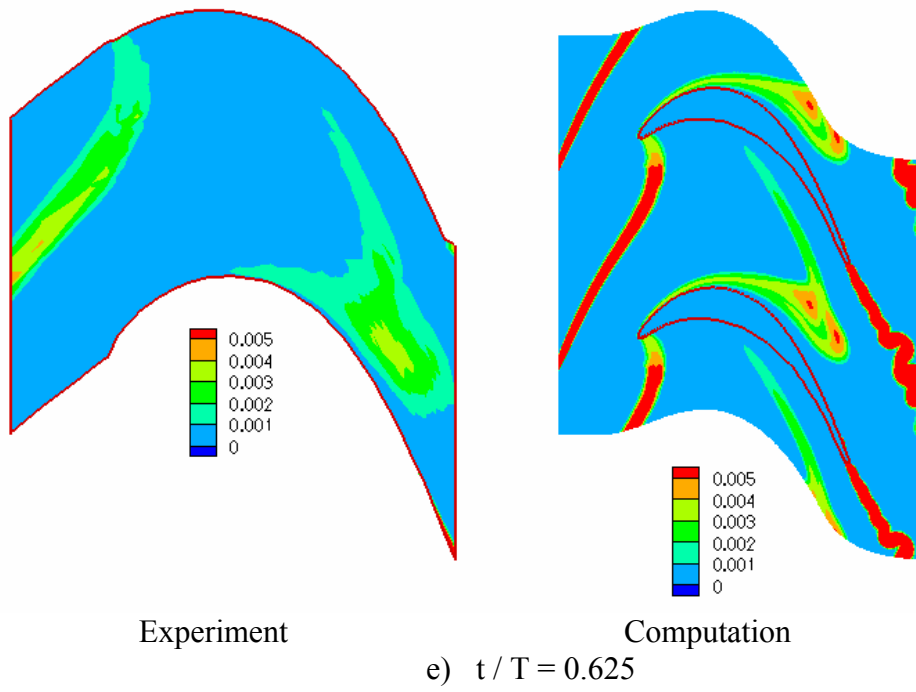


Figure 4.64 : continued

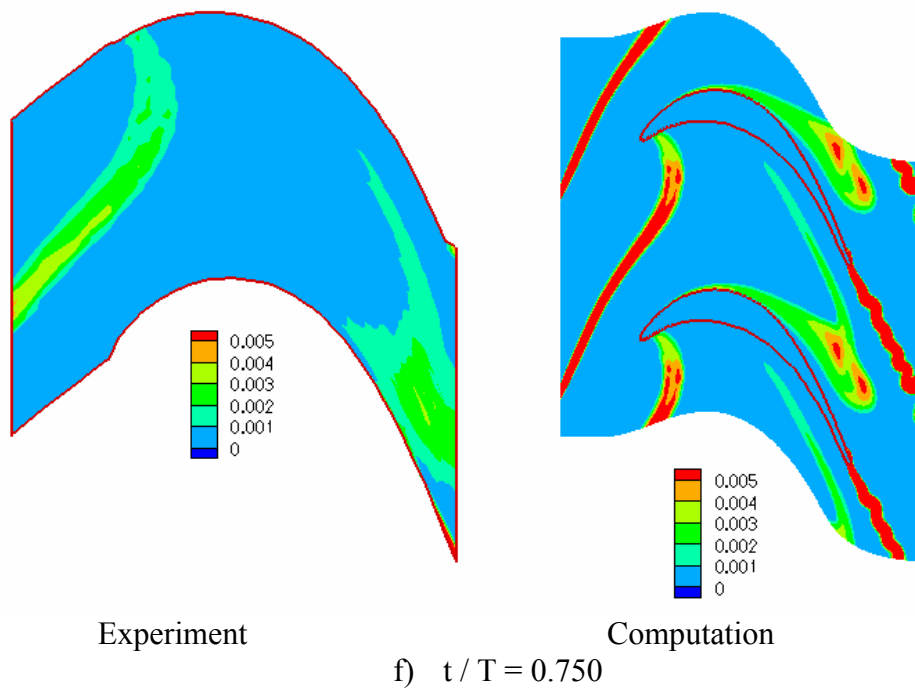
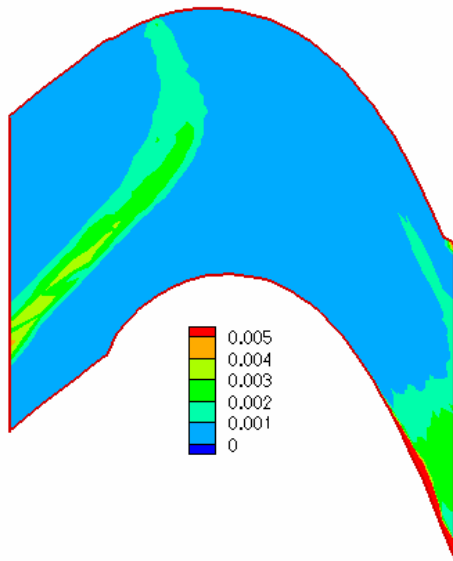
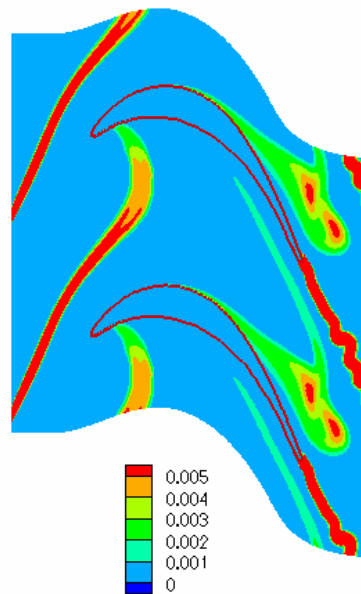


Figure 4.64 : continued



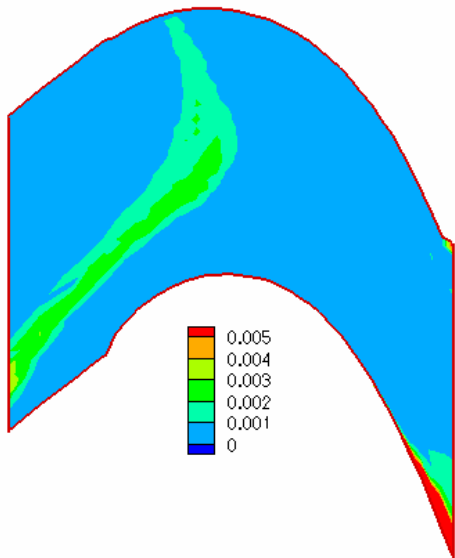
Experiment



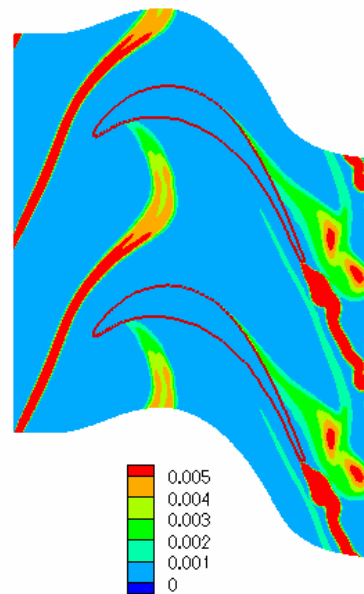
Computation

g) $t / T = 0.875$

Figure 4.64 : continued



Experiment



Computation

h) $t / T = 1.0$

Figure 4.64 : continued

Chapter Five

Conclusions and Future Work

5.1 Conclusions

A systematic approach of testing and validating transition models is developed and employed in testing of a recently developed transition model. The testing methodology uses efficient computational tools and a wide range of test cases. The computational tools include a boundary layer code, single zone Navier Stokes solver, and a multi-block Navier Stokes solver. Test cases include simple flat plate experiments of Savill (1993a, 1993b), Pak-B cascade experiments of Huang et al. (2003), compressor cascade experiments of Zierke and Deutsch (1989), turbine cascade experiments of Ubaldi et al. (1996), and unsteady wake/blade interaction experiments of Stieger et al. (2003). The above test cases investigate the predicting capability of the transition model under the effects of freestream turbulence, Reynolds number, pressure gradient, flow separation, and unsteady wake/blade interaction.

A new correlation based transition model which uses local variables is tested and validated using the available test cases and computational tools. The new transition model is tested and validated for the following experiments.

The new transition model is first tested and validated for T3 flat plate experiments of Savill (1993a, 1993b). These experiments investigate the effect of free stream turbulence intensity on the development and subsequent transition of a laminar boundary layer under zero and variable pressure gradients. T3A, T3B, and T3A- are zero pressure gradient flows and T3C1 and T3C2 are variable pressure gradient flows. The results obtained from the computations are satisfactory when compared to the experiments. The new transition model predicted small transition length in some cases and also the onset of transition is predicted earlier compared to the experiments.

The transition model is then validated using PAK-B blade for the experiments assembled by Huang et al. (2003). The new model is tested for three different free stream turbulence intensities coupled with three different Reynolds numbers. These experiments investigate the capability of

the transition model under the effect of free stream turbulence intensity and Reynolds number. The new model predicted good results for high free stream turbulence and high Reynolds number cases. For low free stream turbulence and low Reynolds number cases the separation bubble predicted is small compared to the experiments and also the reattachment point is not in well agreement compared to the experiment. This deficiency can be eliminated by further improving the separation modification made to the transition model. A parametric study of the separation modification of the new model is made and it is concluded that the onset of transition is not predicted accurately. Thus changing the transition length alone, reattachment length cannot be matched with the experiment. However once the transition onset is predicted accurately using separated flow correlations such as correlation developed by Davis et al. (1987) or the alternate correlation developed by Suzen et al. (2001), the new model can predict good results for low freestream turbulence and low Reynolds number cases.

The new model is then validated for highly loaded compressor cascade experiments of Zierke and Deutsch (1989). Computations are made for two different incidence angles and the Reynolds number is of the order of 500,000. From the pressure coefficient distribution, a separation bubble near the trailing edge on the suction side can be observed. Also on the pressure side transition occurs along the mid chord and the prediction agrees well with the experiment. However due to high Reynolds number there is not much difference between the solution obtained using transition model and fully turbulent solution. There seems to be an error in the measurement for -1.5° incidence angle case as seen from the discrepancy from the pressure coefficient distribution plot.

The new model is then validated for large scale turbine cascade experiments of Ubaldi et al. (1996). From the normalized friction velocity plot it can be observed that the onset of transition is predicted earlier compared to the experiments. Also the length of transition is short compared to the experiment and a sudden rise in the friction velocity can be observed once the transition starts.

Using the unsteady wake/blade interaction experiments of Stieger et al. (2003) the transition model is finally tested for the effect of unsteadiness. This experiment investigates the effect of

periodically passing wakes on laminar to turbulent transition and separation in low pressure turbines. From the computational results it is observed that the wake is captured accurately compared to the experiments. From the pressure coefficient distribution it can be observed that the unsteadiness suppresses the separation bubble. However from the unsteady time averaged results it can be observed that flow separation is still predicted, whereas experimental results indicate attached flow. Also discrepancies are observed near the trailing edge of the T106 cascade in the mean velocity profile comparisons. From the results it is evident that a small separation bubble is predicted according to the computations. These results indicate that the separated flow modification incorporated to the transition model has to be further improved.

5.2 Future Work

Using the available database of test cases and computational tools, transition models can be tested and validated. Also the available test cases and computational tools aid in the development of a new transition model.

For the present transition model, the separation modification has to be further improved to capture the separation bubble accurately for low free stream turbulence and low Reynolds number cases. Also either separated flow correlation developed by Davis et al. (1987) or the correlation developed by Suzen et al. (2001) has to be incorporated to predict the onset of separated flow transition accurately. The new model has to be validated extensively for unsteady cases, further investigating the effect of unsteadiness on flow transition.

Appendix

A.1 Nomenclature

C_p	pressure coefficient, $p_{\text{total}}-p/(0.5\rho U_{\text{ref}}^2)$
C_f	skin friction coefficient, $\tau/(0.5\rho U_{\text{ref}}^2)$
FSTI	freestream turbulence intensity (percent), $100(2k/3)^{1/2}/U_{\text{ref}}$
k	turbulent kinetic energy
K	flow acceleration parameter
L	turbulent length scale, $k^{1/2}/\omega$
L	axial reference length
P	local static pressure
p_{total}	inlet total pressure
Re_x	Reynolds number, $\rho L U_{\text{ref}}/\mu$
Re_θ	momentum thickness Reynolds number, $\rho\theta U_0/\mu$
Re_{θ_t}	transition onset momentum thickness Reynolds number, $\rho\theta_t U_0/\mu$
R_T	viscosity ratio
R_y	wall-distance based turbulent Reynolds number
R_v	vorticity Reynolds number
S	absolute value of strain rate, $(2S_{ij}S_{ij})^{1/2}$
S_{ij}	strain rate tensor, $0.5(\partial u_i/\partial x_j + \partial u_j/\partial x_i)$
U	local velocity
U_o	local freestream velocity
U_{ref}	inlet reference velocity
x/C	axial distance over axial chord
y	distance to nearest wall
y^+	distance in wall coordinates, $\rho y \mu_\tau/\mu$
δ	boundary layer thickness
ε	turbulence dissipation rate
θ	momentum thickness
λ_θ	pressure gradient parameter, $(\rho\theta^2/\mu)(dU/ds)$

μ	molecular viscosity
μ_t	eddy viscosity
μ_τ	friction velocity
ρ	density
τ	wall shear stress
Ω	absolute value of vorticity, $(2\Omega_{ij}\Omega_{ij})^{1/2}$
Ω_{ij}	vorticity tensor, $0.5(\partial u_i/\partial x_j - \partial u_j/\partial x_i)$
Ω	specific turbulence dissipation rate, ε/k

Subscripts

t	transition onset
s	streamline

A2. A Correlation Based Transition Model Using Local Variables (Menter et al., 2004)

1.0 Transport Equation for Intermittency

The intermittency equation is formulated as follows:

$$\frac{\partial(\rho\gamma)}{\partial t} + \frac{\partial(\rho U_j \gamma)}{\partial x_j} = P_{\gamma 1} - E_{\gamma 1} + P_{\gamma 2} - E_{\gamma 2} + \frac{\partial}{\partial x_j} \left[\left(\mu + \frac{\mu_t}{\sigma_f} \right) \frac{\partial \gamma}{\partial x_j} \right] \quad (\text{A1})$$

The transition sources are defined as:

$$P_{\gamma 1} = F_{length} \rho S [\gamma F_{onset}]^{c_{a1}} \quad (\text{A2})$$

$$E_{\gamma 1} = c_{e1} P_{\gamma 1} \gamma \quad (\text{A3})$$

where S is the strain rate magnitude.

$$Re_v = \frac{\rho \gamma^2 S}{\mu} \quad (\text{A4})$$

$$F_{onset 1} = \frac{Re_v}{2.193 \cdot Re_{\theta c}} \quad (\text{A5})$$

$$F_{onset 2} = \min \left(\max \left(F_{onset 1}, F_{onset 1}^4 \right), 2.0 \right) \quad (\text{A6})$$

$$R_T = \frac{\rho k}{\mu \omega} \quad (\text{A7})$$

$$F_{onset 3} = \max \left(1 - \left(\frac{R_T}{2.5} \right)^3, 0 \right) \quad (\text{A8})$$

$$F_{onset} = \max(F_{onset 2} - F_{onset 3}, 0) \quad (\text{A9})$$

$$Re_{\alpha} = f(\overline{Re_{\alpha}}) \quad (\text{A10})$$

The destruction/relaminarization sources are defined as follows:

$$P_{\gamma 2} = c_{a2} \rho \Omega \gamma F_{turb} \quad (\text{A11})$$

$$E_{\gamma 2} = c_{e2} P_{\gamma 2} \gamma \quad (\text{A12})$$

$$F_{turb} = e^{-\left(\frac{R_T}{4} \right)^4} \quad (\text{A13})$$

The constants for the intermittency equation are:

$$c_{e1} = 1.0; \quad c_{a1} = 0.5;$$

$$c_{e2} = 50; \quad c_{a2} = 0.03; \quad \sigma_f = 1.0;$$

The boundary condition for γ at a wall is zero normal flux while at an inlet γ is equal to 1.

2.0 Transport Equation for Transition Momentum Thickness Reynolds Number

The transport equation for the transition momentum thickness Reynolds number $\overline{Re_{\theta}}$ is defined as follows:

$$\frac{\partial(\rho \overline{Re_{\theta}})}{\partial t} + \frac{\partial(\rho U_j \overline{Re_{\theta}})}{\partial x_j} = P_{\theta t} + \frac{\partial}{\partial x_j} \left[\sigma_{\theta t} (\mu + \mu_t) \frac{\partial \overline{Re_{\theta}}}{\partial x_j} \right] \quad (A14)$$

The source term is defined as follows:

$$P_{\theta t} = c_{\theta t} \frac{\rho}{t} (\overline{Re_{\theta t}} - \overline{Re_{\theta}}) (1.0 - F_{\theta t}) \quad (A15)$$

$$t = \frac{500 \mu}{\rho U^2} \quad (A16)$$

where t is a time scale which is present for dimensional reasons.

$$F_{\theta t} = \min \left(\max \left(F_{wake} \cdot e^{-\left(\frac{y}{\delta}\right)^4}, 1.0 - \left(\frac{\gamma - 1/c_{e2}}{1.0 - 1/c_{e2}}\right)^2 \right), 1.0 \right) \quad (A17)$$

$$\theta_{BL} = \frac{\overline{Re_{\theta}} \mu}{\rho U} \quad \delta_{BL} = \frac{15}{2} \theta_{BL} \quad \delta = \frac{50 \Omega y}{U} \cdot \delta_{BL} \quad (A18)$$

$$Re_{\omega} = \frac{\rho \omega y^2}{\mu} \quad (A19)$$

$$F_{wake} = e^{-\left(\frac{Re_{\omega}}{1E+5}\right)^2} \quad (A20)$$

The boundary condition for $\overline{Re_{\theta}}$ at a wall is zero flux. The boundary condition for $\overline{Re_{\theta}}$ at an inlet should be calculated from the empirical correlation based on the inlet turbulence intensity.

The model constants for the transport equation are as follows, where $c_{\theta t}$ controls the magnitude of the source term and $\sigma_{\theta t}$ controls the diffusion coefficient:

$$c_{\theta t} = 0.03$$

$$\sigma_{\theta t} = 10.0$$

3.0 Separation Induced Transition

The modification for separation-induced transition is given by:

$$\gamma_{sep} = \min \left(s_1 \max \left[\left(\frac{Re_v}{2.193 Re_{\theta^*}} \right) - 1, 0 \right] F_{reattach}, 5 \right) F_{\theta t} \quad (A21)$$

$$F_{reattach} = e^{-\left(\frac{R_T}{15}\right)^4} \quad (\text{A22})$$

$$\gamma_{eff} = \max(\gamma, \gamma_{sep}) \quad (\text{A23})$$

$$s_1 = 8$$

The size of the separation bubble can be controlled with the constant s_1 .

4.0 Coupling with the Turbulence Model

The new transition model has been calibrated for use with the SST turbulence model of Menter (1994). The details of the SST turbulence model is given in appendix A3. The transition model is coupled with the turbulence model as follows:

$$\frac{\partial}{\partial t}(\rho k) + \frac{\partial}{\partial x_j}(\rho u_j k) = \tilde{P}_k - \tilde{D}_k + \frac{\partial}{\partial x_j} \left((\mu + \sigma_k \mu_t) \frac{\partial k}{\partial x_j} \right) \quad (\text{A24})$$

$$\frac{\partial}{\partial t}(\rho \omega) + \frac{\partial}{\partial x_j}(\rho u_j \omega) = \alpha \frac{P_k}{\nu_t} - D_\omega + Cd_\omega + \frac{\partial}{\partial x_j} \left((\mu + \sigma_k \mu_t) \frac{\partial \omega}{\partial x_j} \right) \quad (\text{A25})$$

$$\tilde{P}_k = \gamma_{eff} P_k \quad (\text{A26})$$

$$\tilde{D}_k = \min(\max(\gamma_{eff}, 0.1), 1.0) D_k \quad (\text{A27})$$

where P_k and D_k are the production and destruction terms from the turbulent kinetic energy equation in the original SST turbulence model.

The modified blending function is defined as follows:

$$R_y = \frac{\rho y \sqrt{k}}{\mu} \quad (\text{A28})$$

$$F_3 = e^{-\left(\frac{R_y}{120}\right)^8} \quad (\text{A29})$$

$$F_1 = \max(F_{1orig}, F_3) \quad (\text{A30})$$

where F_{1orig} is the original blending function from the SST turbulence model.

5.0 New Empirical Correlation

The new empirical correlation is defined as follows:

$$\lambda_\theta = (\theta^2/\nu)dU/ds \quad (\text{A31})$$

$$K = (\nu/U^2)dU/ds \quad (\text{A32})$$

where dU/ds is the acceleration along in the streamwise direction and can be computed by taking the derivative of the velocity (U) in the x , y and z directions and then summing the contribution of these derivatives along the streamwise flow direction as follows:

$$U = (u^2 + v^2 + w^2)^{\frac{1}{2}} \quad (\text{A33})$$

$$\frac{dU}{dx} = \frac{1}{2}(u^2 + v^2 + w^2)^{-\frac{1}{2}} \cdot \left[2u \frac{du}{dx} + 2v \frac{dv}{dx} + 2w \frac{dw}{dx} \right] \quad (\text{A34})$$

$$\frac{dU}{dy} = \frac{1}{2}(u^2 + v^2 + w^2)^{-\frac{1}{2}} \cdot \left[2u \frac{du}{dy} + 2v \frac{dv}{dy} + 2w \frac{dw}{dy} \right] \quad (\text{A35})$$

$$\frac{dU}{dz} = \frac{1}{2}(u^2 + v^2 + w^2)^{-\frac{1}{2}} \cdot \left[2u \frac{du}{dz} + 2v \frac{dv}{dz} + 2w \frac{dw}{dz} \right] \quad (\text{A36})$$

$$\frac{dU}{ds} = (u/U) \frac{dU}{dx} + (v/U) \frac{dU}{dy} + (w/U) \frac{dU}{dz} \quad (\text{A37})$$

The empirical correlation is defined as:

$$\text{Re}_\theta = 803.73[Tu + 0.6067]^{-1.027} F(\lambda_\theta, K) \quad (\text{A38})$$

$$F(\lambda_\theta, K) = 1 - \left[-10.32\lambda_\theta - 89.47\lambda_\theta^2 - 265.51\lambda_\theta^3 \right] e^{\left[\frac{-Tu}{3.0} \right]}, \lambda_\theta \leq 0 \quad (\text{A39})$$

$$F(\lambda_\theta, K) = 1 + \left[0.0962[K \cdot 10^6] + 0.148[K \cdot 10^6]^2 + 0.0141[K \cdot 10^6]^3 \right] \left(1 - e^{\left[\frac{-Tu}{1.5} \right]} \right) \quad (\text{A40})$$

$$+ 0.556 \left[1 - e^{\left[\frac{-23.9\lambda_\theta}{1.5} \right]} \right], \lambda_\theta > 0$$

where Tu is the local turbulence intensity (in percent) as defined in the nomenclature. For numerical robustness the acceleration parameters and the empirical correlation should be limited as follows:

$$-0.1 \leq \lambda_\theta \leq 0.1 \quad (\text{A41})$$

$$-3 \times 10^{-6} \leq K \leq 3 \times 10^{-6} \quad (\text{A42})$$

$$\text{Re}_\theta \geq 20 \quad (\text{A43})$$

A3. SST Turbulence Model (Menter, 1994)

Menter's SST model is based on a mix of two equation $\kappa - \omega$ and $\kappa - \varepsilon$ turbulence models using a blending function F_1 . The model can be written as

κ -equation:

$$\frac{\partial \rho \kappa}{\partial t} + \frac{\partial \rho u_j \kappa}{\partial x_j} = P_k - 0.09 \rho \omega \kappa + \frac{\partial}{\partial x_j} \left((\mu + \sigma_k \mu_t) \frac{\partial \kappa}{\partial x_j} \right) \quad (\text{A1})$$

ω -equation:

$$\frac{\partial \rho \omega}{\partial t} + \frac{\partial \rho u_j \omega}{\partial x_j} = \frac{c}{\nu_t} P_k - \beta \rho \omega^2 + \frac{\partial}{\partial x_j} \left((\mu + \sigma_\omega \mu_t) \frac{\partial \omega}{\partial x_j} \right) + 2 \rho (1 - F_1) \sigma_{\omega 2} \frac{1}{\omega} \frac{\partial \kappa}{\partial x_j} \frac{\partial \omega}{\partial x_j} \quad (\text{A2})$$

The constants, c , β , σ_k , and σ_ω , are given by the following general expression

$$\phi = F_1 \phi_1 + (1 - F_1) \phi_2 \quad (\text{A3})$$

where ϕ represents any one of these constants; ϕ_1 represents any constant in the $\kappa - \omega$ model;

ϕ_2 represents the corresponding constant in the $\kappa - \varepsilon$ model. These constants are defined as

Set 1 ($\kappa - \omega$):

$$\sigma_{\kappa 1} = 0.85 \quad \sigma_{\omega 1} = 0.5 \quad \beta_1 = 0.075 \quad c_1 = 0.553 \quad (\text{A4})$$

Set 2 ($\kappa - \varepsilon$):

$$\sigma_{\kappa 2} = 1.0 \quad \sigma_{\omega 2} = 0.856 \quad \beta_2 = 0.0828 \quad c_2 = 0.44 \quad (\text{A5})$$

The Production term is given as

$$P_k = \tau_{ij} \frac{\partial u_i}{\partial x_j} \quad (\text{A6})$$

where

$$\tau_{ij} = \mu_t \left[\frac{\partial u_i}{\partial x_j} + \frac{\partial u_j}{\partial x_i} - \frac{2}{3} \frac{\partial u_k}{\partial x_k} \delta_{ij} \right] - \frac{2}{3} \rho \kappa \delta_{ij} \quad (\text{A7})$$

The blending function F_1 is defined as

$$F_1 = \tanh(\arg_1^4) \quad (\text{A8})$$

with

$$\arg_1 = \min \left\{ \max \left[\frac{\sqrt{\kappa}}{0.09\omega d}, \frac{500\nu}{d^2\omega} \right], \frac{4\rho\sigma_{\omega 2}\kappa}{CD_{\kappa\omega}d^2} \right\} \quad (\text{A9})$$

where d is the distance to the closest wall and $CD_{\kappa\omega}$ is the positive portion of the cross-diffusion term in Eq. (A2).

$$CD_{\kappa\omega} = \max \left[2\rho\sigma_{\omega 2} \frac{1}{\omega} \frac{\partial\kappa}{\partial x_j} \frac{\partial\omega}{\partial x_j}; 10^{-20} \right] \quad (\text{A10})$$

The kinematic eddy viscosity is defined as

$$\nu_t = \frac{a_1\kappa}{\max(a_1\omega; \Omega F_2)} \quad (\text{A11})$$

where Ω is the magnitude of vorticity and $a_1 = 0.31$. The function F_2 is given by

$$F_2 = \tanh(\arg_2^2) \quad (\text{A12})$$

with

$$\arg_2 = \max \left[\frac{2\sqrt{\kappa}}{0.09\omega d}, \frac{500\nu}{d^2\omega} \right] \quad (\text{A13})$$

References

- Chen, K.K., and Thyson, N.A., 1971, "Extension of Emmons Spot Theory to Flows on Blunt Bodies." AIAA Journal, Vol.9, pp. 821-825.
- Cho, J.R. and Chung, M.K., 1992, "A $\kappa - \varepsilon - \gamma$ Equation Turbulence Model," Journal of Fluid Mechanics, Vol. 237, pp. 301-322.
- Davis, R.L., Carter, J.E., and Reshotko, E., 1987, "Analysis of Transitional Separation Bubbles on Infinite Swept Wings," AIAA Journal, Vol. 25, No. 3, pp. 421-428.
- Emmons, H.W., 1951, "The Laminar-Turbulent Transition in Boundary Layer-Part I," J.Aero. Sci., Vol. 18, pp.490-498.
- Fan, S., Lakshminarayana, B., 1996, "Computation and Simulation of Wake-Generated Unsteady Pressure and Boundary Layers in Cascades: Part 1 – Description of the Approach and Validation", Transactions of the ASME, Vol. 118.
- Huang, J., Corke, T.C., Thomas, F.O., 2003, "Plasma actuators for separation control of low pressure turbine blades," AIAA paper No. AIAA-2003-1027.
- Kachanov Y.S., 1994, "Physical mechanisms of laminar boundary layer transition", Annu. Rev. Fluid Mech. 26, 411-482.
- Kyriakides, N.K., Kastrinakis, E.G., Nychas, S.G., Goulas, A., 1999, "A bypass wake induced laminar/turbulent transition", Eur. J. Mech. B/Fluids 18, 1049-1065.
- Langtry, R.B., Sjolander, S.A., 2002 "Prediction of Transition for Attached and Separated Shear Layers in Turbomachinery", AIAA 2002-3643.

Langtry, R.B., Menter, F.R., Likki, S.R., Suzen, Y.B., Huang, P.G., and Volker, S., 2004, "A Correlation based transition model using local variables Part II – Test cases and industrial applications", ASME-GT2004-53454, ASME Turbo Expo 2004, Vienna, Austria.

Mayle, R.E., 1991, "The Role of Laminar-Turbulent Transition in Gas Turbine Engines," ASME Journal of Turbomachinery, Vol. 113, pp.509-537.

Menter, F.R., 1994, "Two-equation eddy-viscosity turbulence models for engineering applications", AIAA Journal, Vol. 32, No. 8, pp. 1598-1605.

Menter, F.R., Langtry, R.B., Likki, S.R., Suzen, Y.B., Huang, P.G., and Volker, S., 2004, "A Correlation based Transition Model using Local Variables Part I- Model Formulation", ASME-GT2004-53452, ASME Turbo Expo 2004, Vienna, Austria.

Morkovin, M.V., 1969, "On the many faces of Transition," Viscous Drag Reduction, C.S.Wells, ed., Plenum Press, New York, pp.1-31.

Narasimha, R., 1957, "On the Distribution of Intermittency in the Transition Region of a Boundary Layer," J. Aero. Sci., Vol. 24, pp. 711-712.

Savill, A.M., 1993a "Some recent progress in the turbulence modeling of by-pass transition", In: R,M,C, So, C.G.Speziale and B.E.Lauder, Eds.: Near-Wall Turbulent Flows, Elsevier, pp.829-848.

Savill, A.M., 1993b, "Further Progress in the Turbulence Modeling of Bypass Transition," Engineering Turbulence Modeling and Experiments 2, W.Rodi and F.Martelli, eds., Elsevier Science, pp. 583-592.

Savill, A.M., 1996, "One-point closures applied to Transition, Turbulence and Transition Modelling," M.Hallback et al., Kluwer, pp.233-268.

Schlichting, H., 1979, Boundary-Layer Theory, McGraw-Hill, New York.

Solomon, W.J., Walker, G.J., Gostelow, J.P., 1995 “Transition Length Prediction For Flows With Rapidly Changing Pressure Gradients”, ASME-95-GT-241, International Gas Turbine and Aeroengine Congress & Exposition, Houston, Texas.

Steelant, J., Dick, E., 1996, “Modelling of Bypass Transition with Conditioned Navier-Stokes Equations Coupled to an Intermittency Transport Equation”, International Journal For Numerical Methods In Fluids, Vol. 23, 193-220.

Stieger ,R., Hollis, D., Hodson, H., 2003, “Unsteady Surface Pressures Due to Wake Induced Transition in a Laminar Separation Bubble on a LP Turbine Cascade”, ASME GT2003-38303, Proceedings of ASME Turbo Expo 2003, Atlanta, Georgia, USA.

Suzen, Y.B., Huang, P.G., 1999, “Modeling of Flow Transition Using an Intermittency Transport Equation”, NASA/CR-1999-209313, September 1999.

Suzen, Y.B., Huang, P.G., 2000 “Modeling of Flow Transition Using an Intermittency Transport Equation”, Journal of Fluids Engineering, Vol. 122, pp. 273-284.

Suzen, Y.B., Huang, P.G., Hultgren, L.S., Ashpis, D.E., 2001 “Predictions of Separated and Transitional Boundary Layers Under Low-Pressure Turbine Airfoil Conditions Using an Intermittency Transport Equation”, AIAA-2001-0446, 39th AIAA Aerospace Sciences Meeting & Exhibit, Reno, NV, January 2001.

Suzen, Y.B., Huang, P.G., 2004 “Comprehensive Validation of an Intermittency Transport Model for Transitional Low-Pressure Turbine Flows”, AIAA-2004-1121, 42nd Aerospace Sciences Meeting & Exhibit, Reno, NV, January 2004.

Ubaldi, M., Zunino, P., Campora, U., Ghiglione, A., 1996, "Detailed Velocity and Turbulence Measurements of the Profile Boundary Layer in a Large Scale Turbine Cascade", ASME-96-GT-42, International Gas Turbine and Aeroengine Congress & Exhibition, Birmingham, UK.

Van Driest, E.R. and Blumer, C.B., 1963, "Boundary Layer Transition: Freestream Turbulence and Pressure Gradient Effects," AIAA Journal, Vol.1, No.6, June 1963, pp. 1303-1306.

Westin, K.J.A. and Henkes, R.A.W.M., 1997, "Application of Turbulence Models to Bypass Transition," Journal of Fluids Engineering, Vol.119, pp.859-866.

Zierke, W.C., Deutsch, S., 1989, "The measurement of boundary layers on a compressor blade in cascade – Vols. 1 and 2", NASA CR 185118.

Vita

DATE AND PLACE OF BIRTH

1979, Medipally, Andhra Pradesh, INDIA

EDUCATION

Bachelor of Engineering and Technology in Mechanical Engineering (B.Tech)., Jawaharlal Nehru Technological University, Hyderabad, Andhra Pradesh, INDIA (2001)

PUBLICATIONS

Menter, F.R., Langtry, R.B., Likki, S.R., Suzen, Y.B., Huang, P.G., and Volker, S., 2004, “A Correlation Based Transition Model Using Local Variables Part I- Model Formulation” ASME-GT-2004-53452, ASME TURBO EXPO 2004, Vienna, Austria.

Langtry, R.B., Menter, F.R., Likki, S.R., Suzen, Y.B., Huang, P.G., and Volker, S., 2004, “A Correlation Based Transition Model Using Local Variables Part II- Test Cases and Industrial Applications” ASME-GT-2004-53454, ASME TURBO EXPO 2004, Vienna, Austria.